Overexpression, characterisation, and encapsulation of LRP/LR for treatment of neurodegenerative disorders

by

Chandni Madhav

(1348622)

Dissertation

Submitted in fulfilment of the requirements for the degree

Master of Science

in

Molecular and Cell Biology

in the Faculty of Science, University of Witwatersrand, Johannesburg, South Africa

Supervisor: Dr Eloise van der Merwe

Co-supervisors: Dr Tyrone Otgaar and Prof. Stefan FT Weiss (*in memoriam)*

June 2023

Declaration

I, **Chandni Madhav (1348622)**, declare that this dissertation is my own work, unaided work. It is being submitted for the degree of Master of Science at the University of the Witwatersrand, Johannesburg. It has not been submitted before for any degree or examination at any other university.

: 

05th day of June, 2023 at Johannesburg

Abstract

The neurodegenerative diseases of Parkinson's disease (PD) and Alzheimer's disease (AD) are debilitating conditions affecting millions of people worldwide. Both diseases pose a significant economic burden and require therapeutic strategies. AD is identified by intracellular neurofibrillary tangles and the accumulation of amyloid beta (Aβ) plaques, while PD is characterised by the loss of dopamine-producing neurons and mutations in PINK1, parkin, and α-synuclein proteins. The 37 kDa/67 kDa laminin receptor (LRP/LR) is a multifunctional receptor found to impede the progression of AD and PD. *In-vitro* studies have revealed that the LRP::FLAG overexpression increases hTERT expression and telomerase activity while rescuing cells from Aβ-mediated cytotoxicity. Cuttler *et al.* 2019 also revealed that LRP::FLAG overexpression decreased phosphorylated tau levels and tauopathy-related proteins. Within PD, *in vitro* studies demonstrated that LRP::FLAG overexpression plays a protective role, through the degradation of α-synuclein and rescuing cells from MPP^+ cytotoxicity. Thus, the current study comprised of three parts. The first part aimed at investigating the effect of overexpressing LRP::FLAG in HEK293 cells by assessing LRP/LR and PINK1 protein levels, as well as cell viability after treatment with MPP^+, TBHP, and $A\beta_{42}$, *in vitro* AD and PD models. The results demonstrated that the overexpression of LRP::FLAG rescued cells from MPP^+, TBHP, and $A\beta_{42}$ induced cytotoxicity, and increased LRP/LR and PINK1 protein levels. The second part of the study focussed on overexpressing, purifying, and structurally characterizing the 37 kDa LRP protein. The protein was successfully overexpressed and purified through Co^{2+}-IMAC while structural characterisation indicated that protein was correctly folded and predominantly α-helical, as expected. The purified LRP protein was then encapsulated in PLGA nanoparticles to develop an efficient *in vivo* delivery system. Thus, the third part of the study investigated the effect of empty and LRP-encapsulated PLGA nanoparticles on cell viability, LRP levels, and telomerase activity in SH-SY5Y and HEK 293 cells. The results demonstrated that LRP-encapsulated PLGA nanoparticles successfully delivered the therapeutic protein and increased exogenous LRP protein levels. Additionally, SH-SY5Y cells treated with LRP-encapsulated PLGA nanoparticles exhibited increased cellular viability and telomerase activity. Therefore, the LRP-encapsulated PLGA nanoparticles could be a possible therapeutic for conditions such as ageing and age-related diseases including AD and PD.

Dedications

· ***To my support*** ·

Mom, Papa, Didi & Akshay

Chhikas

Chotus

Madhavs

Maharajs

Mika, Mocha & Hugo

Acknowledgments

I would like to show appreciation to;

My supervisor, Dr Eloise van de Merwe, for providing unconditional guidance, support and opportunities. Thank you for always believing in me and pushing me to achieve more than I ever imagined possible. I will be eternally grateful for the loving environment you created in the lab.

My co-supervisor, Dr Tyrone Otgaar, thank you for pushing me when I felt I wasn't accomplishing enough, thank you for checking in with me every day, and thank you for your support not only as a supervisor but as a friend.

My co-supervisor, the late Prof. Stefan FT Weiss (*in memoriam* - 2023), for providing me with support and opportunities.

My colleagues of Weiss and Van de Merwe labs, thank you for providing a positive work environment in which to share ideas around and for assisting on days I felt overwhelmed. Thank you for the enjoyable moments of shared laughter and heartfelt conversations

Riyadh Mayet and members of the PSFRU unit, thank you for being patient and for welcoming us into your working space. Thank you for all the advice, assistance and mentorship during our protein purification.

My family, thank you for your endless support and for allowing me the freedom to pursue my dreams.

Financial Aid

The National Research Foundation (NRF) – Postgraduate Scholarships (2021-2022)

Wits Seed Fund (2021-2023)

Research outputs

Bignoux, M.J., Bernert, M., Otgaar, T.C., **Madhav, C.,** Weiss, S.F.T., & Ferreira, E. PLGA nanocapsules as a delivery mechanism for LRP/LR targeting molecules. *In preparation*

Table of Contents

List of abbreviations

Aß	Amyloid Beta
AD	Alzheimer's Disease
Aß40	40 amino acid isoform of amyloid beta
Aß42	42 amino acid isoform of amyloid beta
APP	Amyloid precursor protein
BCA	Bicinchoninic acid assay
BSA	Bovine serum albumin
DNA	Deoxyribonucleic acid
CD	Circular dichroism
CHAPS	3-[(3-cholamidopropyl) dimethylammonium]-1-propanesulfonate
CNS	Central nervous system
CTD	C-terminal domain
CTRD	C-terminal ring domain
DMEM	Dulbecco's modified eagle medium
DMSO	Dimethyl sulfoxide

EDTA	Ethylenediaminetetraacetic acid
ELISA	Enzyme linked immunosorbent assay
FBS	Foetal bovine serum
FT	Flow through
HRP	Horseradish peroxide
HEK293	Human embryonic kidney cell line
hTERT	Human Telomerase Reverse Transcription
hTERC	Human telomerase RNA component
IgG1-iS18	High affinity LRP/LR-specific antibody
IMAC	Immobilized metal ion affinity chromatography
IPTG	isopropyl ß-D-1-thiogalactopyranoside
ITF	Intrinsic tryptophan fluorescence
LB	Lewy body
LRP/LR	37-kDA/67-kDA laminin receptor precursor/high affinity laminin receptor
MRE	Mean residue ellipticity
Mt-DNA	Mitochondrial deoxyribonucleic acid
MMP	Mitochondrial membrane potential
MPP	Mitochondrial processing peptide
MPP+	1-Methyl-4-phenylpyridinium iodide
MTT	3-(4,5-dimethylthiazol-2-yl)-2,5-diphenyltetrazolium bromide
MWM	Molecular weight marker

OMM	Outer mitochondrial membrane
PAGE	Polyacrylamide gel electrophoresis
PBS	Phosphate buffered saline
PCR	Polymerase chain reaction
PD	Parkinson’s disease
PMSF	Phenylmethylsulphonyl fluoride
qPCR	Quantitative Polymerase Chain reaction
PBS	Phosphate buffered saline
PBST	Phosphate buffered saline with Tween-20
PCA	Protocatechuic acid
PD	Parkinson's disease
Pink-1	PTEN induced putative kinase 1
PTEN	Phosphatase and tensin homolog
PVDF	Polyvinylidene fluoride
RIPA	Radioimmunoprecipitation assay lysis buffer
ROS	Reactive oxygen species
RNA	Ribonucleic-acid
ROS	Reactive oxygen species
RPM	Revolutions/minute
SDS	Sodium dodecyl sulphate
SNPc	Substantia nigra pars compacta

SH-SY5Y	Neuroblastoma cell line
SW	Salt wash
TEMED	Tetramethyl ethylenediamine
TERC	Telomerase reverse transcriptase RNA component
TERT	Telomerase reverse transcriptase
UBL	Ubiquitin-like domain
UPS	Ubiquitin proteasome system
UV	Ultraviolet
WB	Western Blotting

List of figures

List of tables

1. Introduction

1.1. Epidemiology of Alzheimer's disease and Parkinson's disease

Alzheimer's and Parkinson's disease are classified as progressive neurodegenerative disorders which are categorized as continuing degeneration of the function and structure of the central and peripheral nervous system (Cummings *et al.,* 2002). In particular, Alzheimer's disease (AD) is considered an incurable and advancing type of cognitive disorder that leads to a decline in memory and cognitive abilities while on the other hand, Parkinson's disease (PD) is identified as a chronic, degenerative nervous system disorder that impacts the motor system, resulting in impaired movement (Bekris *et al.,* 2011; Nussbaum *et al.,* 2003). While AD and PD share mutual causes and effects, the diseases each have different pathological mechanisms which impacts the brain (Nussbaum *et al.,* 2003). Individually, Alzheimer's disease is known as an age-related disease and the leading form of progressive neurodegenerative diseases. AD is a common form of dementia, making up over 80% of all dementia cases (Goedert *et al.,* 2006). Worldwide, the prevalence of AD is estimated to affect over 55 million patients, with over 10 million patients diagnosed yearly (Li *et al.,* 2022). According to the world Alzheimer's report there is an estimation of approximately 187 000 patients within South Africa living with dementia, mostly those who are over the age of 60 (Alzheimer's Disease International, 2015). Additionally, given that both developing and developed countries are rapidly aging, it is estimated that the frequency will double every 20 years (Mayeux *et al.,* 2012). According to the worldwide projections of AD, it is estimated by 2050 that there will be over 139 million AD cases (World Health Organisation, 2022). The rising prevalence of dementia, which causes cognitive decline, imposes a significant physical and economic burden on society (Reitz *et al.,* 2011). Presently, the only available treatments for AD simply assist with symptoms of cognitive changes including memory loss and behaviour changes. One of those treatments are drugs such as cholinesterase inhibitors, these drugs are administered to help improve the neuropsychiatric symptoms of AD such as depression and agitation, however it has been found that these drugs have adverse side effects such as nausea, loss of appetite, and cardiac arrhythmia (Neugroschl *et al.,* 2011). Additionally, treatment plans such as adaptive living and routine habits are used to create a safe and supportive environment for the patients, to assist with the AD sufferers' well-being and ability to function (Alzheimer's Disease International, 2015). Palliative treatments have only been used due to poor understanding of the disease's molecular mechanisms. In essence, this highlights the significance of creating new and targeted treatments that can slow down

the advancement of AD, ultimately decreasing the demand for care and expense associated with it.

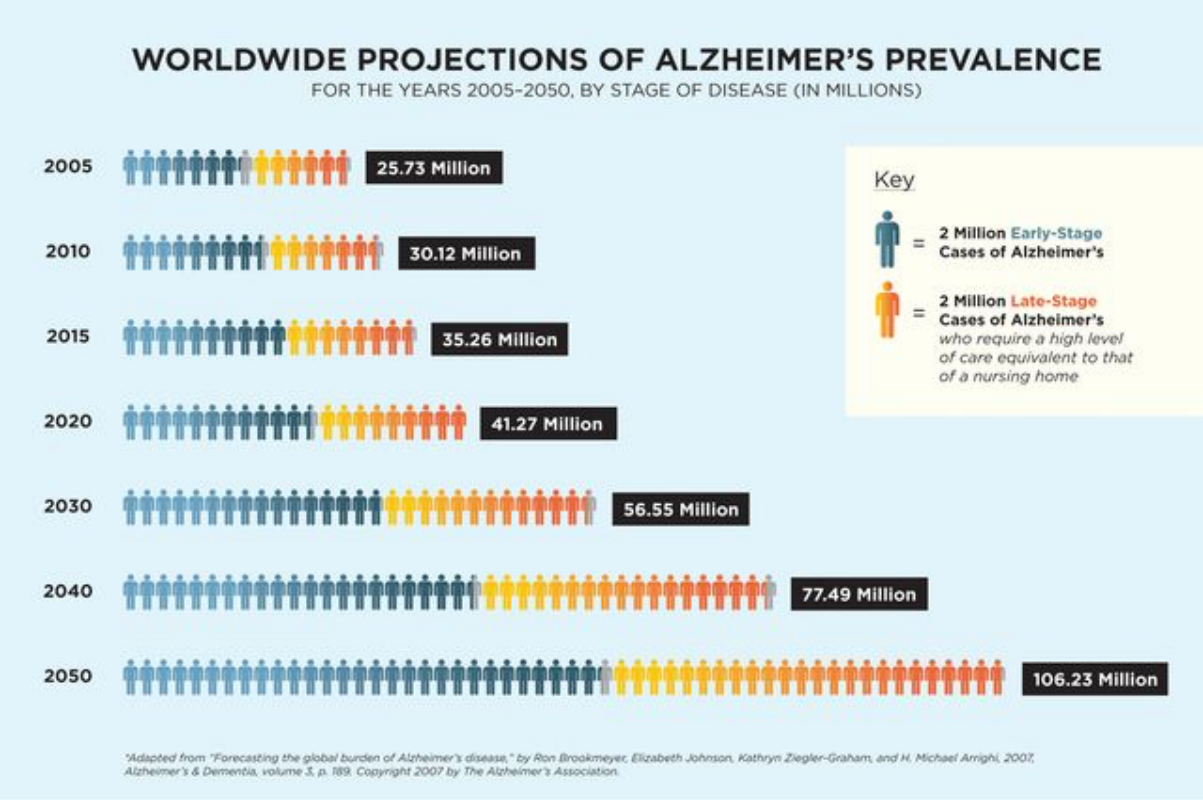

Figure 1: The worldwide projections of AD prevalence. *Currently there is over 40 million cases of Alzheimer's disease worldwide, and it is predicted that by 2050 over 100 million cases will be prevalent (Adapted from Brookmeyer et al., 2007).*

PD, which affects more than 10 million people worldwide, is the second most prevalent neurodegenerative illness (Parkinson's Foundation, 2019*)*. Worldwide, the prevalence of PD is known to increase with age, affecting 1 in 100 people over the age of 60, and 4 in 100 over the age of 80 (Reeve *et al.,* 2014). Unfortunately, South African and African PD epidemiology and statistics are limited; but even so, PD has been found to be most common in people of Northern European origin (De Lau *et al.,* 2006). Symptoms of PD progress gradually, starting with slight tremors in the hand, eventually leading to the onset of body stiffness and slow movement (Sveinbjornsdottir *et al.,* 2016). As of now, there are palliative treatments available for PD, including care homes and occupational therapy, since a curative treatment has not yet been established (Singh *et al.,* 2007). Furthermore, a commonly used drug which assists in symptom control of PD is levodopa, which is a dopamine precursor, known as an effective dopamine enhancer agent. Studies have found that levodopa does in fact improve symptoms associated with the disease; however it has adverse side effects from

prolonged usage such nausea and vomiting (Tarakad & Jankovic, 2017). Additionally, non-pharmacological treatments are available which aims at treating the symptoms which arise from PD, these include functional stereotaxic neurosurgery, physiotherapy, and dietary changes (Oertel & Schultz, 2016). These treatment options are not curative as it can only alleviate symptoms of the disease or impede the pathogenesis of the disease. In conclusion, there is a pressing demand for cost-effective and non-palliative therapies that can impede the advancement of AD and PD by preventing the degeneration of neurons with minimal or no adverse effects.

1.2. Alzheimer's disease pathology and molecular mechanisms

There are two fundamental neuropathological features distinguish AD; (a) the neurotoxic amyloid beta-42 ($A\beta_{42}$) peptide accumulation which results in the Aβ plaque formation, extracellularly (Xiao *et al.,* 2015) and (b) the hyper-phosphorylated tau aggregation of which produces intracellular neurofibrillary tangles (NFT), each of which result in the degradation of neural networks and cerebral tissue (Choi *et al*., 2014). Collectively, these factors cause the characteristic impairments of the behavioural and cognitive functions in those patients who suffer from AD (Serrano-Pozo *et al*., 2011).

Amyloid plaques are composed of the 4 kDa Aβ peptides, more specifically an isoform $A\beta_{42}$ (42 amino acid (aa)) product of proteolytic cleavage (Caetano *et al*., 2011). The Aβ peptide is generated through the cascade of the amyloidogenic pathway where the amyloid protein precursor (APP) is cleaved by γ-secretase and β-secretase (Choi *et al*., 2011). Firstly, the cleavage of APP is by β-secretase at the N-terminus releasing the secreted APPβ (sAPPβ) fragment. The process of Aβ shedding involves the cleavage of the C-terminal region of APP by γ-secretase, which results Aβ fragments being released into the extracellular space (Caetano *et al.,* 2011) (Figure 2). This process results in the formation of the Aβ oligomers, such as the isomers $A\beta_{40}$ and $A\beta_{42}$, each which are produced according to a specific cleavage pattern of APP (Selkoe, 1996). In normal physiological circumstances, the processing of APP occurs via the non-amyloidogenic pathway. In this pathway, α-secretase initiates cleavage of APP, producing APPsα (which inhibits the formation of Aβ). This is followed by γ-secretase cleavage, resulting in the creation of AICD (Figure 2). While the exact physiological roles of these substances are not entirely clear, some evidence suggests that APPsα functions in growth promotion and brain development. Furthermore, research has indicated that APPsα

may facilitate neurite growth, contribute to pro-survival pathways and enhance memory formation (Chow *et al.,* 2010). In contrast, the advancement of AD happens when the non-amyloidogenic pathway is disturbed, or when the degradation of $A\beta_{42}$ is reduced, leading to the formation of clumps that create neurotoxic plaques (Jarrett *et al*., 1993). The accumulation of the $A\beta_{42}$ peptides are favoured because they have a higher propensity to aggregate and is known to be more cytotoxic than the $A\beta_{42}$ isomer (Verdier & Penke, 2004). The accumulation of Aβ plaques enhances lipid oxidation and thereby oxidative stress which impairs the mitochondrial DNA (mtDNA) and induces mitochondrial dysfunction (Choi *et al*., 2014). Furthermore, the accumulation of the $A\beta_{42}$ peptides lead to the production of ROS initiating the intracellular oxidative damage potential (Sayre *et al*., 2000; Serrano-Pozo *et al.,* 2011). This leads to the ROS mediated mtDNA damage, mitochondrial dysfunction, and cytotoxicity (Mattson, 1997). Consequently, the formation of Aβ plaques induces oxidative stress thereby increasing cytotoxicity, senescence (permeant cell cycle arrest) and cell apoptosis (Stebbins *et al.*, 2009).

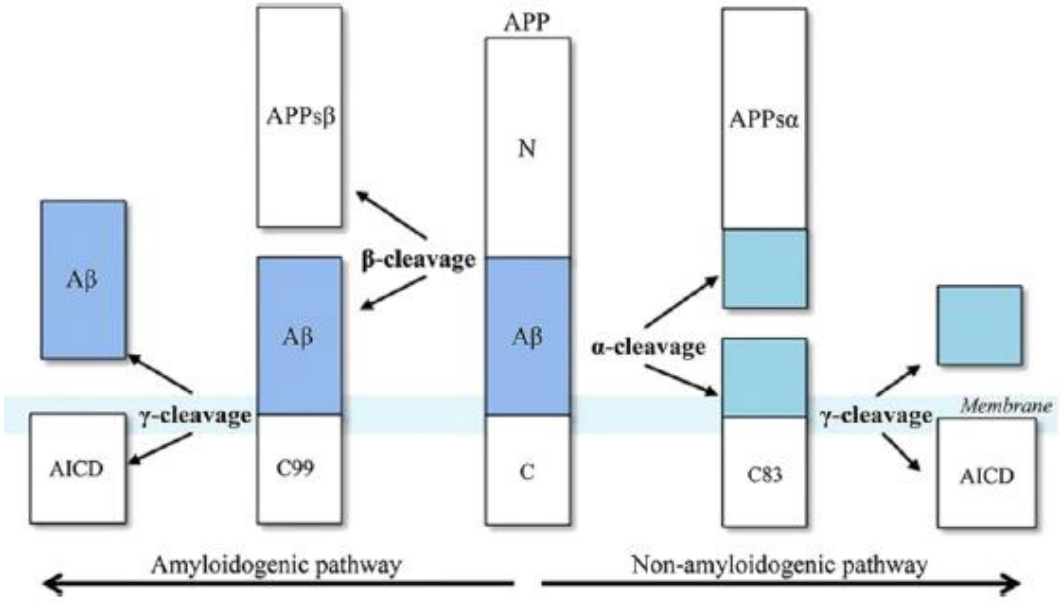

Figure 2: The two pathways of APP. *APP can be metabolised by the non-amyloidogenic and the amyloidogenic pathway. Under normal circumstances, APP is cleaved by α-secretase and by γ-secretase releasing sAPPα and p3. In the amyloidogenic pathway, the APP is cleaved by β-secretase and γ-secretase producing APPβ and AICD (Adapted from Menting and Claassen, 2014).*

On the other hand, the accumulation of NFTs is also associated with AD pathology, which consists of hyperphosphorylated and misfolded tau proteins (Choi *et al*., 2014). These

proteins have been found to increase the production of ROS, which results in neuronal dysfunction (Caetano *et al.,* 2011). Essentially, it is this relationship between Aβ, NFTs and ROS which mitigate mitochondrial dysfunction and ROS production (Avlia, 2006). Ultimately, these hallmarks enhance the accumulation and thus the oxidative damage potential of ROS which consequently induces senescence and apoptosis, thereby promoting the formation of cerebral lesions that further the progression of AD (Avlia, 2006).

1.3. Parkinson's disease pathology and molecular mechanisms

AD and PD are both defined as protein misfolding diseases and are characterised by the aggregates of protein deposits in the brain (Pimentel *et al.,* 2012). Specifically, PD is defined through the impairment of the dopamine-producing neurons which are found in the substantia nigra pars compacta (SNPc). The loss of these neurons are ultimately responsible for the altered motor behaviour of PD patients, which are resultant of organ shrinkage and the accumulation of Lewy bodies (Dauer & Przedborski, 2003). The progression of SNPc neural death is yet to be fully understood however is thought to be compromised by oxidative stress (OS), mitochondrial dysfunction, neuro-inflammation, and genetic alterations (Paillard *et al*., 2015) (Figure 3).

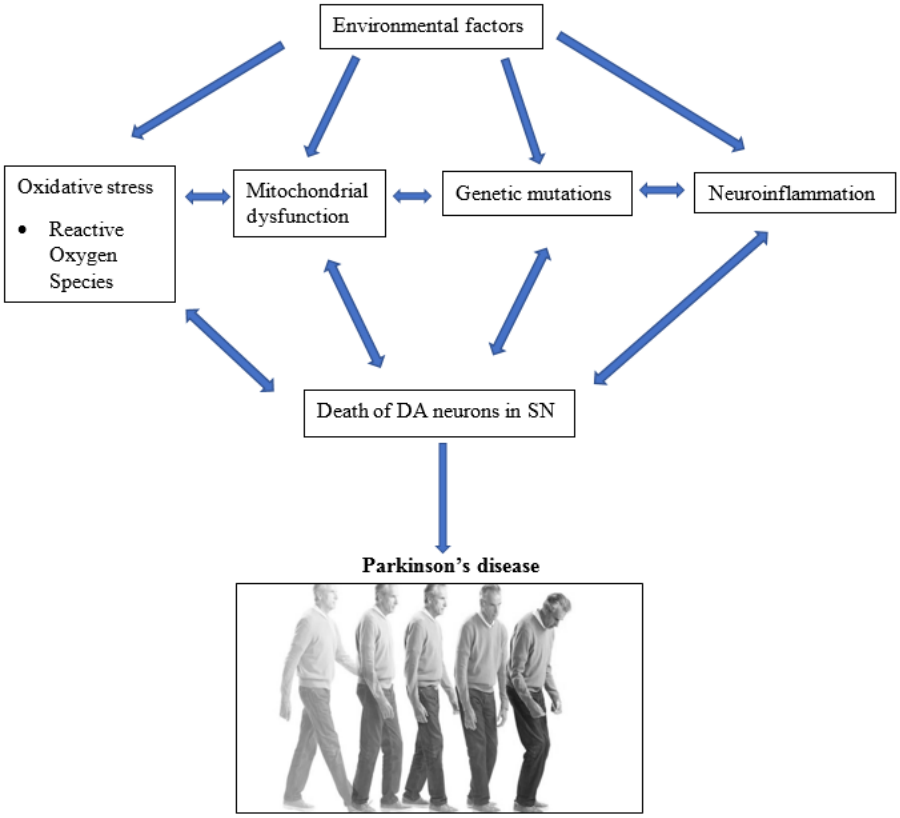

Figure 3: The potential factors which can attribute to the progression of Parkinson's disease. *Potential causes which may cause PD is environmental factors inducing oxidative stress, mitochondrial dysfunction and genetic mutations which contribute to the neural death of the SNPc dopaminergic neurons. (Paillard et al., 2015)*

Although the majority of PD cases occur intermittently, there are several cases which have linked gene mutations to the disease. It has been established that familial PD is caused by mutations in PD related genes such as α-synuclein and parkin (Yasuda & Mochizuki, 2010). Accordingly, α-synuclein is a presynaptic neuronal protein encoded by *SNCA*, and mutations in this gene form aggregations of α-synuclein which is a constituent of Lewy bodies (Moraitou *et al.*, 2011). Furthermore, α-synuclein is known to be intrinsically unstable and can natively unfold in aqueous solution, supporting that the protein has a high propensity for aggregation (Meade *et al*., 2019). The α-synuclein protein is composed of 140 amino acids and can be divided into three distinct domains the N-terminal domain (NTD), the hydrophobic core region - NAC (non Aβ-component) and the C-terminal domain (CTD) (Rodriguez *et al.,* 2015; Emamzadeh, 2016). The hydrophobic core domain of α-synuclein generates cross-β structures, which promote the formation of fibril aggregation (Meade *et al.,*

2019). Conversely, the acidic C-terminal end of α-synuclein interacts with the NAC region and is responsible for suppressing α-synuclein fibril aggregation (Emamzadeh, 2016). Mutations in the α-synuclein gene are known to generate the fibrillar form of α-synuclein, which is the primary component of Lewy bodies (LB). It is the fibrillar aggregation of Lewy bodies which disrupt the neurotransmitter transmission of dopamine which allows the onset of parkinsonism (Poulopoulos *et al.,* 2012).

Another protein which furthers the pathogenesis of PD is parkin which is a 465-residue ligase (Mizuno *et al.,* 2001). In normal circumstances, parkin plays a role in the covalent labelling of molecules with ubiquitin, which then undergo degradation in lysosomes and proteasomes (Song *et al*., 2016; Seirafi, 2015). The parkin protein can be divided into three domains, the N-terminal ubiquitin like domain (UBL), the in between RING finger domain (IBR), and the C-terminal RING domain (Van Coelln *et al,* 2004). Furthermore, parkin is responsible for the ubiquitin-mediated degradation of O-glycosylated forms of α-synuclein, and mutations in parkin have been linked to the aggregation of α-synuclein and the formation of Lewy bodies, which eventually contributes to the progression of Parkinson's disease (Shimura *et al*., 2000). Furthermore, the overexpression of parkin has shown to protect cells from α-synuclein induced aggregation. Furthermore, parkin has been shown to regulate mitochondrial integrity by interacting with the PTEN-induced putative kinase 1 (PINK1) protein (Bingol *et al.,* 2016). PINK1 is found on the mitochondrial surface, where it recognizes mitochondrial dysfunction and recruits' parkin from the cytoplasm to the mitochondria, thereby inducing mitophagy (Miklya *et al.,* 2014). As a result, parkin is an important protein with several neuroprotective functions, two of which are the regulation of dysfunctional mitochondria and the prevention of α-synuclein aggregation (Dawson & Dawson, 2010)

1.4. 37 kDa Laminin Receptor Precursor/ 67 kDa high affinity Laminin Receptor (LRP/LR)

Neurodegenerative diseases and cancer have been found to associated with the 37 kDa laminin receptor precursor/67 kDa high affinity laminin receptor (LRP/LR) (Da Costa Dias *et al.,* 2013). LRP/LR or namely, LamR is a type II transmembrane receptor containing two functional domains; extracellular C terminal domain and the globular intracellular N terminal (Zidane *et al*., 2012). It is mostly located in the area of the plasma membrane known as the lipid raft permitting a considerable number of interactions with the proteins found in the

extracellular matrix, but also has been found within the nucleus and cytoplasm (Mbazima *et al.,* 2010). As a result, due to the interactions between LRP/LR receptors in the areas surrounding cells, it attaches to various molecules, including laminin-1, elastin, heparin sulphate proteoglycans (HSPGs), and cellular prion proteins (PrP^c and PrP^{sc}) (Gauzynski *et al.,* 2006), and the AD-causing agent $A\beta_{42}$ (Jovanovic *et al*., 2013). Specifically, composed of 295 amino acid residues, the receptor contains multiple binding sites including two high affinity binding sites for laminin 1 (Otgaar *et al.*, 2017) (Fig. 4). Under normal conditions, LRP/LR plays part in cell growth, differentiation, migration, and adhesion which are vital for survival of cells (DiGiacomo & Meruelo, 2015; Omar *et al.,* 2012).

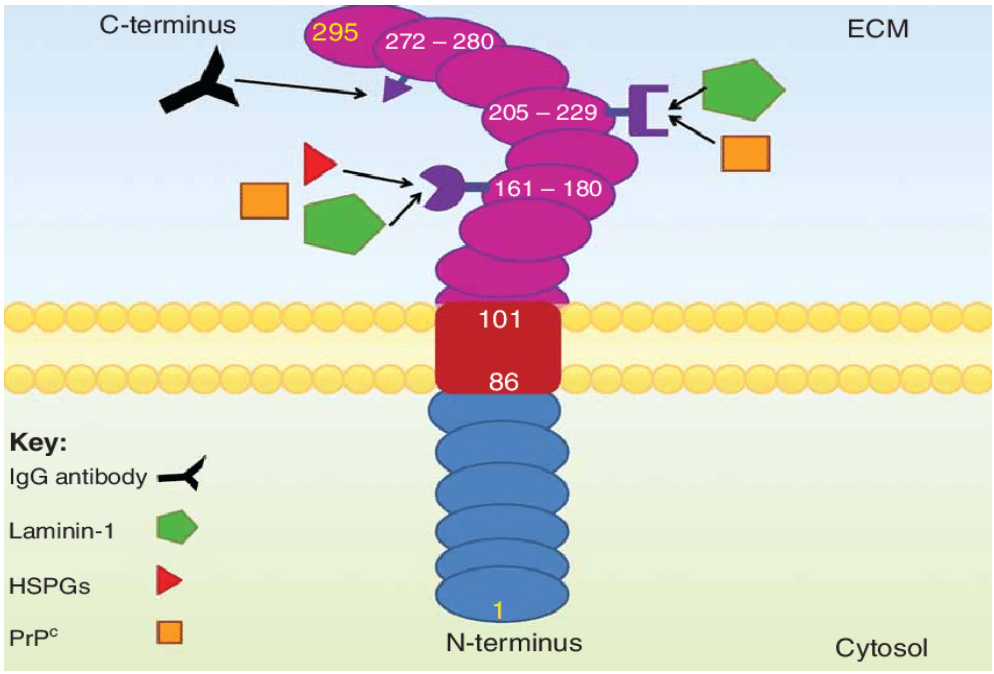

Figure 4: A schematic representation LRP/LR. *There are three sections to the receptor, namely the cytosolic N-terminal domain (coloured blue), the transmembrane domain (coloured red), and the ECM C-terminal domain (coloured purple). The C-terminus region of the receptor comprises binding sites for various substrates, including* PrP^c *and a peptide G-binding site. The latter serves as a binding location for laminin-1 and heparin. Both laminin-1 and* PrP^c *bind to the 209-229 aa site, while the IgG binding domain is found between the 272-280 aa region. (Image adopted from Jonanovic et al., 2015)*

1.4.1. Protein structure of LRP/LR

The first identified receptor of laminin was the non-integrin 67 kDa laminin receptor (LR) identified through laminin-1 binding (Lesot *et al.* 1983). The 67 kDa LR is assumed to arise

from the 37 kDa LR via post translational modifications, however, this is still poorly understood (Landowski *et al*., 1995). Previous efforts to sequence the 37 kDa LRP protein has been met with limited success attributed to the restricted capability to extract the protein in adequate amounts and with a high degree of purity (Wewer *et al.,* 1986). Furthermore, the amino acid composition of purified 67 kDa LR has been resolved, but efforts to further sequence the protein is absent from literature. LRP has been discovered to be targeted to the membrane at the cell surface by fatty acid acylation, and exists as both a monomer (37 kDa) and a dimer (67 kDa) (Butò *et al.,* 1998; Fatehullah *et al.,* 2010). Though they are both reported to bind laminin, the homodimeric and heterodimeric states of LRP have not yet been thoroughly resolved (Jamieson *et al.,* 2008). Despite the fact that the characterization of the interactions between LRP and laminin has not been definitively determined, some regions of the protein, such as residues 161-180 (peptide G) and residues 205-229, have been suggested as binding sites for laminin- (Castronovo *et al.,* 1991; Landowski *et al.,* 1995).

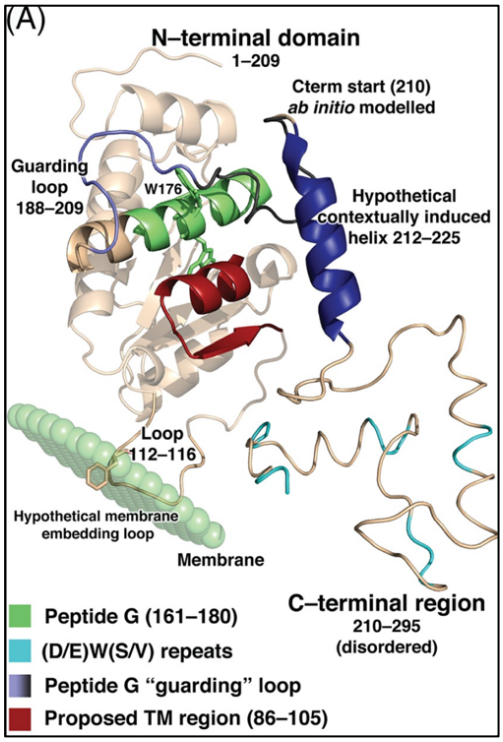

Figure 5: 37 kDa laminin receptor (full length). *Model showing the laminin binding sites: Peptide-G binding site (green), peptide 205-229 (blue) and transmembrane (TM) region (red) (Adapted from DiGiacomo et al., 2015)*

Analysing the structure of LRP/LR will help comprehend how the receptor associates with its binding partners, and it will support the development of treatments that can imitate or prevent

LRP/LR interactions in situations related to viral infections, neurodegenerative diseases, and cancer. The aa 9–205 were resolved in the crystal structure of the 37 kDa human LR (LAMR, 1-220) at resolution 2.15 Å (Jamieson *et al.,* 2008). According to the study, the globular NTD (aa 1-209) and composed of a central β-sheet surrounded by α-helices, whereas the CTD (aa 210-295) has been found to be intrinsically disordered as seen in far UV CD (Jameison *et al.,* 2008; Schlessinger *et al.,* 2009). The CTD consists of aspartic acid and glutamic residues, giving it a highly negative charge, particularly found in the 205-229 amino acid region which is assumed to be a laminin binding site (Jamieson *et al.,* 2008). Taken all together, the function and structure of LRP plays a definitive role in various disease pathogenesis, including AD.

1.4.2. LRP/LR role in diseases

It is especially important to note that LRP/LR interactions are linked many forms of diseases, including neurodegenerative diseases (prion disorders and AD), viral infections and various forms of cancer (Leucht *et al.,* 2003; Jovanovic *et al*., 2013; Jovanovic *et al.,* 2014; Naidoo *et al.*, 2015; Weiss *et al.,* 2017). LRP/LR has been discovered to be significantly overexpressed in cancer, which results in increased adhesion and invasion leading to metastasis. Additionally, it inhibits apoptosis and triggers angiogenesis, as evidenced by various studies (Zuber *et al.,* 2008; Omar *et al*., 2012; Moodley and Weiss., 2013; Khumalo *et al.,* 2013; Khusal *et al.,* 2013; Chetty *et al.*, 2014; Rebelo *et al.,* 2016; Vania *et al.,* 2016). Moreover, additional research has shown that LRP/LR plays a role in the aging process by interacting with telomerase, an enzyme that is recognized for hindering the aging process (Otgaar *et al*., 2017). Subsequently, studies have revealed overexpression LRP/LR overexpression enhances telomerase activity and thus, decrease senescence markers (Otgaar *et al.,* 2017).

Initially, LRP/LR is found to be involved in AD, through cell surface interaction with Aβ as well as the enhancement of the Aβ shedding, due to the interaction with APP, γ-secretase and β-secretase which are AD-related proteins (Jovanovic *et al.,* 2014). Studies have exhibited that LRP/LR and Aβ co-localise and that a receptor for $A\beta_{42}$ peptides could be LRP/LR (Da Costa Dias *et al.,* 2013). Studies have revealed that when IgG1-iS18 antibody and short hairpin RNA (shRNA) technologies were used to mediated LRP/LR blockade and downregulation, respectively, it was found that there was a significant reduction in Aβ shedding and cytotoxicity (Jovanovic *et al.,* 2013; Da Costa Dias *et al.,* 2013). Therefore, it

was established that LRP/LR is involved in the pathogenesis of AD which endorsed further study. Additionally, it was noticed that the interaction between LRP/LR and $A\beta_{42}$ on the surface of cells suppressed cell growth and caused apoptosis. This was demonstrated by the detection of apoptotic fragments after exposure to significant quantities of $A\beta_{42}$ (Da Costa Dias *et al.,* 2014). Subsequently, it was due to the involvement of LRP/LR in the $A\beta_{42}$ internalization which led to the accumulation of intercellular $A\beta_{42}$ and ultimately $A\beta_{42}$-related cytotoxicity (Jovanovic *et al.,* 2014; Da Costa Dias *et al.,* 2013). Furthermore, observations indicated that LRP/LR co-localises with AD related proteins (APP, γ-secretase and β-secretase) both inside and at the cell surface. However, treatment with the shRNA and IgG1-iS18 did not change APP, γ-secretase and β-secretase expression but rather reduced sAPPβ levels and release of the Aβ extracellularly. Interestingly, there was an indirect interaction between LRP/LR and β-secretase and a direct interaction with the catalytic subunit of γ-secretase which initiated APP cleavage thus releasing sAPPβ. Therefore, the downregulation of LRP/LR demonstrated β- and γ-secretase activity impediment thereby reducing sAPPβ and ultimately reducing Aβ shedding (Jovanovic *et al*, 2013).

Upon further investigation, Aβ shedding and intracellular $A\beta_{42}$ levels were significantly reduced in cells overexpressing LRP::FLAG and thus rescues cells from cytotoxicity mediated by Aβ (Bignoux *et al*., 2019) The study showed that the overexpression of LRP::FLAG increased hTERT expression which increased telomerase activity while decreasing intracellular $A\beta_{42}$ levels and shedding (Bignoux *et al.,* 2019). Cuttler *et al* demonstrated that LRP/LR and tau coexist in the perinuclear section of cells and verified that LRP/LR interacts directly with tau. The study also showed that overexpressing LRP::FLAG caused a reduction in phosphorylated tau levels, as well as a reduced PrP^{c} levels, a tauopathy linked protein (Cuttler *et al.,* 2020).

1.5. Telomerase in Alzheimer's and Parkinson's Disease

As mentioned earlier, LRP/LR plays a crucial role in age-related illnesses, and recent studies demonstrate that LRP/LR supports telomerase activity in both cancer and aging (Naidoo *et al.,* 2015; Otgaar *et al.,* 2017). Extensive research has established that cell viability is preserved through the telomerase-mediated maintenance of telomeres (Shay *et al.,* 2004). Telomeres are a segment of genetic material consisting of repeating sequence (TTAGGG) that are found at the ends of chromosomes. Their primary function is to protect the DNA

against fusion and deterioration of chromosomes. Telomeres are sustained by telomerase, a ribonucleoprotein enzyme that adds telomeric repeats to the ends of telomeres, enabling their maintenance (Cong *et al.,* 2002). The human telomerase comprises two units, the telomerase RNA component (TERC) subunit and the telomerase reverse transcriptase (TERT) subunit, that work together to produce telomeres in a 3' to 5' direction. (Nakamura & Cech, 1998) (Fig. 6). The activity of telomerase is crucial in both cellular senescence and the process of immortalization. Therefore, it holds great importance in both the aging process and the cancerous state (Shay & Wright, 2005). Cellular senescence occurs from cellular stresses such as telomere shortening, instability of the genome and mitochondrial disruption, which consequently disrupt tissue due to the replicative and regenerative limit of the cells (Molofksy *et al.,* 2006).

While telomerase primarily functions in extending telomeres, its catalytic subunit, hTERT, possesses additional cellular roles that are essential for maintaining cell viability (Ahmed *et al.,* 2008). Firstly, proteins which are involved in the Wnt pathway are activated by hTERT, regulating transcription and promoting cell replication (Cong & Shay, 2008). Additionally, hTERT plays a crucial role in protecting mitochondria (Ahmed *et al.,* 2008). It has been found that hTERT contains a signal peptide (20 aa) on its N terminal, which facilitates its mitochondrial translocation in response to increased ROS levels (Haendeler *et al*., 2009). Once in the mitochondria, the role that hTERT has is preventing cytochrome C release (inhibition of apoptosis) and prevents oxidative damage in mtDNA (Santos *et al.,* 2006; Zhang *et al.,* 2003).

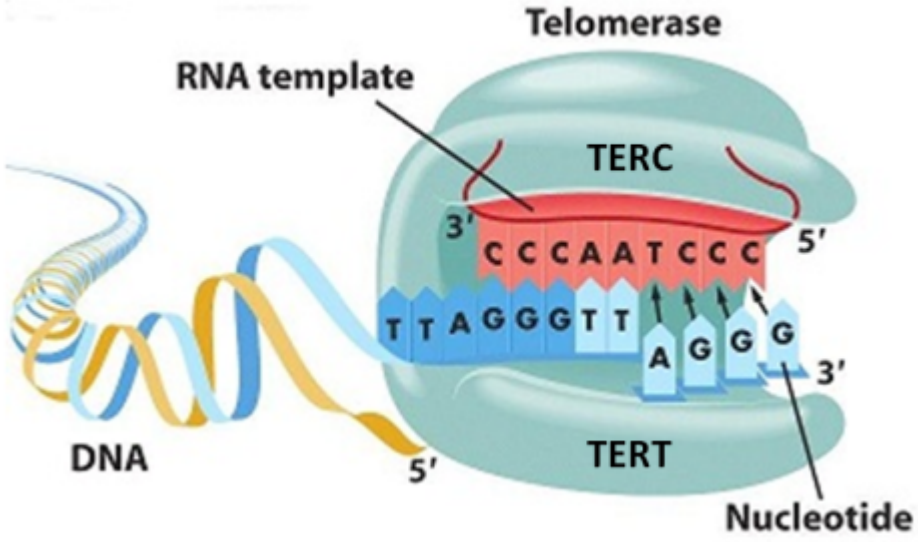

Figure 6: A schematic representation of the enzyme, telomerase, and two essential domains hTERC & hTERT. *Telomere elongation occurs when the TERT and TERC subunits catalyse the addition of TTAGGG repeats to the 3' end of the chromosome. (Adopted from Townley et al., 2014)*

Supporting evidence suggests that AD pathogenesis may be implicated by telomerase, which consequently results in the presence of short telomere lengths in the neural and T cells of AD sufferers (Franco *et al.,* 2006). Furthermore, it has been shown that ROS preferably binds to the guanine rich region of telomeric DNA resulting in telomere instability and reducing the binding of telomerase to telomeres ultimately leading to telomere shortening (Thomas *et al.,* 2008; Lee *et al*., 2017). Additionally, *in vitro* studies have shown that $A\beta_{42}$ inhibits telomerase activity, through direct binding of Aβ-peptides to the telomeric complex of DNA-RNA (Wang *et al.,* 2015). Therefore, this suggests that there is a conflicting association between Aβ and telomerase in nerve cells, and that telomere reduction plays a role in the development of Alzheimer's disease in individuals. Interestingly, it has been discovered that hTERT and LRP/LR interact for allowing cell survival.

LRP/LR and hTERT have been observed to interact and co-localize in perinuclear and at the cell surface. It has been found that downregulation of LRP/LR using small interfering RNAs (siRNAs) leads to a decrease in telomerase activity, and on the other hand, overexpression of LRP::FLAG is associated with an increase in hTERT expression, telomerase activity, and telomere lengthening, which ultimately protects cells from Aβ-induced apoptosis (Otgaar *et*

al., 2017). These findings suggest that increasing TERT and telomerase activity levels through LRP::FLAG overexpression could be a potential therapeutic strategy for AD.

The extent to which TERT is involved in PD has not been extensively researched, however, a recent study by Wan *et al* investigated the role of TERT expression in transgenic PD mice models. The results showed that when treated with telomerase activators, the total aggregated α-synuclein levels were significantly reduced in the hippocampus and neocortex of mice. This reduction was attributed to improved markers of autophagy, indicating better degradation of toxic α-synuclein. The study also concluded that increased TERT expression was linked to decreased α-synuclein protein levels, through activating autophagy thereby reducing the impairment degradation mechanisms during progression of the disease (Wan *et al.,* 2021). Furthermore, it was discovered that when cells were treated with a PD inducer, MPP, the overexpression of LRP::FLAG rescued cells from the MPP^+ induced cytotoxicity (Burns *et al., in preparation)*

1.6. PLGA nanoparticles as a drug delivery system

As previously stated, numerous studies have shown that the use of LRP::FLAG, specifically the *in vitro* overexpression of LRP/LR, impedes the pathogenesis of neurodegenerative diseases. For that reason, it is required to assess the effect of LRP/LR overexpression *in vivo.* Although the mammalian expression system offers suitable protein folding and post translational modifications, there are major limitations to using this method, including the high cost of production due to the slow cell growth, expensive media and transfection reagents, but more specifically delivery systems inability to cross the blood brain barrier (BBB) (Pardridge *et al*., 2012). The BBB protects the central nervous system (CNS) from substances and most biologics which contributes to the lack of progress in the treatment of CNS diseases including AD and PD (Li *et al.,* 2013). Therefore, a promising alternative is the use of polymeric nanoparticles as a delivery vehicle for drugs to the target tissue while regulating the rate and location of drug release.

A promising alternative to the regular drug delivery systems is the use of polymeric encapsulated nanoparticles. These serve as nanocarriers for macromolecular drugs. In recent years, nanoparticles have gained popularity for their applications in the field of medicine and molecular biology as a delivery system for small hydrophilic, hydrophobic drugs, and

biological macromolecules (Danhier *et al.,* 2012). These nanoparticles have four main benefits. First of all, cell membranes and the BBB can be bypassed by using nanoparticles with diameters between 1 to 1000 nm (Irving, 2007). Secondly, encapsulation allows for the protection from chemical and enzymatic breakdown, thus, extending their *in vivo* half-life (Mudshinge *et al.,* 2011). The particles' biodegradability, which enables a controlled release of the drug, is the third benefit. The fourth benefit is that the particles' surfaces can be modified to enable cell, tissue, and organ specificity, such as the addition of cell-specific ligands (Abhilash, 2010). Thus, a potential option for the encapsulation of the LRP protein are the biodegradable polymer matrix nanoparticles made up of polylactic-co-glycolic-acid (PLGA).

PLGA encompass all of the advantages mentioned above as they are FDA approved, highly stable and allow for controlled drug release to a disease localised site (Basarkar & Singh, 2007). PLGA has become increasingly popular due to its ability to break down into lactic acid and glycolic acid, which are natural metabolites that can be easily processed by the body via the tricarboxylic acid (TCA) cycle (Krebs cycle) and released water and carbon dioxide, therefore resulting in a minimal systemic toxicity (Semete *et al.,* 2010). There are many methods of nanoparticle preparation, and depending on the method the structural organisation differs. The drug is either entrapped within the core of the nano capsule or entrapped on the surface of the nanosphere matrix (Barratt, 2000; Couvrar *et al.,* 1995). The primary technique employed to create PLGA nanoparticles is the process of single or double-emulsion-solvent evaporation. In the single-emulsion method, an oil in water (o/w) emulsion is used for water insoluble (hydrophobic) drugs such as steroids, whereas, in the double emulsion method a water in oil in water (w/o/w) method is used and suited for water soluble (hydrophilic) drugs such as proteins (Garti *et al.,*1998) (Figure 7). Briefly, PLGA is added into an organic phase which is emulsified with water, the drug is either directly added to the oil phase (hydrophobic drugs) or can be initially emulsified with the polymer (hydrophilic drugs) before the formation of nanoparticles (Perez-Moral *et al.,* 2014).

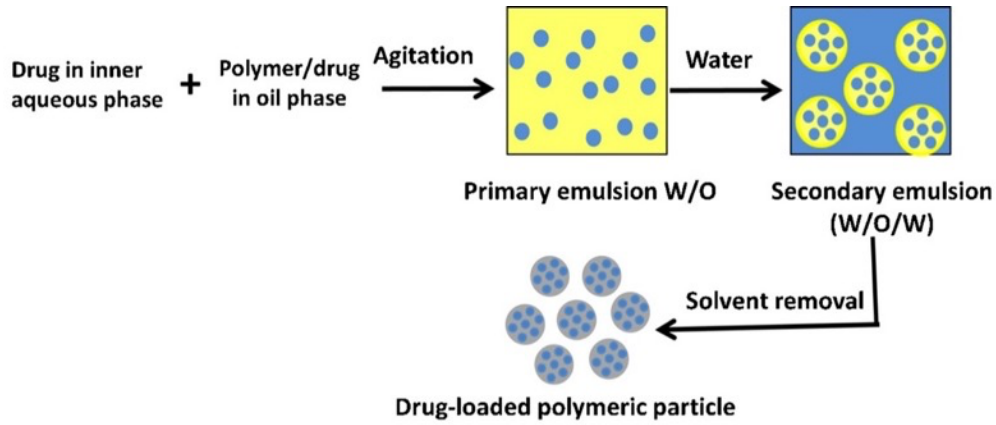

Figure 7: A schematic representation of the double emulsion technique (Adapted from Iqbal et al., 2015)

Ultimately, the PLGA nanoparticles used as a delivery vehicle for LRP, would be prepared by the double emulsion method and would require nanoparticles to be smooth, round, hollow and within 250-500 nm in size.

2. Rationale

AD and PD progressive neurodegenerative disorders affecting globally over 50 million and 10 million patients, respectively. Due to the high occurrence and economic burden of these diseases there is a need for non-palliative therapeutic strategies, as only palliative treatments are available. It has been discovered that LRP/LR contributes to the prevention of AD and PD. *In vitro* studies have demonstrated that the overexpression of LRP::FLAG impedes Aβ shedding, reduces intracellular $A\beta_{42}$ levels thus rescuing cells from Aβ-mediated cytotoxicity. Furthermore, the overexpression of LRP::FLAG has been found to increase hTERT expression which concurrently decreased telomerase activity while decreasing intracellular $A\beta_{42}$ levels and shedding. Cuttler *et al*. demonstrated that LRP/LR and tau co-localize and interact directly. They also found that overexpression of LRP:FLAG led to a decrease in total and phosphorylated tau levels, as well as a decrease in PrP^{c} levels, a protein related to tauopathies. Within PD, *in vitro* studies demonstrated that LRP/LR plays a protective role in PD, likely through the degradation of α-synuclein and by increasing cell viability and the MMP of cells treated with the PD-inducer, MPP^{+}. As demonstrated, the use of LRP::FLAG, specifically the *in vitro* overexpression of LRP/LR, impedes the progression

of these neurodegenerative diseases. For that reason, it is required to assess the effect of LRP/LR overexpression *in vivo.*

Therefore, the present study was divided into three parts, with the initial part focusing on exploring the impact of LRP::FLAG overexpression in HEK293 cells. This was done to determine whether the overexpression of LRP plays an important role in both AD and PD, and if targeting LRP/LR can provide a novel and potentially effective strategy for these diseases. The overexpression of LRP::FLAG assessed LRP and PINK1 protein levels by western blotting, as well as the resultant effect on cell viability after treatment with MPP^+, TBHP, and $A\beta_{42}$ by MTT analysis. However, the translation of this research to an *in vivo* investigation required isolated 37 kDa LRP and an effective delivery system. Thus, the second part of the study focused on successfully overexpressing and purifying the 37 kDa (1-295 residue) LR protein, to produce large amount of the isolated therapeutic protein for PLGA nanoparticle encapsulation. This also involved the structural characterisation of the 37 kDa LRP through ITF and far UV CD which assessed the structural integrity of the protein. Lastly, the third part of the study focused on assessing the use of PLGA nanoparticles as a potential delivery system for the LRP-encapsulated nanoparticles. This involved investigating the effect of the empty and LRP encapsulated nanoparticles on cell viability, LRP levels, and telomerase activity in HEK293 and SH-SY5Y cells.

3. Aims and Objectives

3.1. Aims

3.1.1. Aim 1: To assess the effect of LRP::FLAG in Parkinson's and Alzheimer's disease cell culture models

3.1.2. Aim 2: To purify and characterise LRP protein for the downstream application of encapsulating in PLGA nanoparticles

3.1.3. Aim 3: To investigate the effect of treatment with exogenous LRP encapsulated in PLGA nanoparticles in Parkinson's and Alzheimer's disease cell culture models

3.2. Objectives

3.2.1. Aim 1

a. To overexpress LRP::FLAG and to determine whether LRP::FLAG overexpression affects LRP and PINK-1 protein levels in HEK293 cells

b. To investigate the effect of LRP::FLAG overexpression on cell viability in Alzheimer's like-state $A\beta_{42}$ and TBHP treated HEK293 cells

c. To investigate the effect of LRP::FLAG overexpression on cell viability in Parkinson's-like state MPP^+ treated HEK293 cells

3.2.2. Aim 2

a. To optimise the overexpression of hLRP protein in T7 Express pLysS competent *E.coli* cells

b. To scale-up hLRP solubilisation using the 0.5% Triton X-100 detergent

c. To purify the hLRP protein using immobilized metal ion affinity chromatography

d. To characterise the structure of hLRP through intrinsic tryptophan fluorescence and far UV circular dichroism

3.2.3. Aim 3

a. To optimise the production of empty and LRP encapsulated PLGA nanoparticles

b. To assess the effect of empty and LRP (1-5% (v/v)) encapsulated PLGA nanoparticles on cytotoxicity and LRP protein levels in SH-SY5Y cells

c. To investigate the effect of treatment with empty and LRP (1-10% (v/v)) encapsulated nanoparticles on cell viability in SH-SY5Y cells

d. To assess the effect of empty and LRP (1-5% (v/v)) encapsulated PLGA nanoparticles on telomerase activity in SH-SY5Y cells

4. Methods and Materials

4.1. LRP Protein Production and Purification

This study was performed using the LRP protein (295 amino acid residues) containing both laminin binding sites. A pure and soluble form of the protein was required to perform the downstream experiments of the study.

4.1.1. Plasmid and Protein construct

The gene sequence of the full length of the LRP protein (residues 1-295) was constructed and inserted into a pET-11a plasmid (GenScript, USA). The LRP gene sequence contained a Hexahistidine-tag (His-tag). The His-tag were used to facilitate the downstream purification by immobilized metal-ion affinity chromatography (IMAC).

Plasmids are circular, dsDNA molecules found naturally in yeast and bacteria that replicate independently from the cell's DNA. Multiple copies of the plasmid are produced during DNA replication, which occurs prior to each cell division, ensuring continuous propagation through successive host cell generations (Esser *et al.,* 1986). Plasmids are inexpensive, easy to use, and stable, making them ideal for producing a large amount of protein in a short period of time. Plasmids' circular nature may limit insert size and make them unsuitable for longer sequences (Rosano and Ceccarelli, 2014). The pET-11a plasmid used was 5.7 kb long, while the gene that was inserted was 295 bp long, which made it appropriate for the study.

The T7 Express pLysS Competent *E.coli* cells (New England Biolabs, USA) were transformed using the pET-11a LRP plasmid. Using the T7 lac promoter in bacteria, this vector expression system generates a high level of heterologous protein (Briand *et al.,* 2016). The T7lac promoter cassette includes a T7 promoter and a T7 terminator, as well as the lac operon and a ribosomal binding site. The T7 promoter initiates a high level of gene expression if the T7 RNA is present. The pET-11a plasmid also includes a pBR322 replication origin, which allows for a high plasmid copy number while also reducing leaky protein expression in the absence of an inducer. The AmpR gene provides bacteria with ampicillin resistance by encoding the β-lactamase enzyme, which is required to degrade the β-lactam ring in ampicillin, allowing for bacterial selection after transformation (Neu, 1969).

Plasmids can replicate independently within the host cell; however, the host cell replication machinery, polymerases, are required to promote plasmid replication. Bacteria are frequently used as plasmid expression vectors because they replicate quickly, resulting in the production of many plasmids and thus increased protein production (Rosano *et al.,* 2016). Furthermore, the T7 RNA polymerase required to initiate transcription of the T7 promoter is coded for in the host cell by the *T7 RNA polymerase* gene under the control of the LacUV6 promoter, which is induced by a non-hydrolysable allolactose analogue, isopropyl β-d-1-thiogalactopyranoside (IPTG) (Gomes, 2020).

Additionally, the lac repressor protein is encoded by the *LacI* gene, and functions to bind and block expression of the *lacO* gene, preventing leaky basal expression of LRP in the absence of IPTG. Furthermore, the lac repressor protein binds to and inhibits the lacUV5 promoter in the host-cell thereby blocking the transcription of the T7 RNA polymerase in the absence of IPTG. Once IPTG is added, it aids in blocking the inhibitory action of the lac repressor, thereby promoting the expression of the T7 RNA polymerase in the host-cell, as well as preventing lac repressor inhibition in the gene of interest within the plasmid (Tan *et al.,* 2012).

4.1.2. Transformation

Using the heat shock method, the pET-11a plasmid, containing the LRP insert was used to transform the T7 Express Competent *E.coli* cells. Initially, the competent *E.coli* cells was thawed for 15 minutes on ice. Transformation was initiated by adding 2 µl of the plasmid (50 ng/µl) which was incubated with 50 µl of cells and was placed on ice for 30 minutes allowing for stabilization of the lipid membranes in the cells. Thereafter, cells were heat shocked for at $42°C$ for 45 seconds and incubated for 5 minutes on ice. When cells are exposed to higher temperatures, the kinetic energy of the molecules in the fluid membrane increases, destabilizing it. This makes the cells more permeable to the plasmid. Therefore, lowering the temperature after the cells were heat shocked allows for the cells to recover. The pellet was resuspended in 1ml of prewarmed ($37°C$) sterile Super Optimal broth with Catabolite repression (SOC) media (0.5% (w/v) yeast extract, 2% (w/v) tryptone, 10 mM NaCl, 10 mM $MgCl_2$, 20 mM glucose, and 2.5 mM KCl). SOC media allows for cell recovery following the heat shock-induced stress. Thereafter, the transformed cells were grown for 1 hour at $37°C$, while shaking at 230 rpm for aeration.

Following cell growth, the cells were spread onto freshly prepared sterile Luria Broth (LB)-agar (0.5% (w/v) yeast extract, 1% (w/v) tryptone, 1.5% (w/v) agar, and 1% (w/v) NaCl) plates, supplemented with 0.1 mg/ml ampicillin (Melford, UK) used to select for a successful transformation. Incubation of the LB agar plates were at 37°C for 19 hours. To ensure there were no contamination, spread plates of SOC medium, LB agar and untransformed *E.coli* cells were prepared. Once cells were transformed, an isolated colony was picked and used to inoculate into 100 ml of fresh sterile 2x Yeast extract-Tryptone (YT) media (1% (w/v) yeast extract, 1.6% (w/v) tryptone, and 0.5% (w/v) NaCl) containing 0.1 mg/mL ampicillin. Supplementation of ampicillin is added for the prevention of growth of any untransformed cells, as well as for contamination prevention. Additionally, an isolated small colony was picked to ensure cells were genetically identical. The cell culture was then grown at 37°C for 16 hours, while shaking at 180-190 rpm to ensure aeration.

Glycerol stocks (1 ml) were prepared by mixing this culture with 80% sterile glycerol (v/v) at 1:1 ratio. The stocks were snap frozen in liquid nitrogen and placed at -80°C for storage. The culture was also used to isolate the pET-11a plasmid, containing the LRP insert using GeneJET plasmid mini-prep kit (Thermo Fisher Scientific, USA), as per suggested protocol. The purpose of this kit is to efficiently and affordably extract plasmid DNA from recombinant *E.coli* cultures in a small quantity. The kit utilizes a unique spin column, which is composed of a silica-based membrane technology. The plasmids (100 ng/µl) were sent for sequencing (Inqaba Biotechnical Industries, RSA) to ensure LRP gene integrity.

4.1.3. Protein expression

Following bacterial transformation with the pET-11a plasmid containing the LRP insert, the 37 kDa LRP protein was produced by heterologous protein overexpression in T7 Express pLysS competent *E.coli* cells. This was performed to ensure that enough protein was produced for the downstream applications of this project. Glycerol stocks (1 ml) were used in a 1 in 1000 dilution to inoculate freshly prepared, sterile 2x YT media which contained 0.1 mg/mL ampicillin. The prepared culture was grown at 37°C overnight, while shaking at 180-195 rpm which allowed for aeration and growth. Thereafter, a large volume of freshly prepared 2x YT media with 0.1 mg/ml ampicillin was inoculated in a 1 in 50 dilution of the overnight culture. Thereafter, cells were grown until an OD_{600} of 0.6 AU was reached, which

indicated that the *E.coli* cells were in the exponential phase of growth, which is optimal for the induction of heterologous expression. Once the OD_{600} was obtained, the culture was cold-shocked on ice for 30 minutes. Thereafter, overexpression was induced using 0.3 mM IPTG (Melford, UK). IPTG effectively turns the lacUV5 promoter on which induces protein expression. Cold shocking the cells allowed for the rate of protein synthesis to be lowered, resulting in soluble and functionally folded protein. The cells were then incubated at $20°C$ for 20 hours, while shaking a 230 rpm. The temperature was reduced to $20°C$ as it decreased the rate of protein folding, thereby reducing the possibility of obtaining nonfunctional and misfolded protein. Following incubation, cells were pelleted by centrifugation (5000 xg for 30 minutes at $4°C$) and resuspended in 50 ml of equilibration buffer. Resuspended cell lysates were stored at -$20°C$.

4.1.4. Purification

Cell lysis was performed to successfully isolate protein from the cell lysate. The cell lysates were thawed up at $20°C$, after which, 0.1 mg/ml lysozyme (Sigma-Aldrich, USA) and 1 mM phenylmethylsulphonyl fluoride (PMSF) (Roche, Germany) were added. Lysozyme was used to cleave the peptidoglycan component of gram-positive cell walls, allowing them to rupture. PMSF is a serine protease inhibitor that is commonly used to prevent protease-mediated proteolytic degradation of overexpressed proteins. After adding lysozyme and PMSF, the mixture was incubated and slowly inverted for 30 minutes at $20°C$. Thereafter, the lysate was incubated with 0.01 mg/ml DNase 1 (Merk, Germany) at $20°C$ for 30 minutes. DNase 1 was added to the bacterial DNA fragments to prevent DNA contamination in downstream applications and to reduce solution viscosity. Centrifugation (18 000 xg for 30 minutes at $4°C$) was used to separate the soluble and insoluble fractions of the lysates. The supernatant was then filtered through a 0.45 µm filter to remove insoluble matter before being used in the subsequent purification steps.

4.1.4.1. Immobilized metal-ion affinity chromatography (IMAC)

IMAC is a purification technique commonly used to purify proteins which are fused to a short affinity peptide tag. IMAC relies on the interaction between multiple electron donors found on the tag with a transition metal cation such as Co^{2+}, Ni^{2+}, Cu^{2+}, Zn^{2+} bound to the solid phase support (Sepharose) (Falke *et al.,* 2013). A chelating agent such as iminodiacetic acid (IDA) is covalently bound to the solid phase support and is used to entrap the metal ions.

The affinity tag is a polyhistidine (6-12 residues) fused to either the N or C terminus of the protein, the most common form is the 6-His where the electron donor is the histidine imidazole ring. Since the LRP protein was fused with a His-tag, it was purified from the soluble crude cell lysate by IMAC. The protein was eluted using a high concentration of imidazole which competes for the metal ions with the histidine residues therefore displacing the protein from the IDA ligand (Falke *et al.,* 2013).

The LRP protein was purified on a 5 ml IMAC column (1.6 x 2.5 cm His Trap column (GE Healthcare, USA) attached to the ÄKTA Prime Liquid Purification System (GE Healthcare, USA) (Flow rate of 5 ml/minutes and pressure limit of 0.3 MPa). The column was packed with Sepharose, used the IDA ligand and was charged with either Ni^{2+} or Co^{2+} ions.

Initially, 10 column volumes of equilibration buffer were used to equilibrate the IMAC column which ensured that the protein molecules interacted with the ligand. Subsequently, the column was loaded with 50 ml of filtered (0.45 µm) supernatant the flow through was collected. Thereafter, a salt wash (1.5 M NaCl, 30 mM imidazole and 20 mM tris-HCl, pH 7.5) was carried out by passing 5 column volumes through the column (and collected). A high concentration of salt is used to remove any DNA contamination while removing non-specific proteins bound to the column. Thereafter, the column was re-equilibrated with equilibration buffer (10 column volumes). The His-Tagged LRP was then eluted from the column using elution buffer (5 column volumes) (500 mM NaCl, 300 mM imidazole and, 20 mM tris-HCl, pH 7.5) and collected.

4.1.5. Protein concentration and purity

4.1.5.1. SDS-PAGE

Smith *et al*. (1984) explained that Sodium Dodecyl Sulphate Polyacrylamide Gel Electrophoresis (SDS-PAGE) is employed to segregate proteins based on their molecular size. In this technique, SDS is utilized as a negatively charged denaturing detergent that binds to the protein's backbone, prompting the protein to unravel into primary chains and producing a net negative charge that is proportional to the protein's molecular weight. The protein mixture is then placed on a porous acrylamide gel that is prepared at various concentrations. The concentration of the gel is inversely proportional to the protein size. The proteins move through the gel in response to an electric field, migrating from the cathode

(negative terminal) to the anode (positive terminal) of the electric field (Smith *et al.,* 1984). Proteins do not have a constant charge to mass ratio, hence, they need to be linearised and coated with a uniform charge. The protein samples are reduced with β-mercaptoethanol and denatured by heat. The discontinuous buffer system has provided great resolution and consists of a stacking gel on top of a separating gel. In the stacking gel (pH 6.8) the large, negative chloride ions migrate at a fast rate due to their high ionic charge, followed by the negatively charged protein and the positive glycinate ions. Whereas, in the separating gel (pH 8.8), the glycinate ions migrate ahead of the protein due to their large negative charged creating a uniform electric field for the proteins to migrate in based on their molecular size.

SDS-PAGE was used to identify contaminates and to determine the size of the LRP protein. The size of the protein was predicted to be ≈ 37 kDa based on the sequence. Initially, samples were prepared by diluting the protein into reducing sample buffer (4% (w/v) SDS, 125 mM tris-HCl (pH 6.8), 20% (v/v) glycerol, 3.5 µg/ml bromophenol blue and, 10% (v/v) β-mercaptoethanol) and heating the sample at $95°C$ for 5 minutes. This ensured that the protein sample was denatured, linearized and in a uniform negative charge.

SDS-PAGE was performed using the Bio-Rad Mini Protean™ Tetra Cell electrophoresis system (Bio Rad Laboratories, USA). Once the gel plates were setup, 12.5% acrylamide separating gel (12.5% (w/v) acrylamide, 1.08% (w/v) bis-acrylamide, 250 mM tris-HCl (pH 8.8), 0.1% (w/v) SDS, 0.2% (v/v) TEMED and, 0.05% (w/v) ammonium persulfate) was prepared and poured. Once it had polymerised, a 4% acrylamide stacking gel (4% (w/v) acrylamide, 0.36% (w/v) bis-acrylamide, 50 mM tris-HCl (pH 6.8), 0.1% (w/v) SDS, 0.2% (v/v) TEMED and, 0.005% ammonium persulfate) was prepared and poured. A 10-well comb was inserted into the stacking gel after it was poured. Once polymerization had occurred, the gels were placed into the electrophoresis tank containing the SDS-PAGE electrophoresis buffer (250 mM tris-HCl pH 8.3, 192 mM glycine and, 0.1% (w/v) SDS).

The samples were then loaded into each well (10 µl) and electrophoresis was carried out at 120 V until the dye front reached the 1 cm from the bottom of the gel. Gels were carefully removed and stained with Coomassie stain solution (0.1% (w/v) Coomassie Brilliant Blue R-250 in 1:5:4 (v/v/v) acetic acid:methanol:water) for 3 hours. Subsequently, destain solution (1:5:4 (v/v/v) acetic acid:methanol:water) was added to the gels for 24 hours. The unknown

molecular weight of the samples were calculated relative to the migration of the proteins in the BLUeye Prestain protein Ladder (Merck, Germany). Protein purity was assessed through densitometric analysis and protein samples that were at least 85% pure were used for the downstream experiments.

4.1.6. Protein characterisation

4.1.6.1. Absorbance spectroscopy

Due to tyrosine, tryptophan, and phenylalanine (aromatic) amino acid residues, proteins absorb light at 280 nm (A_{280}). Therefore, A_{280} is quantitively used to determine protein concentration using the Beer-Lambert law. Additionally, nucleic acids are known to absorb light at 260 nm (A_{260}) due to the resonance structure in purine and pyrimidine bases, therefore the 260 nm absorbance is used to detect nucleic acid contamination. Thus, $A_{280/260}$ is used as an indicator for the amount of nucleic acid contamination in a purified protein ($\geq$1.8).

Briefly, absorbance spectroscopy was used to determine the protein concentration, as well as to quantify contamination. Initially, the protein was centrifuged (13 200 rpm for 15 minutes, at 4°C) to remove any aggregation. Using a Jasco V630 spectrophotometer (Jasco, USA), the absorbance spectrum was obtained from 240 to 340 nm, in triplicate with 3 biological repeats. The resultant A_{280} was used to calculate the molar concentration of the protein according to the Beer lambert law

$$c = \frac{A_{280}}{\varepsilon \cdot \ell}$$

c *is the protein concentration* (M), A_{280} *is the corrected absorbance at* 280 *nm,* ε *is the molar extinction coefficient at* 280 *nm and* ℓ *is path length* (cm)

The molar coefficient is the sum of the aromatic contributions of all the aromatic amino acids present in the protein and was predicted to be 67045 $M^{-1}.cm^{-1}$ for LRP protein.

4.1.6.2. Circular Dichroism (CD) Spectroscopy

CD is a method used in absorption spectroscopy based on the unequal absorption of left and right circularly polarized light. Optically active chiral molecules absorb one of the directions of circularly polarized light, and it is possible to quantify the disparity in absorption between the left and right circularly polarized light. UV CD is commonly used to determine aspects of the secondary structure in a protein (Li *et al.,* 2011). CD is typically reported as a difference between the absorbance of E_L and $E_R(\Delta E)$ by an asymmetrical molecule and can be expressed as degrees of ellipticity. For proteins, the ΔE is representative of the secondary structure composition when measured in the far UV range, producing a distinct CD-spectra for different secondary structural features found in proteins. The far-UV CD spectrum of α-helical protein has troughs at 208 nm and 222 nm, and a peak at around 190 nm. Whereas, in β-sheeted protein there is a trough at 218 nm and a peak at 195 nm (Greenfield, 2006).

Far UV CD spectropolarimetry was used to characterize the secondary structure of the LRP protein. This was done to confirm that the protein was predominantly α-helical as expected, which would indicate that the protein is correctly folded. The far-UV CD spectra were obtained from 200-250 nm, in triplicates, on the Jasco J-1500 spectropolarimeter (Jasco, USA). Each replicate was averaged from 10 accumulations. The spectra were obtained using a bandwidth of 5 nm, a scanning spread of 200 nm/minute and a path length of 2 mm (20°C). The protein sample consisted of 10 µM of protein, diluted five times with Milli-Q® water such that the final NaCl concentration was only 20 mM (to minimize background noise caused by the presence of chloride ions). The average spectrum of the samples was corrected by subtracting the spectrum of the buffer. The signal of the far UV was obtained in millidegrees (mdeg) and normalised to mean residue ellipticity using;

$$\theta_{MRE} = \frac{\theta\ (mdeg)\ \times\ 10^6}{\ell \cdot C\ \cdot n}$$

θ_{MRE} *is the mean residue ellipiticity* $(deg.cm^2.dmol^{-1})$, $\theta\ (mdeg)$ *is the recorded signal,* ℓ *is the path length* (mm), C *is the protein concentration* (µM) and
n is the number of peptide bonds in the protein backbone

4.1.6.3. Intrinsic tryptophan fluorescence (ITF) spectroscopy

Tryptophan, tyrosine, phenylalanine, and cysteine amino acids act as fluorophores and exhibit an intrinsic fluorescence in proteins. Specifically, tryptophan contributes significantly to fluorescence as it has a high quantum yield as compared to tyrosine, and can be selectively excited at 295 nm (Ghisaidoobe *et al.,* 2005). ITF is commonly used as a probe to assess the tertiary structure of a protein due to the indole group of tryptophan which is solvatochromic, meaning that the emission wavelength is dependent on the polarity of its environment. When the tryptophan residues are buried within the protein core, a blue shift in the fluorescence emission occurs (hypochromic) due to the decreased tryptophan exposure to the polar solvent. Whereas, when the tryptophan residues are exposed to the polar solvent (unfolded protein), a red shift occurs in the fluorescence emission (bathochromic) (Royer, 1995).

ITF spectroscopy was utilised to determine if the LRP protein is folded correctly. The spectra was obtained both in the presence and absence of denaturants (8 M Urea), which allowed for comparisons between the native and unfolded protein. Initially, samples were incubated with the allocated denaturant for 2 hours, at $20°C$. On the Jasco FP-6300 spectrofluorometer (Jasco, USA), using the excitation wavelength of 280 and 295 nm, the emission spectra were obtained from 280 – 350 nm, in triplicates. The spectra were obtained at $20°C$ using excitation and emission bandwidths of 5 and 2.5 nm, a scanning speed of 200 nm/minute and a path length of 1 cm. In the absence of a denaturant, the sample consisted of 2 µM of protein, while in the presence of the denaturant, the sample contained 2 µM protein and 8 M Urea. Both samples were normalised by subtracting the spectrum of the buffer. Thereafter, the data was corrected by dividing the corrected fluorescence intensity value by the maximum fluorescence intensity value of the protein.

4.2. LRP encapsulated nanoparticle production and *in vitro* studies

4.2.1. LRP encapsulated PLGA Nanoparticle production

The purified 37 kDa LRP protein was encapsulated using PLGA nanoparticle technology. PLGA is the most popular and well-known polymer for controlled release drug delivery systems because of its biocompatibility, biodegradability, and mechanical strength (Kumari *et al.,* 2010; Makadia *et al.,* 2011). There are multiple methods used to prepare nanoparticles, the drug can either be trapped within the core or entrapped on the surface of the matrix. The

double-emulsion-evaporation method is utilised for the encapsulation of hydrophilic drugs such as nucleic acids and proteins whereas the single emulsion technique is suitable for hydrophobic drugs such as steroids. In this study, the single emulsion technique was not performed with the LRP protein since it is hydrophilic and will result in the LRP diffuse into the aqueous solution before encapsulation (McCall *et al.,* 2013).

In preparation, glass test tubes were marked at the 1 ml level, a polymer solution was prepared with 100 mg of PLGA dissolved in 1 ml of ethyl acetate. The test tubes were tightly sealed and incubated overnight at room temperature. Due to the high evaporation rate of ethyl acetate, the 1 ml level was monitored, and the solvent was replaced if lost. Emulsification of LRP with the polymer solution was prepared by adding 700 ug/µl of LRP protein into the polymer solution. The drug was emulsified with the polymer until a homogenous, opaque solution was achieved. Subsequently, 50 ml of 0.3% (w/v) Vitamin E-TPGS was prepared, and 4 ml of the solution was added to a new 50 ml centrifuge tube. The tube was vortexed, and the polymer solution was added in a dropwise manner using a glass Pasteur pipette. Once added, the emulsion solution was vortexed for an additional 15 seconds and thereafter sonicated on ice (3x for 10 seconds at 40% amplitude) with a 700 W probe sonicator. Subsequently, 45 ml of the 0.3% Vitamin E-TPGS solution was added to a 100 ml beaker and placed on a magnetic stirrer. The emulsion solution was added into the stirring Vitamin E-TPGS solution and incubated 3-4 hours at room temperature. The emulsion solution was partially covered with foil to ensure evaporation of the ethyl acetate. After 3-4 hours, the emulsion solution was left overnight at $4°C$ allowing the nanoparticles to harden.

Thereafter, the nanoparticles were purified to collect uniform and smaller particles of the PLGA particles. Initially, the larger nanoparticles were separated out by low centrifugation (8 000 xg for 10 minutes) and the supernatant (containing smaller nanoparticles) was transferred into 1.5 ml Eppendorf tubes. The smaller nanoparticles were purified out by high centrifugation (17 000 xg for 15 minutes) and the clear supernatant was discarded. The nanoparticles were washed by resuspending the pellet in 200 µl dH_2O using a water bath sonicator. Thereafter, the solution was centrifuged (17 000 xg for 15 minutes) and the clear supernatant was discarded, this step was repeated for a total of three times, and subsequently resuspended in 500 µl of dH_2O and placed at -80 ºC in preparation for lyophilisation. Once frozen, the solution was transferred to the lyophiliser where the lid of the tube was removed

and covered with parafilm (with small holes) to allow for water sublimation. The lyophilised nanoparticles were stored at -80°C until further use.

4.2.1.1. Treatments of cells with empty and LRP PLGA nanoparticles

The HEK293 and SH-SY5Y cells were treated with 1-10% (v/v) of empty and LRP-encapsulated PLGA nanoparticles. This was done to assess their effect on cellular viability, LRP levels and telomerase activity.

Briefly, the cell lines were seeded into a 24-well plate and incubated overnight (at 37°C and 5% CO_2) until confluency reached 60-70% (see 4.2.2.). Thereafter, the cells were treated with 1, 5 and 10% (v/v) of empty and LRP-encapsulated PLGA nanoparticles in a final volume of 1 ml/well for 48 hours under standard conditions. The next day, media was changed to remove nanoparticles that were not taken up by the cells and to replenish with 1 ml/well. The treated cells were either used to extract protein for western blotting (see 4.2.4.-4.2.7.), cellular viability (see 4.2.8.) and telomerase activity (see 4.2.9.).

4.2.2. Cell culture

This study utilized two different cell lines: the SH-SY5Y human neuroblastoma cell line and the HEK293 human embryonic kidney cell line. The HEK293 cell line was grown in Dulbecco's Modified Eagle's Medium (DMEM) with 10% foetal bovine serum (FBS) and 1% penicillin/streptomycin (P/S) antibiotics, while the SH-SY5Y cell line was grown in a mixture of 1:1 DMEM and Ham's F12 nutrient with the same supplements. These media were used to supplement cells with vital nutrients and prevent bacterial and/or fungal growth. The cells were cultured in an incubator at 37°C and 5% CO_2 to simulate *in vivo* conditions, and were sub-cultured when they reached 70-90% confluency. Seeding and sub-culturing involved washing the cells with 1x phosphate buffered saline (PBS), detaching them with 1x Trypsin/EDTA, and suspending them in fresh media.

4.2.3. pCIneo-moLRP::FLAG stable transfection

To overexpress LRP::FLAG, cell transfections were carried out using the pCIneo-moLRP::FLAG DNA construct (Vana & Weiss, 2006). The cells were seeded at a confluency of 60-70% in a 6-well plate, and 5 µg of the plasmid DNA was mixed with 100 µl Xfect™ Reaction Buffer and 1.5 ml Xfect™ Polymer which formed nanoparticle complexes after 10

minutes. The complexes were added dropwise to the cell culture, and incubated at 37°C and 5% CO_2 for 4 hours. After incubation, the media was replaced with fresh growth media, and the cells were incubated for an additional 48 hours at 37°C. To select for transfected cells, cells were treated with 800 ng/ml Geneticin followed by 400 ng/ml, which removed the population of non-transfected cells. This was done to investigate the effects of overexpressing LRP::FLAG in TBHP/ $A\beta_{42}$ and MPP^+ mediated cytotoxicity (see 4.2.8.).

4.2.4. Extraction of protein

The cells were detached from the culture flasks by adding 2 ml of Trypsin/EDTA and incubating for 5 minutes at 37°C. To inactivate the Trypsin/EDTA, 8 ml of cell culture media was added, and the resulting cell suspension was added to a 15 ml falcon centrifuge tube and centrifuged for 10 minutes at 5000 rpm. The supernatant was removed, and the cells were lysed by adding 0.5-1 ml of radioimmunoprecipitation assay (RIPA) buffer (1% Triton X-100, 10 mM NaCl, 0.1% sodium dodecyl sulphate (SDS), 0.5% sodium deoxycholate, 50 mM tris-HCl (pH 8.0), and 5 mM ethylenediaminetetraacetic acid (EDTA) (pH 8.0), followed by incubation at 4°C for 10 minutes. The total protein concentration was determined using a BCA assay for western blot analysis.

4.2.5. BCA™ Protein Assay

The (Bicinchoninic acid assay) BCA assay is used to measure the quantity of protein and ensure that the samples are loaded evenly for western blot analysis. This assay works by detecting a colour change, which can be quantified using an absorbance spectrophotometer. This reaction is due to the protein's peptide bonds and the temperature. Peptide bonds within the protein reduce copper ions (Cu^{2+}) from copper sulphate (Cu^{+}) to form a purple-coloured product with bicinchoninic acid. The more peptide bonds present, the greater the amount of copper ions that are reduced, allowing for a direct measurement of the protein concentration.

Subsequently, bovine serum albumin (BSA) standards were prepared through a serial dilution, for protein concentration quantification a standard curve was constructed. Briefly, the following concentrations of BSA were prepared: 0, 0.025, 0.125, 0.25, 0.5, 0.75, 1.0, 1.5, and 2 mg/ml. In a 96 well plate, 25 µl of each standard was added. Subsequently, a 1:5 ratio of diluted cell lysates (25 µl) were added into each well. Accordingly, in a 1:50 and 49:50 ratio, the bicinchoninic assay (BCA) and copper (II) sulphate ($CuSO_4$) reagents were

combined. In the plate containing the cell lysate sample and BSA standards, 200 µl of the BCA and $CuSO_4$ solution was added. Until colour change occurred, the 96 well plate was Incubated at 37°C for 40 minutes. Using the Multiskan® GO ELISA plate reader (Thermo Scientific, Massachusetts, USA) absorbance was measured at 562 nm. Thereafter, using the absorbance of the standards, a linear regression curve was constructed where the equation of the curve was used to calculate protein concentration of the samples.

4.2.6. SDS PAGE

SDS-PAGE was performed as mentioned above, 4.1.5.1.
The protein samples were heated at 95°C for 5 minutes in the Blue Loading buffer (New England Biolabs) containing 40 mM dithiothreitol. Initially, 2-3 µl of PageRuler Prestained Protein Ladder (Thermo Fisher) was loaded into the first well of each gel. For β-actin and LRP, 10 ug was loaded, while 20 ug of PINK1 was loaded into wells. The samples were separated on a 12% polyacrylamide gel in 1x running buffer for 60-90 minutes at 120 V using the Mini Protean gel system (Bio-rad, California, USA).

4.2.7. Western Blotting

Once the proteins were separated by SDS PAGE, the gel was transferred to a polyvinylidene fluoride (PVDF) membrane via electro-blotting. At first, the Whatman papers were trimmed to the required size and immersed in a 1x transfer buffer containing 20% methanol, 25 mM tris, and 19.2 mM glycine. At the same time, the PVDF membranes were trimmed to the desired size and soaked in methanol for a duration of 5 minutes. Next, the gels were trimmed to the appropriate size and three sheets of filter paper were arranged on the semi-dry electrophoretic transfer device. The membranes were then placed on top of the filter papers, and the gels were positioned above them, followed by an additional three sheets of filter paper. The apparatus used for the transfer was closed and placed into the Trans-blot® Turbo™ Transfer system (Bio-rad, California, USA) for 30 minutes at 25 V - 1.0 A. After transferring the proteins onto the membranes, the membranes were placed in a blocking buffer comprising of 5% low-fat milk powder in PBST (1x PBS and 0.1% Tween 20) for a period of 1 hour. This step aimed to prevent the primary and secondary antibodies from binding non-specifically. Subsequently, the membrane was incubated with the primary antibody (Table 1) overnight at a temperature of 4°C on a shaker. Subsequently, the

membranes were washed in 1x PBST 5 times, for 5 minutes each, to remove primary antibodies which were not bound. Thereafter, the membrane was incubated with the secondary antibody (Table 1) for 2/3 hours (in the dark at room temperature). Following the incubation, the membranes were subjected to the washing step. They were rinsed 5 times with 1x PBST for 5 minutes each time. The Clarity™ Western ECL Blotting Substrate (Bio-Rad) and the ChemiDoc™ Imaging System (Bio-Rad) were used to visualise and capture the membranes. Densitometric analysis was calculated using The Image Lab 5.1 software (Bio-Rad) where β-actin was used as the loading control to normalise all values.

Table 1: *Antibodies (primary and secondary) used for western blotting*

Target Protein	Primary antibody	Dilution	Secondary antibody	Dilution
LRP::FLAG	Murine anti-FLAG® M2, (Sigma F3165)	1:4000	Anti-murine IgG-HRP (Sigma A4416)	1:2500
LRP/LR	Human anti-LRP/LR IgG-iS18, (Affimed)	1:6500	Anti-human IgG-HRP, (abcam 6858)	1:6500
PINK1	Rabbit anti-Pink-1 (Sigma P0076)	1:1500	Anti-rabbit IgG-HRP, (Cell Signaling Technology® 7074S)	1:2500
β-actin	Murine anti-β-actin-peroxidase, (Sigma A3854)	1:5000		

4.2.8. MTT Assay

The MTT (3-[4,5-dimethylthiazol-2-yl]-2,5diphenyl diphenyltetrazolium bromide) assay was used for cellular viability assessment of LRP::FLAG overexpressed SH-SY5Y and HEK293 cells. Furthermore, The assay was used to determine cellular viability in SH-SY5Y cells treated with exogenous LRP encapsulated in PLGA nanoparticles. The MTT assay employs a colorimetric method that relies on the capacity of metabolically active cells to convert a yellow tetrazolium salt into purple formazan crystals. This reduction reaction is facilitated by specific oxidoreductase enzymes that are present in viable cells and depend on the coenzyme

NAD(P)H. The extent of formazan crystal formation is directly proportional to the mitochondrial activity of the cells and is indicative of their viability (Mosmann *et al.,* 1983).

Briefly, TBHP/Aβ and MPP^+ were used to treat transfected and non-transfected cell lines while LRP encapsulated PLGA nanoparticles were used to treat SH-SY5Y cells. Furthermore, PCA is a well-known agent that triggers apoptosis and was utilized as a positive control in this study. Briefly, non-transfected and transfected LRP::FLAG cells were seeded in a 48 well plate at 1 x 10^5 cells/well and incubated overnight at standard conditions to allow for attachment. Once confluency of 60-70% was obtained, cells were treated with either 250 nM, 500 nM and 750 nM $A\beta_{42}$/ml, 50 µM, 100 µM and 200 µM TBHP/ml or 500 µM and 750 µM MPP^+/ml for 48 hours. Thereafter, to each well the MTT solution (100 µl of 1 mg/ml) was added, and incubated at $37°C$ for 3-4 hours. Post incubation, the media was carefully removed from each well and 300 µl of dimethyl sulfoxide (DMSO) was used to dissolve the purple formazan crystal. In a 96 well-plate, 100 µl of each sample was transferred into the wells in triplicates. Using the VICTOR® Nivo™ Multimode Microplate Reader the absorbance was measured at 570 nm.

4.2.9. Telomerase activity detection using quantitative polymerase chain reaction (qPCR)

Telomerase activity in cells treated with empty and LRP-encapsulated nanoparticles was quantified using the TRAPeze® RT Telomerase Detection Kit. The method is sensitive and uses fluorescence to detect telomerase activity in real time, and it relies on the telomeric repeat amplification protocol (TRAP), which makes use of the fluorescence energy transfer primers (Amplifluor® primers) that directly measure the fluorescence emission to detect and quantify telomerase activity. Initially, in an extracted sample the telomerase adds telomeric repeats to the 3' end of the substrate over a period of time. Subsequently, the extended products are amplified by Taq polymerase, using the Amplifluor® primers. Once incorporated into the telomeric repeat amplification products, these primers generate a fluorescent signal. The quantity of fluorescence emission generated is directly proportional to the quantity of TRAP products produced.

At first, the RNA and protein were extracted following the specified protocol. In this step, the samples were suspended in 200 µl of CHAPS lysis buffer and left on ice for 30 minutes.

Afterwards, the samples were subjected to centrifugation at 12 000 xg for 20 minutes at $4^{\circ}{}^{\circ}C$. The supernatant was transferred to a 1.5 ml Eppendorf tube and snap frozen (-80°C) in liquid nitrogen. Subsequently, the NanoDrop® ND-1000 (Thermo Fishe Scientific, Massachusetts, USA) was used to quantify the protein where it was and standardized to 500 ng/µl. In a 96-well plate, the TRAP reaction mixture and 1 µg/µl of protein samples was loaded into each well to 12.5 µl as the final volume. This reaction Mastermix consisted of Luna® Universal qPCR Mastermix (New England Biolabs, Massachusetts, USA), TS and ACX primers, EGTA (to inhibit RNases), and PCR-grade water. The CFX96™ Touch qPCR System from Bio-Rad, California, USA, was employed to perform qPCR analysis on all samples. The cycling parameters used in this study consisted of an initial cycle of 30 minutes at 37°C, followed by 2 minutes at 95°C, and subsequently 45 cycles of amplification with denaturation at 95°C for 15 seconds, annealing at 59°C for 60 seconds, and extension at 45°C for 10 seconds. To ensure that the buffer was not contaminated and had no telomerase activity, a minus telomerase negative control (consisting only of CHAPS lysis buffer) was included. A no template negative control (PCR-grade water) was included to adjust for any primer dimer formation in the absence of telomerase activity. Additionally, a heat-treated negative control was included, where the samples were incubated at 90°C for 10 minutes to inactivate any telomerase activity. A positive cell extract was provided as a positive control and made up as per protocol. The Bio-Rad CFX Maestro software was used to analyse the Cq values. The values were normalized as a percentage of the untreated controls, with the heat-treated samples serving as the background after subtraction.

4.2.10. Statistical Analysis

The statistical analysis will be conducted using Microsoft Excel 2018 (Microsoft Corporation) and QuickCalcs Outlier Calculator ©2017 GraphPad Software. Each experiment will include at least three biological replicates with error bars representing the standard deviation. The ANOVA and Student's *t*-test will be conducted at a 95% confidence interval, with p values less than 0.05 being considered statistically significant (*$p < 0.05$, **$p < 0.01$, and ***$p < 0.001$).

5. Results

5.1. LRP::FLAG plasmid *in vitro* study

The study was conducted in three parts. The first part focused on evaluating the impact of LRP::FLAG overexpression on HEK293 cells, with the aim of comparing its effects with LRP protein treatment to assess their potential role in impeding the progression and pathogenesis of AD and PD. This investigation aimed to determine whether targeting LRP could provide a new and effective strategy for treating these diseases. The second part of the study aimed to overexpress, purify and characterise the 37 kDa LRP protein in preparation for its encapsulation in PLGA nanoparticles. Finally, the third part of the study evaluated the *in vitro* therapeutic potential of PLGA encapsulated LRP nanoparticles in treating PD and AD. The study aimed to provide insights into the potential of LRP as a therapeutic target and the usefulness of PLGA encapsulated LRP nanoparticles as a novel treatment approach for these debilitating diseases.

5.2.1. Confirmation of transfection with LRP::FLAG

The main method used to achieve stable overexpression of LRP::FLAG within the HEK293 cell line was by transfecting the cells with the pCIneo-moLRP::FLAG plasmid. This resulted in a new cell line called transfected HEK293. The HEK293 cells were selected for these experiments since they express neuronal markers and are easily transfectable. Briefly, 48 hours after the cells were transfected, they were treated with geneticin, whereafter geneticin resistant cells were pooled and analyzed. Subsequently, western blot analysis was used to determine the effect of LRP::FLAG overexpression on LRP/LR and PINK1 protein levels. PINK1 protein levels were determined, as it is a protein known to play a significant role in the implication of PD. Thus, PINK1 was assessed to determine if LRP::FLAG overexpression may alter the protein levels of PINK1.

The results of the western blot analysis (shown in Figure 8, lanes 4-6) confirmed that the HEK293 cells that were transfected with pCIneoLRP::FLAG successfully expressed LRP::FLAG. This indicates that the transfection was successful and the subsequent experiments using LRP/LR to study PD and AD could be carried out.

A.

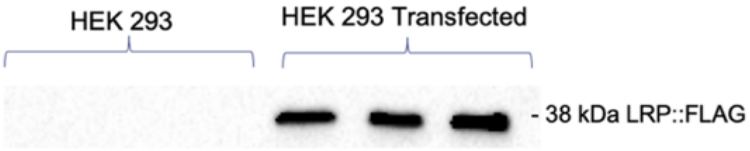

Figure 8. Transfection of HEK293 with pCIneo-LRP::FLAG plasmid was successful (A) *The presence of LRP::FLAG was determined via western blotting in transfected and non-transfected HEK293 cells. Accordingly, it was discovered that the transfected cells exclusively expressed a band at 38 kDa, which indicates the presence of LRP::FLAG, with an absence of bands in the non-transfected samples (A, lanes 4-6). LRP::FLAG was detected using the rabbit anti-FLAG HRP-conjugated antibody.*

5.1.2. LRP::FLAG overexpression in HEK293 cells increase LRP/LR and PINK1 protein levels

Western blotting was used to determine the effects of LRP::FLAG on LRP and PINK1 protein levels in both transfected and non-transfected cells. In order to normalize data, ß-actin (HRP) was used as a loading control.

Here, it was exhibited that the LRP::FLAG did indeed increase the total LRP/LR and PINK1 protein levels (Figure 9. A). After analysing the western blots using densitometry and comparing the non-transfected cells with LRP::FLAG transfected cells, it was found that the overexpression of LRP::FLAG significantly increase the levels of both LRP and PINK1 by 11.7% and 8.3%, respectively, in HEK293 cells (Figure 9. B). PINK1 is a mitochondrial kinase which enhances cell survival through selective mitophagy. PINK1 is a mitochondrial kinase that promotes cell survival through selective mitophagy, and studies have shown that increasing PINK1 expression can help with neurodegenerative diseases by regulating mitochondrial integrity (Matsuda *et al.,* 2013).

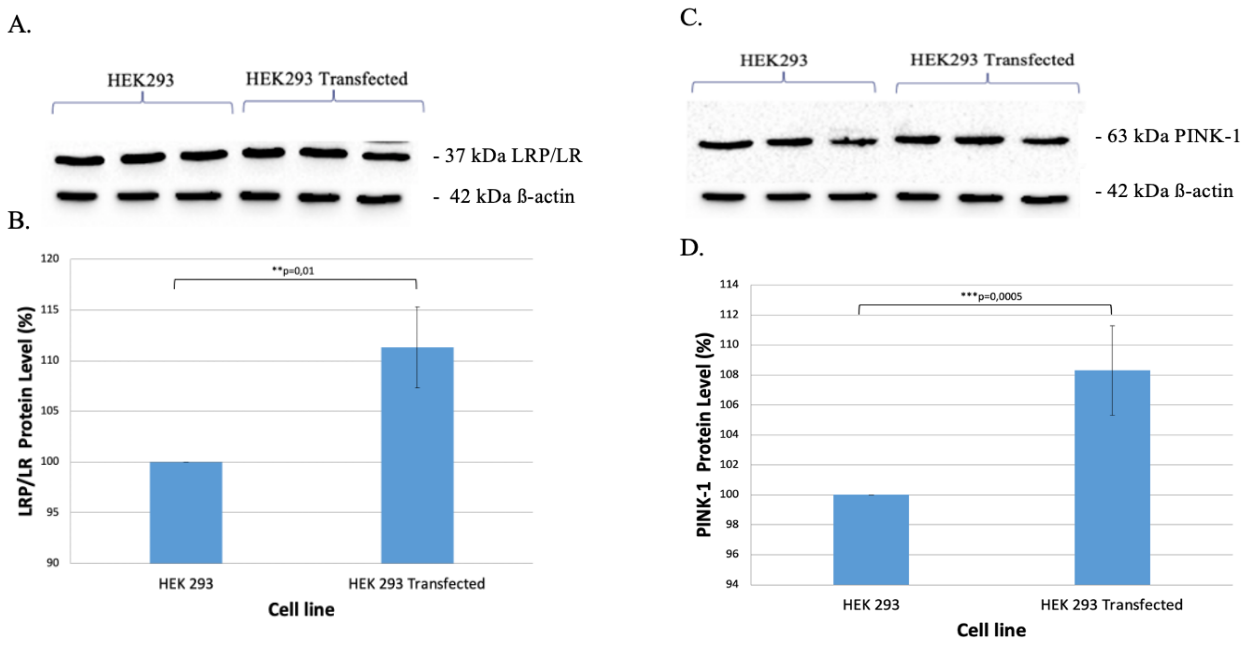

Figure 9. Western blot analysis reveals that LRP::FLAG overexpression increases total LRP/LR and PINK1 protein levels in HEK293 cells. *Western blot analysis was conducted on the HEK293 transfected with pCIneo-LRP::FLAG and non-transfected HEK293 cells. (A) LRP/LR expression is higher in the transfected HEK293 cells (B) Analysis revealed a significant 11.7% increase in LRP/LR protein levels after LRP::FLAG transfection in HEK293 cells. (C) PINK1 expression is increased in transfected HEK293 cells (D) Analysis revealed a significant 8.3% increase in PINK1 protein levels after LRP::FLAG transfection in HEK293 cells. Standard deviation is shown by the error bars, n = 3 biological repeats. *p<0.05, **p<0.01 and ***p<0.001; Student's t-test.*

5.1.3. LRP::FLAG overexpression in HEK293 cells increases cell viability after MPP^+ treatment

To evaluate the impact of LRP::FLAG overexpression on cell viability, an MTT assay was conducted on both non-transfected and transfected HEK293 cells following treatment with 1-methyl-4-phenylpyridinium (MPP^+) at concentrations of 250 µM and 500 µM. MPP^+ is a neurotoxin that can induce PD-like state by inhibiting dopaminergic neurons in the substantia nigra region of the brain. MPP^+ is a commonly used neurotoxin that can cause cell death in dopamine neurons and induce PD in various experimental models, including cell cultures, mice, rats, and primates (Braungart *et al.,* 2004). Briefly, to induce a PD-like state within cells, the HEK293 cells were treated with 250 µM and 500 µM of MPP^+ for 48 hours.

Protocatechuic acid (PCA), which is recognized as a substance that can induce apoptosis, was utilized as a positive control in the HEK293 cells. Here, it was exhibited that the overexpression of LRP::FLAG resulted in a significant increase in cell viability after treatment with 250 µM and 500 µM of MPP^+ as compared to then non-transfected HEK293 cells (Figure 10).

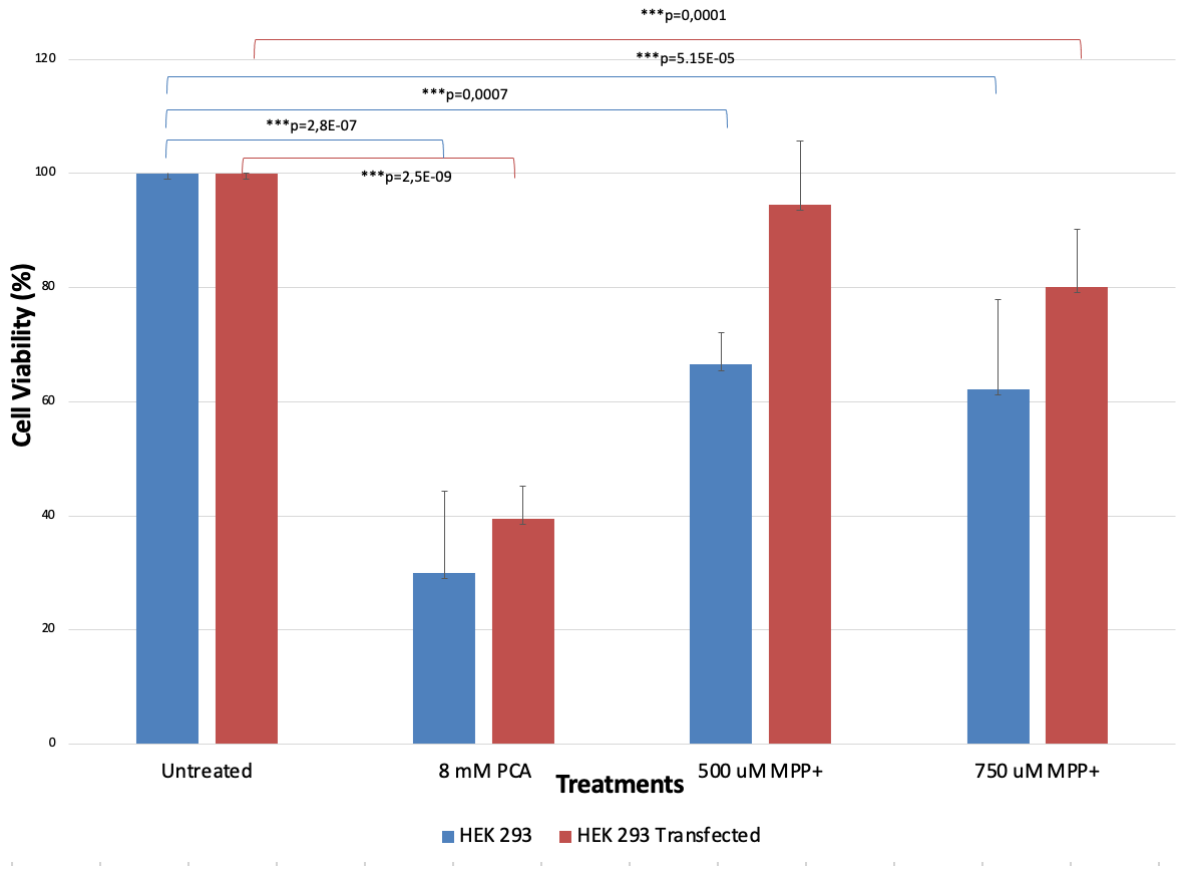

Figure 10. LRP::FLAG overexpression rescues HEK293 cells at 500 µM and 750 µM MPP^+ treatment. *Initially, data obtained normalized and compared to the non-treated, non-transfected HEK293 cells (viability was set to 100%). Cell viability was assessed 48 hours post treatment and PCA was used as a positive control. At increasing concentrations of MPP^+, quantitative analysis of cell viability indicated that LRP::FLAG overexpression maintained a higher level of cell viability as compared to the non-transfected HEK293 cells. Firstly, transfected cells showed a 26% higher cell viability compared to the non-transfected cells at 500 µM. Whereas, transfected cells showcased a 17% higher cell viability as compared to the non-transfected cells at 750 µM. Standard deviation is shown by the error bars, n = 3 biological repeats. *p<0.05, **p<0.01 and ***p<0.001; Student's t-test.*

As previously mentioned, the overexpression of LRP::FLAG in HEK293 cells resulted in an increase in PINK1 protein levels (Figure 9). These results suggested that LRP/LR plays a part in the impediment of PD, however, a definitive role has not been yet established. The results showed that compared to the non-transfected HEK293 cells, 500 µM and 750 µM had a significant 28% and 17% increase in cell viability, respectively (Figure 10). Therefore, indicating that the overexpression of LRP::FLAG may rescue cells from the cytotoxic effects of MPP^+.

5.1.4. LRP::FLAG overexpression in HEK293 cells increases cell viability after TBHP and $A\beta_{42}$ treatment

Neurodegenerative diseases (AD and PD) are thought to be influenced by oxidative stress in their pathogenesis by increasing ROS-induced neuronal damage (Mandel *et al.,* 2003; Von Armin *et al.,* 2010). A known inducer of cellular oxidative stress is t-butyl hydroperoxide (TBHP), and therefore, a MTT assay was performed to examine the protective effect of LRP/LR on oxidative damaged in nerve cells by treating non-transfected and LRP::FLAG transfected HEK293 cells with cytotoxic levels of TBHP (50, 100 and 200 µM)

Cellular viability analysis (Figure 11) revealed that treatment with cytotoxic TBHP increased cell viability in LRP::FLAG transfected HEK293 cells. Firstly, at 50 µM, transfected cells showed a 49.6% increase in cell viability as compared to non-transfected cells. Second, at 100 µM transfected cells revealed a 62.5% increase in cell viability as compared to the non-transfected cells. Finally, at 200 µM, transfected cells showed a 19% increase cell viability as compared to non-transfected cells.

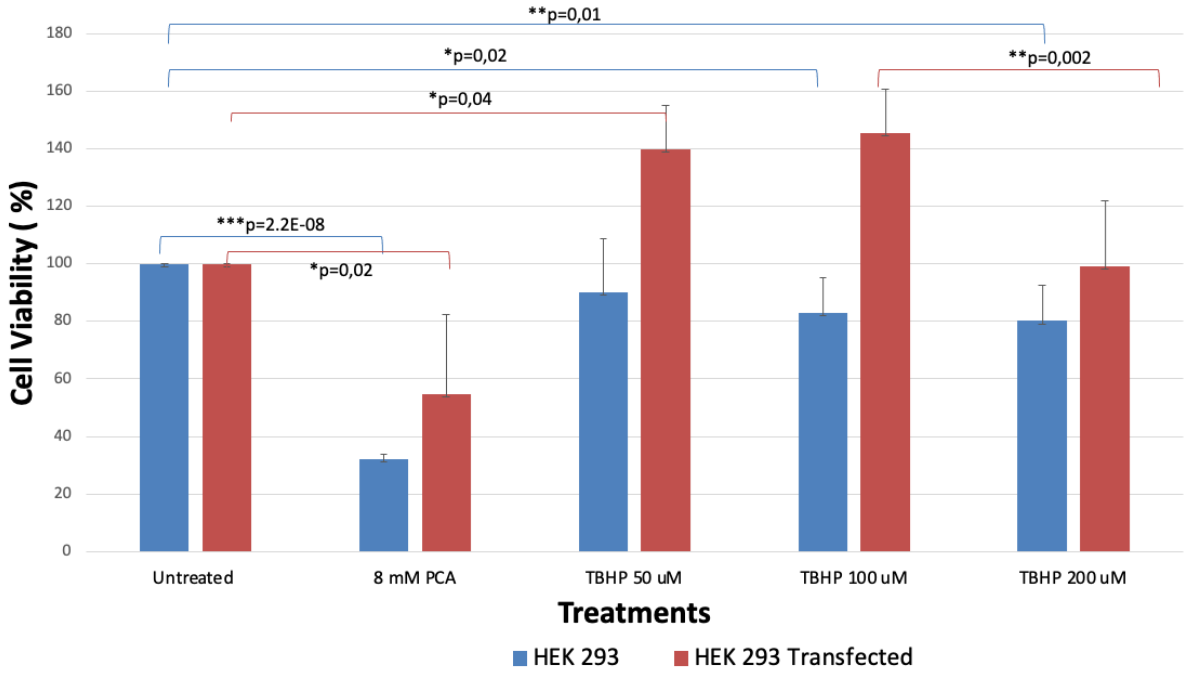

Figure 11. LRP::FLAG overexpression enhances HEK293 cell viability at 50 µM, 100 µM and 200µM TBHP. *Initially, data obtained normalized and compared to the non-treated, non-transfected HEK293 cells (viability was set to 100%). Cell viability was assessed 48 hours post treatment and PCA was used as a positive control. Briefly, compared to non-transfected cells, the LRP::FLAG overexpression maintained a higher level of cellular viability at increasing concentrations of TBHP. Standard deviation is shown by the error bars, n = 3 biological repeats. *p<0.05, **p<0.01 and ***p<0.001; Student's t-test.*

Given that LRP::FLAG overexpression has been shown to rescue cells from oxidative stress-induced cytotoxicity, and previous research has demonstrated a bidirectional relationship between oxidative stress and $A\beta_{42}$ accumulation where each factor contributes to and exacerbates the other (Cheignon *et al.,* 2018), further investigation was performed to evaluate the impact of LRP::FLAG overexpression on HEK293 cells treated with cytotoxic levels of $A\beta_{42}$ peptides.

Previous research has identified LRP/LR as a receptor for $A\beta_{42}$, which is involved in the uptake and accumulation of $A\beta_{42}$ within cells. This accumulation has been linked to a decrease in cell growth and an increase in apoptosis (Da Costa Dias *et al.,* 2014). Furthermore, it has been discovered that the administration of synthetic $A\beta_{42}$ at a concentration of 500 nM can replicate the cytotoxic effects of $A\beta_{42}$ (Da Costa Dias *et al.,* 2014). Newer studies have demonstrated that overexpression of LRP::FLAG inhibits the

shedding of Aβ and decreases the levels of $A\beta_{42}$ within cells, thereby protecting them from the cytotoxic effects of $A\beta_{42}$ (Bignoux *et al.,* 2019). The study revealed that the LRP::FLAG overexpression increased hTERT expression which increased telomerase activity while decreasing intracellular $A\beta_{42}$ levels and shedding (Bignoux *et al.,* 2019). Cuttler *et al*. 2020 demonstrated that overexpression of LRP::FLAG led to a reduction in both total and phosphorylated tau levels, as well as a decrease in levels of PrP^{c}, a protein associated with tauopathies (Cuttler *et al.,* 2020). Therefore, an MTT assay was performed to determine whether there was an effect on the viability in LRP::FLAG transfected HEK293 cells treated with cytotoxic levels of $A\beta_{42}$ peptides.

Cellular viability analysis in HEK293 cells (Figure 12) exhibited that post-treatment with $A\beta_{42}$, there was a significant increase in cellular viability in LRP::FLAG transfected HEK293 cells as compared to non-transfected HEK293 cells. Firstly, at 250 nM, transfected cells had 58.9% significantly higher cell viability than non-transfected cells. Second, at 500 nM, transfected cells had 28.5% significantly higher cell viability than non-transfected cells. Finally, at 750 nM, transfected cells had 33.3% significantly higher cell viability than non-transfected cells. Therefore, indicating that transfection with LRP::FLAG may rescue HEK293 cells from $A\beta_{42}$-induced cytotoxicity.

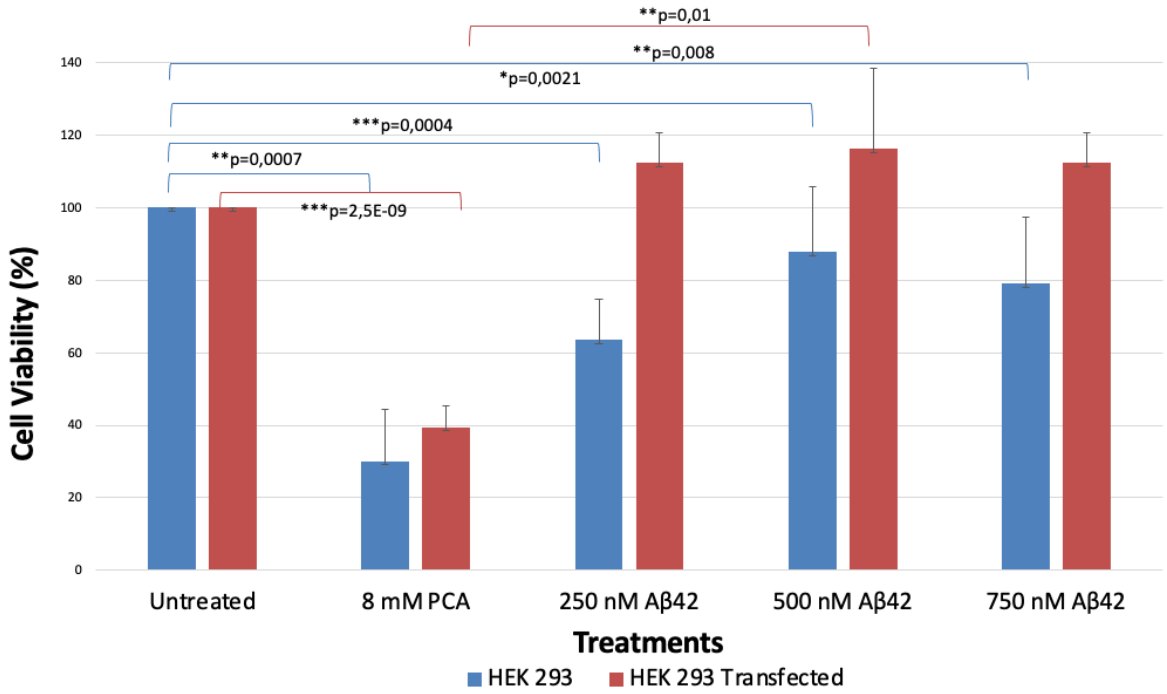

Figure 12. LRP::FLAG overexpression enhances HEK293 cell viability after $A\beta_{42}$ induced cytotoxicity. *Initially, data obtained normalized and compared to the non-treated, non-transfected HEK293 cells (viability was set to 100%). Cell viability was assessed 48-hours post treatment and PCA was used as a positive control. Cells were treated with 250 nM, 500 nM and 750 nM $A\beta_{42}$ and a MTT cell viability assay was performed. Briefly, compared to non-transfected cells, the LRP::FLAG overexpression maintained a higher level of cellular viability at increasing concentrations of $A\beta_{42}$. Standard deviation is shown by the error bars, n = 3 biological repeats. *p<0.05, **p<0.01 and ***p<0.001; Student's t-test.*

5.2. LRP Protein Purification

To investigate whether exogenous LRP protein could produce similar results as LRP::FLAG transfection, this part of the study focussed on overexpressing, purifying, and characterising the 37 kDa LRP protein. Here, express competent *E. coli* cells were transformed with a pET-11a vector expression system containing the gene for the 37 kDa laminin receptor precursor (LRP) protein. The protein was overexpressed and subsequently purified using liquid chromatography. The His-tag was included to facilitate downstream purification with immobilized metal ion affinity chromatography (IMAC). The structure was thoroughly characterized using ITF and Far UV-CD.

5.2.1. Overexpression trials for the optimization of LRP expression

Optimal conditions for the overexpression of the 37 kDa LRP protein had not yet been determined. Hence, protein overexpression trials of LRP were conducted to determine the optimal conditions to produce a high quantity of soluble 37 kDa LRP protein. Here, two different conditions were trialed for the optimal overexpression of LRP, using different concentrations (1.0 mM and 0.3 mM) of IPTG. The resultant SDS PAGE gel is shown below in Figure 13. After induction with different concentrations of IPTG, samples were collected at different time intervals, the samples were centrifuged to separate the insoluble (pellet (P)) from the soluble (supernatant (S)) LRP protein.

A. 1.0 mM IPTG

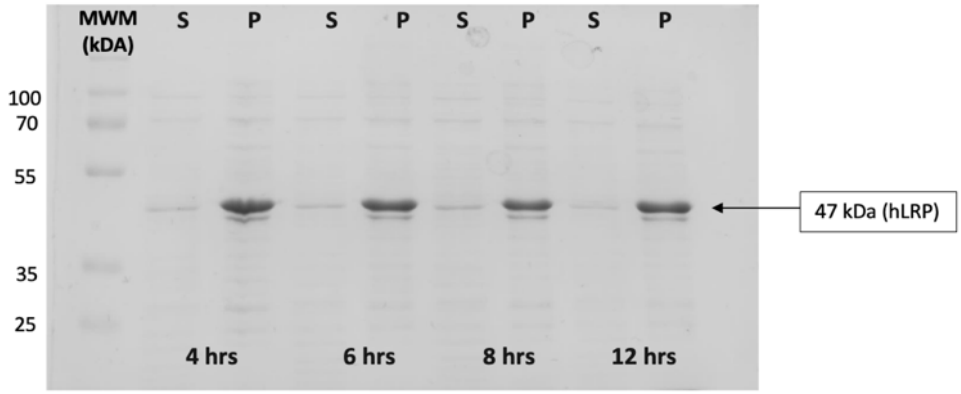

B. 0.3 mM IPTG

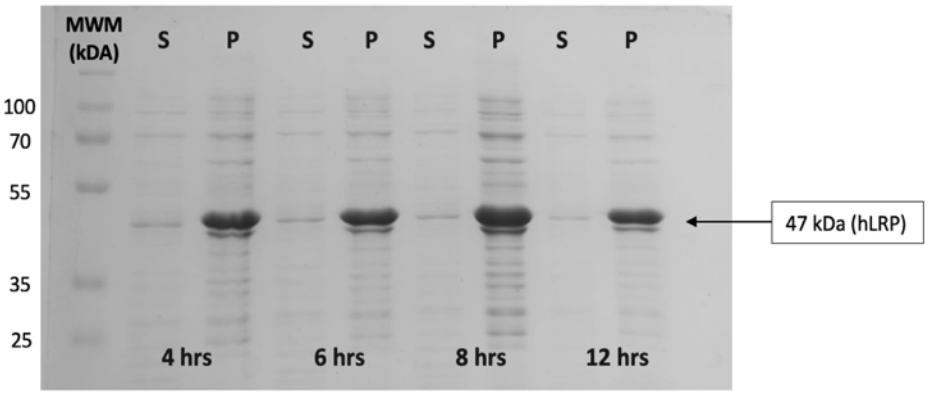

C.

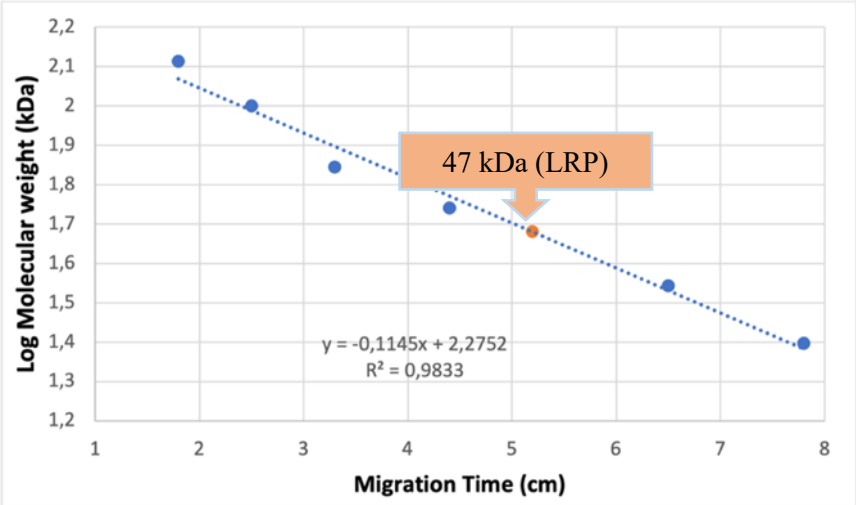

Figure 13. Overexpression trials of LRP to identify optimal conditions for soluble protein production. *(A) SDS-PAGE gel samples showing overexpression trials under the condition of 1.0 mM IPTG at different time intervals (4, 6, 8, 12 hours). (B) SDS-PAGE gel samples showing overexpression trials under the condition of 0.3 mM IPTG at different time intervals (4, 6, 8, 12 hours). S: Supernatant (soluble 37 kDa LRP), P: Pellet (insoluble 37 kDa LRP). The size of the bands was determined by linear interpolation of a standard curve (C) constructed from standards of the known molecular weight marker (PreStained Protein Ladder (Merck, Germany)). The size of the bands in (A) and (B) correspond to the molecular weight of 47 kDa.*

As seen above, two different conditions were tested for the optimal overexpression of the 37 kDa LRP. As seen in Figure 13 (A) after induction with 1.0 mM IPTG, incubated at 20°C and at 230 rpm, samples were collected at intervals of 4 hours, 6 hours, 8 hours, and 12 hours. The SDS-PAGE gel (Figure 13. A) exhibited higher intensity bands in the pelleted samples which presented that the protein was highly insoluble, yet at a low concentration. Therefore, a lower concentration of IPTG was trialed, as seen in Figure 13 (B), after induction with 0.3 mM IPTG, incubated at 20°C and at 230 rpm, samples were collected at intervals of 4 hours, 6 hours, 8 hours, and 12 hours. The SDS-PAGE gel (Figure 13. B) exhibited that there was a higher concentration of protein after 8 hours of overexpression, yet the protein was insoluble (P). The molecular weight corresponding to the band of interest was determined by linear interpolation of a standard curve constructed from a set of standards of known molecular weight (Figure 13. C). The standard curve indicates that the band of interest corresponds to

the molecular weight of 47 kDa, unexpectantly. Studies have shown that membrane proteins have an anomalous migration on SDS-PAGE but has yet to be conclusively explained (Imamura *et al.,* 2002).

5.2.2. LRP solubilization using Triton X-100

Using the optimal conditions for the expression of large quantities of the insoluble from the protein, large scale solubilization of the membrane protein was performed using Triton X-100. Studies have found that there are many challenges faced when purifying membrane proteins due to their highly hydrophobic characteristics and strong propensity to aggregate. The aggregated protein is often referred to as inclusion bodies which are commonly found in the cytoplasm and the transmembrane space (Palmer *et al.,* 2004). Here, the protein was subjected to an extraction protocol where the insoluble LRP protein was recovered from the cell lysate by low-speed centrifugation (5000 xg) and subsequently, washed with Triton X-100, therefore obtaining a high yield of soluble protein.

A.

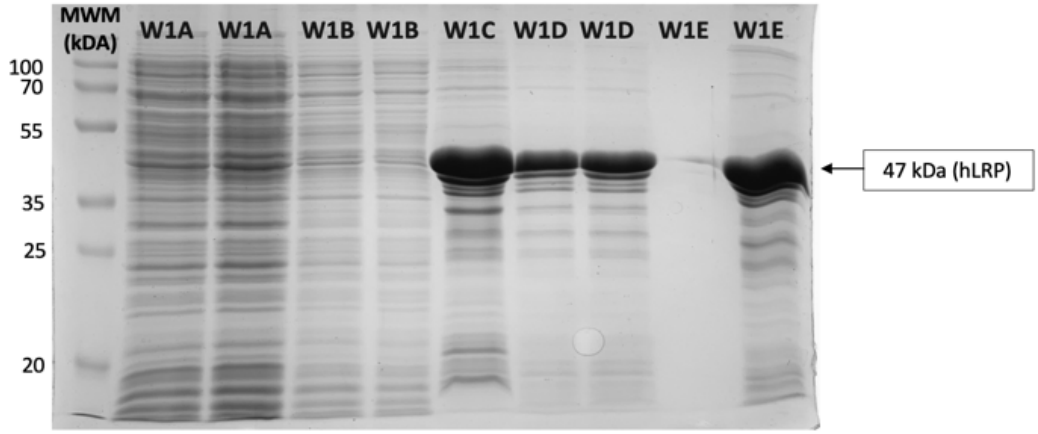

B.

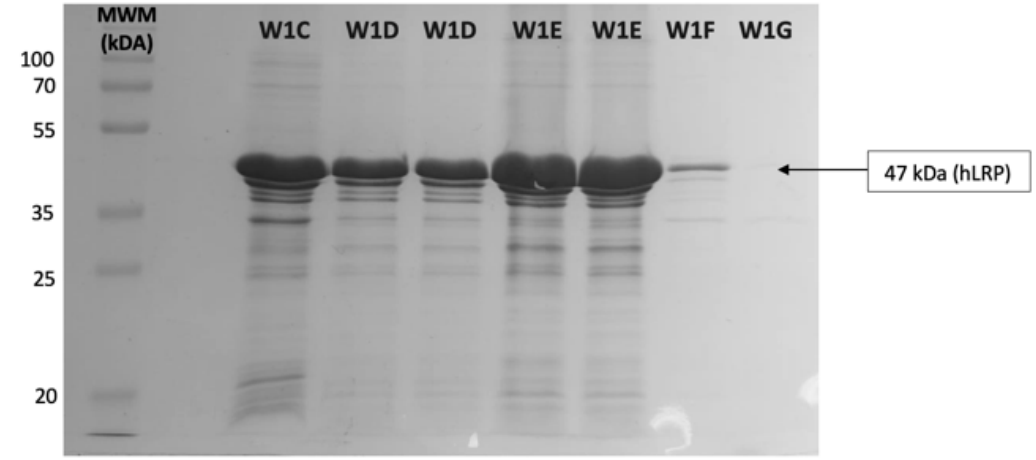

Figure 14. Solubilization of overexpressed LRP from the insoluble pellet with Triton X-100. *(A) and (B) SDS PAGE gels of the 10 aliquots of the soluble fractions collected (Wash 1A – W1G) from insoluble pellets via protein extraction. The insoluble fractions were solubilized in a detergent containing 0.5% (w/v) Triton X-100, each fraction was centrifuged at 18 000 xg for 30 minutes, soluble supernatant was collected. *2 repeats for samples (W1A-W1D) and samples W1C-W1E were run again on gel B for further confirmation.*

The cell lysates were solubilized in a detergent containing 0.5% (w/v) Triton X-100, and each fraction was centrifuged for 30 minutes at 18 000 xg, thereafter the soluble supernatants were collected. Upon the resultant SDS-PAGE gel (Figure 14. A and B), the supernatant collected from wash 1C (W1C)(Figure 14. A) to wash 1E (W1E)(Figure 14. B), contained high yields of soluble protein which were later used for further analysis.

5.2.3. Nickel Immobilised Metal-Ion Affinity Chromatography (IMAC)

The LRP protein was overexpressed with a N-terminal His-tag which allowed resolubilized protein collected from the insoluble fraction lysate to be purified by IMAC. Initially, a nickel (Ni^{2+})-IMAC resin was used as it provides higher affinity for His-tagged protein purification. The resultant IMAC elution profile and SDS-PAGE gel is shown below in Figure 15.

The resolubilized protein collected from the insoluble fraction lysate was loaded onto the IMAC column, any unbound contaminating proteins were eluted as the flow through (FT)(Figure 15. A; lane 3). Thereafter, a wash using a high salt concentration removed any non-specifically bound contaminant proteins (Figure 15. A; lane 4), where the elution profile (Figure 15. B) indicates that the salt wash peak was relatively small, indicating a low concentration of contaminants. The protein-bound to the column were then eluted with a high concentration of imidazole resulting in a small peak where multiple fraction of the elution (E1-E4) was collected (Figure 15 A; lane 4-8). The trailing of the elution peak was a result of uneven levels of retention in the column, at different points during the elution. The eluted protein fraction was pooled together. The LRP protein was not completely pure after the IMAC as the eluted fraction contained a few contaminants as seen in the bands in the elution lane (E3)(Figure 15. A; lane 6). The high levels of non-specifically bound proteins could be accounted for by the low specificity with which His-tags bind Ni^{2+}. Therefore, the soluble lysate was purified using a Co^{2+}-IMAC resin.

A.

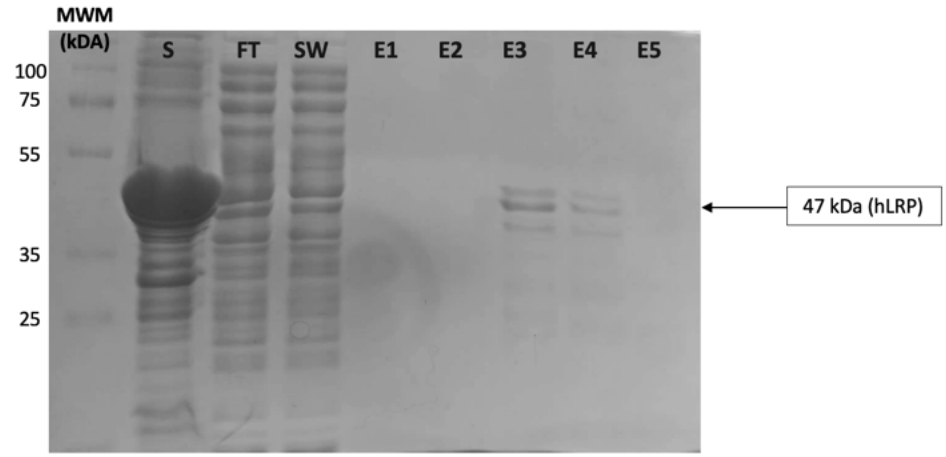

B.

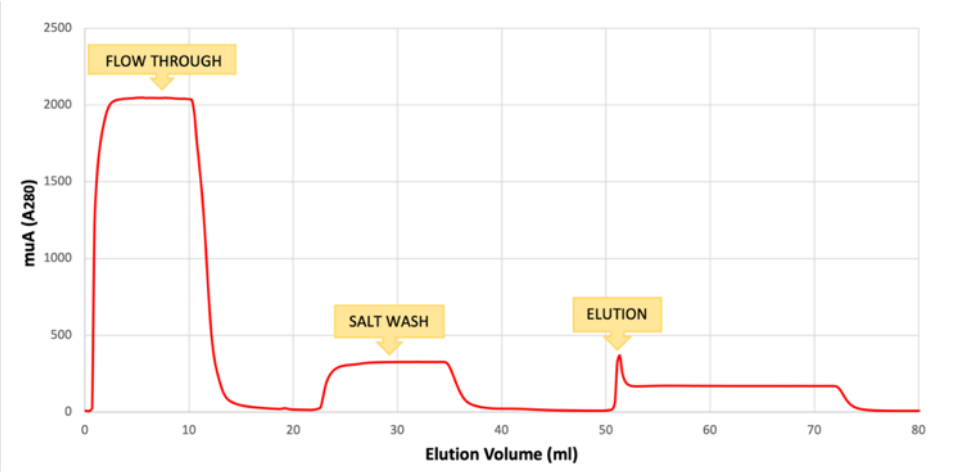

Figure 15. Immobilized nickel metal ion affinity chromatography purification of LRP*. (A) SDS-PAGE gel with the samples collected from immobilized metal-ion affinity chromatography. S: supernatant. SW: salt wash. FT: flow through. E (1-5): elution 1-5. (B). Elution profile from nickel immobilized metal-ion affinity chromatography. The protein of interest is shown in the blue box at 47 kDa molecular weight. The soluble lysate was loaded onto the column. The flow through contained many unbound contaminant proteins, as can be seen by the large number of bands in the flow through lane of the gel. Non-specifically bound contaminants were then removed by a salt wash containing detergent and a high salt concentration. These contaminants were detected by SDS-PAGE as indicated in (A). A high concentration of imidazole was used to elute the column-bound proteins. Bands E1 to E5 on the gel are multiple small volume fractions of the elution. There was presence of contamination indicating that the protein was not completely pure and required subsequent purification.*

5.2.4. Cobalt Immobilised Metal-Ion Affinity Chromatography (IMAC)

A cobalt (Co^{2+})-IMAC resin was subsequently used as it provides greater specificity for His-tagged protein purification. The resultant IMAC elution profile and SDS-PAGE gel is shown below in Figure 16.

The soluble lysate was loaded onto the IMAC column which allowed for the flow through (FT) (Figure16. A; lane 3) of any unbound protein contaminants. The column was then washed with high salt concentration allowing the removal of any non-specifically bound contaminant proteins (Figure 16. A; lane 4). As seen in the elution profile (Figure 16. B) the salt wash peak is very small, indicating a low concentration of contaminants. The salt wash (SW) did not show up on the gel indicating that there is a low concentration of contaminants (Figure 16. A; lane 3). The protein-bound to the column was then eluted with a high concentration of imidazole resulting in a small peak. The trailing of the elution peak was a result of uneven levels of retention in the column, at different points during the elution. The eluted protein fraction was pooled together. The LRP protein was not completely pure after the IMAC as the eluted fraction contained a few contaminants as seen in the bands in the elution lane (E4/5/6) (Figure 16. A; lane 8/9/10), however it was more pure than with the Ni^{2+}-IMAC resin. This resulted in a higher yield of specifically bound protein which is accounted for by the increased specificity with which His-tags bind Co^{2+}. The molecular weight of the protein was ≈ 47 kDa.

A.

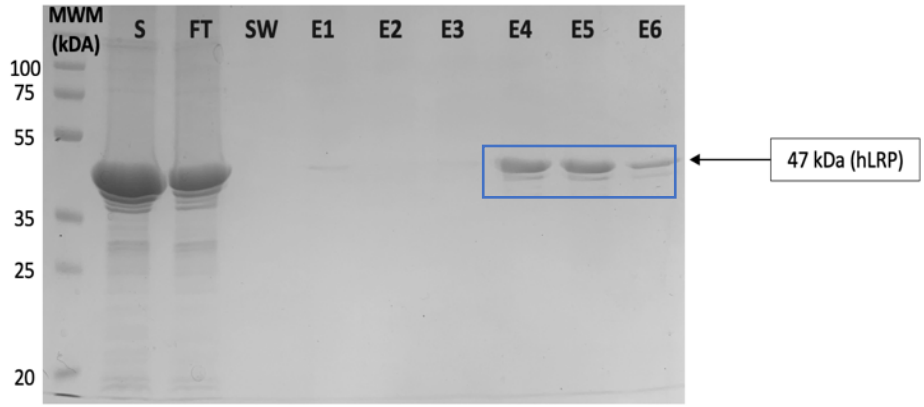

B.

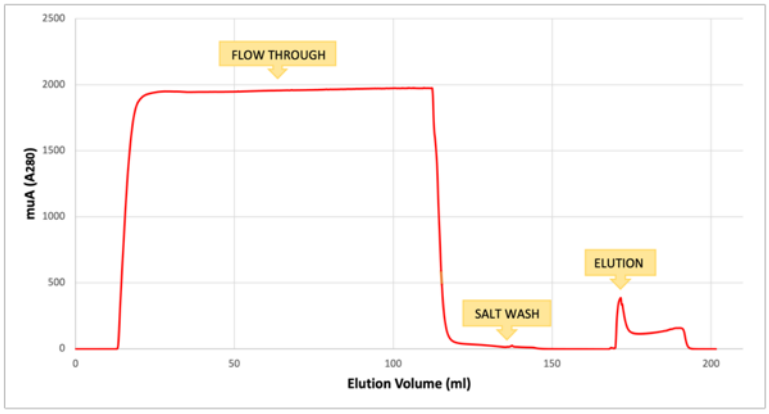

Figure 16. Immobilized cobalt metal ion affinity chromatography purification of LRP*. (A). The samples obtained from immobilized metal-ion affinity chromatography were analysed using SDS-PAGE gel. S for supernatant, P for pellet, SW for salt wash, FT for flow through, and E for elution. (B). The cobalt immobilized metal-ion affinity chromatography yielded an elution profile. The protein of interest, which weighs 47 kDa, is highlighted in the blue box. Initially, the soluble lysate was loaded onto the column. The flow through lane of the gel displayed numerous bands, indicating the presence of unbound contaminant proteins. Subsequently, a salt wash containing detergent and a high salt concentration was employed to eliminate non-specifically bound contaminants. These contaminants could not be detected by SDS-PAGE as indicated by the absence of the bands in salt wash lane of the gel. Column-bound proteins were then eluted with a high concentration of imidazole. The elution was successful as shown by the bands in the elution lane of the gel. The presence of bands in the elution lane indicate that the protein was not completely pure and required subsequent purification.*

Studies have shown that membrane proteins have an anomalous migration on SDS-PAGE but has yet to be conclusively explained. Therefore, a western blot was performed to confirm the presence of the 37 kDa LRP protein using human anti-LRP/LR IgG-iS18 antibody.

A.

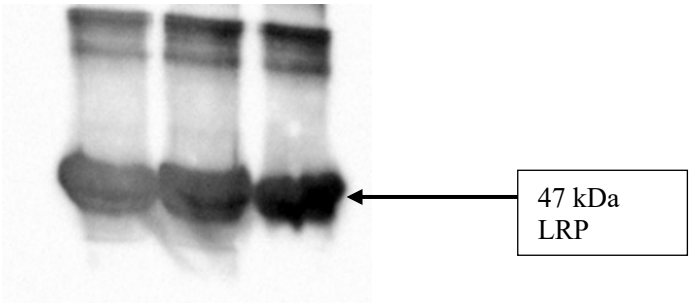

Figure 17. Western blot analysis reveals the presence of LRP protein. *The presence of the 47 kDa and 67 kDa LRP was confirmed through western blot analysis of elution fraction from the immobilized cobalt metal-ion affinity chromatography purification.*

Upon densitometric analysis, it is shown that the 37 kDa LRP and 67 kDa LR protein was present in the IMAC eluted fractions. However, due to anomalous migration, the 37kDa LRP migrated to a molecular weight of 47 kDa. The bands present at the higher molecular weight is likely due to non-specific binding of the primary/secondary antibodies.

5.2.5. LRP purity and concentration through absorbance spectroscopy

Absorbance spectroscopy was utilised to determine the concentration of the protein, and to further determine if the protein contained nucleic acid contamination. The absorbance spectrum shown below in Figure 18 is characteristic of a protein absorbance spectrum. There is a peak at 280 nm based on the presence of aromatic amino acids (tyrosine, tryptophan, and phenylalanine which absorb at 280 nm. Furthermore, the absorbance at 280 nm was used to calculate the protein concentration of 12.6 µM using the extinction coefficient of 67045 $M^{-1}.cm^{-1}$. There is a shoulder at 295 nm due to the presence of the tryptophan residues which exclusively absorb at 295 nm. The absence of an absorbance at 340 nm indicated that the protein was free from aggregation. Nucleic acids absorb at 260 nm, the A_{280}/A_{260} ratio is 1.54 indicating that the protein is sufficiently free from nucleic acid contamination.

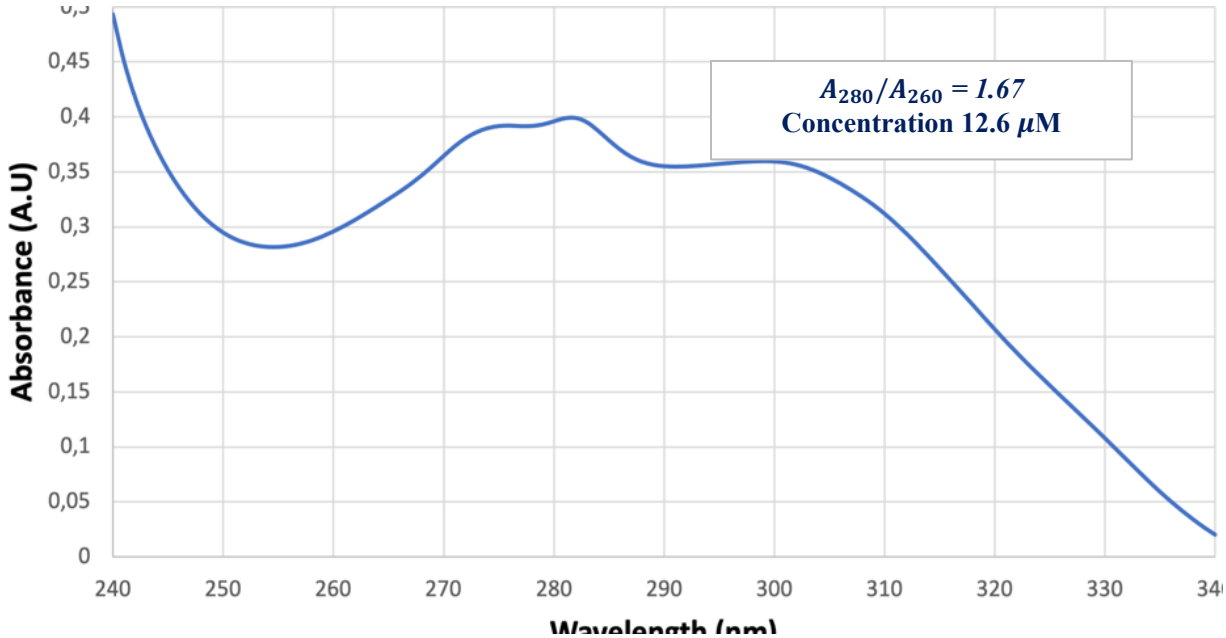

Figure 18. Absorbance spectrum of LRP. *The spectrum has a peak at 289 nm due to the presence of aromatic amino acids (tyrosine, phenylalanine, and tryptophan) and a shoulder at 295 nm due to the presence of 10 tryptophan residues. The protein is free from aggregation due to the lack of absorbance at 340 nm. The absorbance at 280 nm was used to calculate protein concentration using the extinction coefficient of 67045* $M^{-1}.cm^{-1}$*. The protein concentration was 12.6 μM. The* A_{280}/A_{260} *ratio is 1.54 indicating that the protein is relatively free from nucleic acid contamination.*

5.2.6. Intrinsic Tryptophan Fluorescence

After a sufficient amount of pure protein was obtained, the structure and stability of LRP was characterised. ITF was used to study the tertiary structure of the protein and to indicate if the protein is properly folded. Tryptophan residues contain a indole fluorophore which excite at 295 nm. When tryptophan residues are in a polar environment, they emit light at 350 nm, however, when they are in a hydrophobic environment, such as inside the protein core, they emit light at 320 nm. In order to confirm that the protein was properly folded, the ITF spectra was obtained in the presence and absence of a denaturant (8 M urea), after excitation at 280 nm and 295 nm.

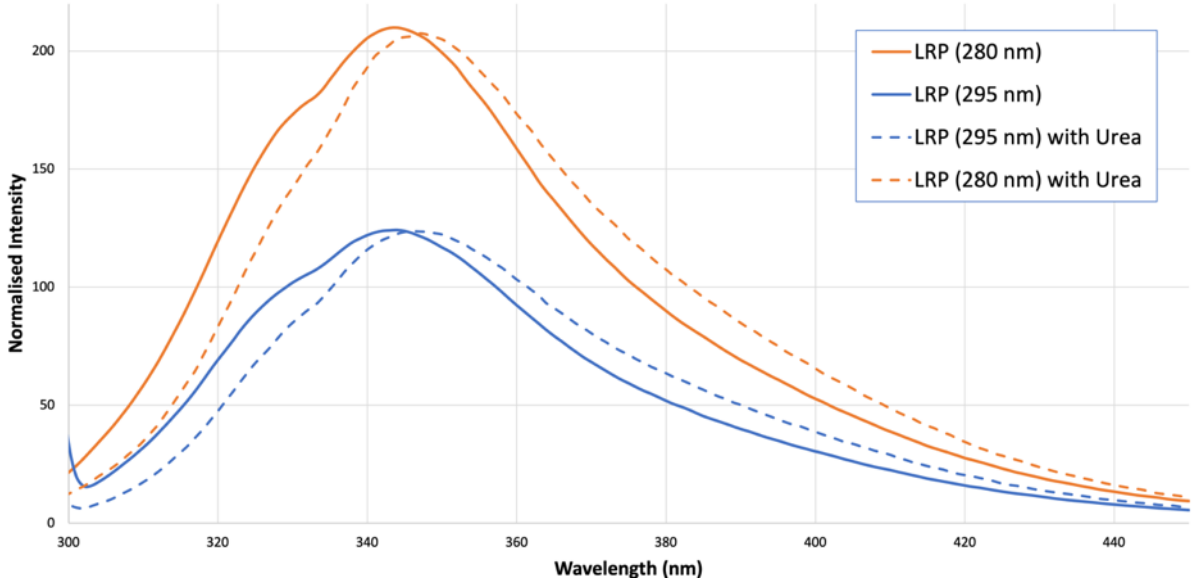

Figure 19. Intrinsic tryptophane fluorescence spectrum of LRP in the presence and absence of a denaturant. *The spectra were obtained after exciting the tryptophan residues at 280 nm and 295 nm. The protein (2 µM) was denatured with 8 M urea. The spectrum of the denatured protein was normalised against the spectrum of the wild-type. The native spectrum has a peak at 345 nm suggesting the presence of the tryptophan residues in the same environment. The denatured spectrum has a single peak at 350 nm.*

After excitation at 280 and 295 nm, the native protein's emission spectrum (absence of 8 M urea) shows a peak at 345 nm confirming that the tryptophan residues are in the same environment. However, the ITF emission spectrum of the unfolded protein (presence of 8 M urea) shows a single peak at 350 nm. In the presence of urea, the emission maximum is shifted by 5 nm (Figure 19). This bathochromic shift exhibits that the tryptophan residues in the native protein were in a hydrophobic environment and is evidence that the protein is folded correctly. If the native protein was unfolded, the bathochromic shift observed would not occur in the presence of urea.

5.2.7. Circular Dichroism Spectropolarimetry

The secondary structure of LRP was determined using circular dichroism spectropolarimetry. The far-UV CD spectrum of α-helical protein has troughs at 208 nm and 222 nm, and a peak at approximately 190 nm (Greenfield, 2006).

The far UV circular dichroism spectra were obtained by normalizing the circular dichroism signal (millidegrees) to mean residue ellipticity (MRE), which takes into consideration both the concentration of the protein and the total number of amino acids present. The spectrum, as shown above (Figure 20), exhibits a trough at 207 nm and a peak at 190 nm. Indicating that the LRP protein is predominantly an α-helical protein, as mentioned in previous studies (Jamieson *et al.,* 2008).

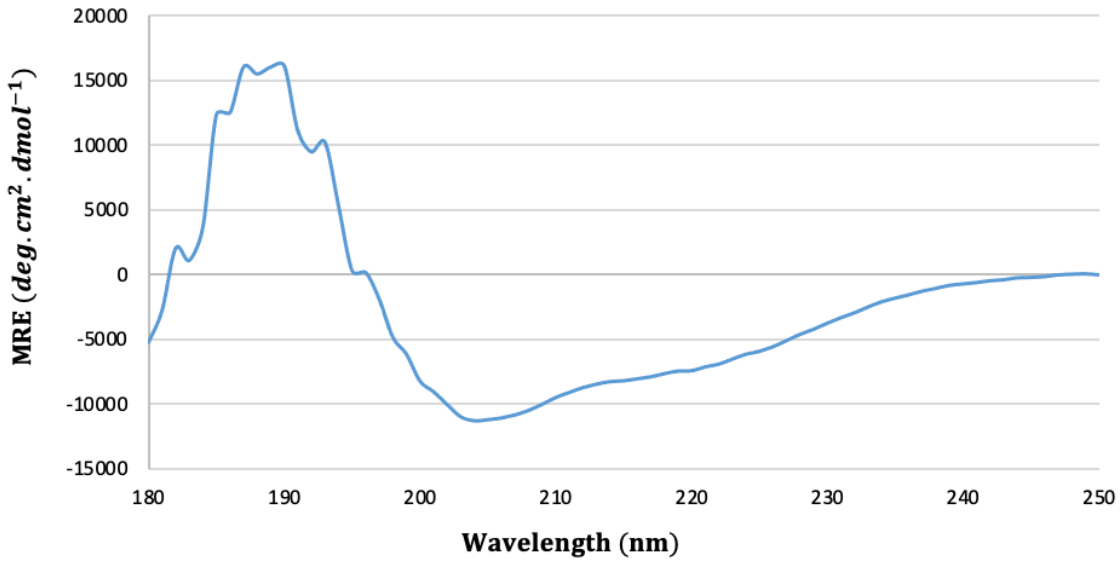

Figure 20. Circular dichroism spectrum of LRP. *The far UV circular dichroism spectrum was obtained by normalizing the circular dichroism signal (millidegree) to mean residue ellipticity (MRE), which accounts for the protein concentration and the number of amino acids present. The spectra contain a trough at 207 nm and peak at 190 nm. The spectra indicates that the protein is predominantly α-helical as expected.*

5.3. Encapsulation of the 37 kDa LRP in PLGA nanoparticles as a delivery system

The overexpression of LRP::FLAG has shown to be an effective treatment for PD and AD *in-vitro* (Bignoux *et al.,* 2019; Cuttler *et al.,* 2020; Burns *et al.,* in preparation). However, for this to be further tested *in-vivo* an effective, non-toxic delivery system needs to be used to

overcome the blood brain barrier which can be a challenge and contributes to the lack of progress in treatment of these CNS diseases. Therefore, this part of the study focused on the optimisation of encapsulating LRP in PLGA nanoparticles and to further establish whether these LRP PLGA nanoparticles would have an effect on LRP/LR levels, cellular viability, and telomerase activity in both HEK293 and SH-SY5Y cells.

5.3.1. LRP PLGA nanoparticle treated cells exhibit an increase in LRP protein levels in HEK293 cells

Once the batch production of the LRP PLGA encapsulated nanoparticles had been optimised, western blotting was performed to determine whether the empty and LRP encapsulated nanoparticles exhibited any effect on LRP/LR levels after a 48 hour treatment with 1% and 5% (v/v) of the empty and LRP nanoparticles on HEK 293 cells (Figure 21). The HEK293 cells showed a significant increase in LRP levels by 39% and 17%, respectively, when treated with 1% and 5% (v/v) LRP nanoparticles as compared to the untreated samples (Figure 21. A).

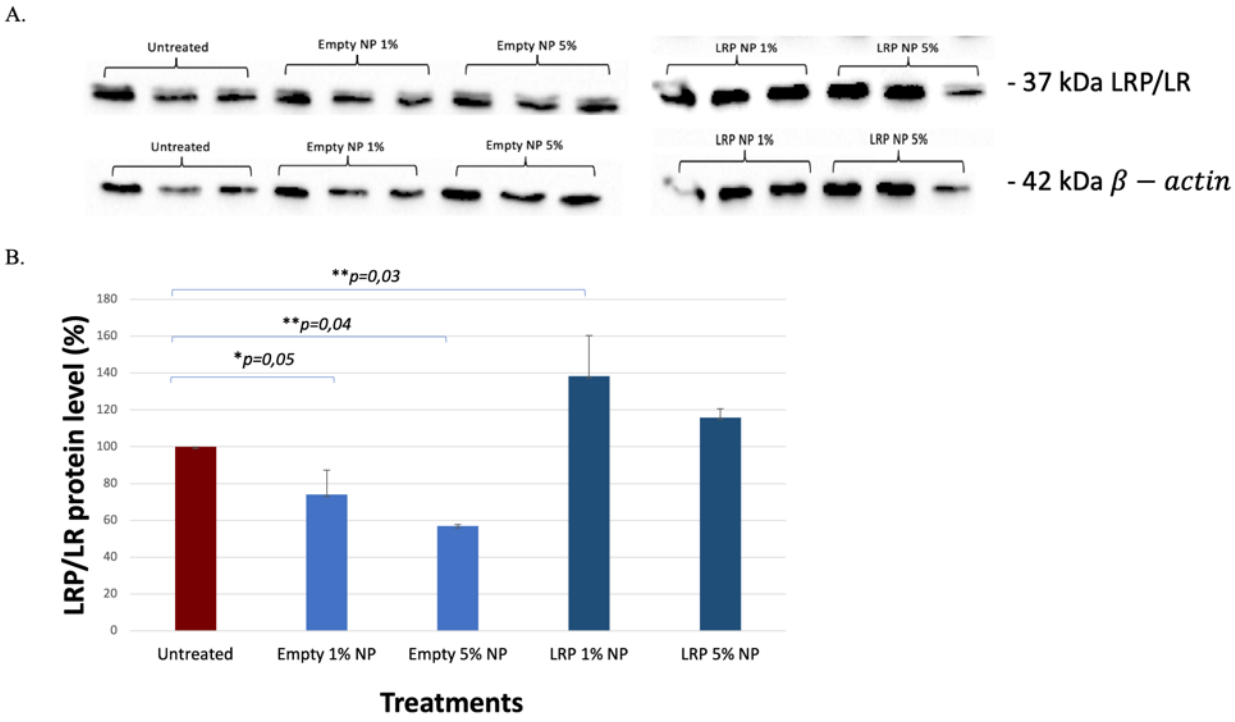

Figure 21. Determination of total LRP/LR levels in HEK293 cells after treatment with empty and LRP-encapsulated PLGA nanoparticles. *Western blotting (A) with densitometric analysis (B) indicates a significant increase in LRP levels after a 48-hour treatment of HEK23 cells with 1% and 5% (v/v) LRP PLGA nanoparticles. Analysis revealed that 1% and 5% (v/v) LRP nanoparticle treated cells resulted in a 39% and 17% increase of LRP/LR (B). Untreated is set to 100%, with all samples expressed as a percentage of the untreated samples. Standard deviation is shown by the error bars, n = 3 biological repeats. *p<0.05, **p<0.01 and ***p<0.001; Students t-test.*

5.3.2. LRP PLGA nanoparticles exhibit a higher cell viability than empty PLGA nanoparticles in treated SH-SY5Y cells

Since the LRP PLGA nanoparticles exhibited an increase in LRP levels, confirming the presence of exogenous LRP (Figure 21), the empty and LRP PLGA nanoparticles were thereafter assessed on cell viability in neuronal SH-SY5Y cells. The cells were treated with a 1%, 5%, and 10% (v/v) of empty and LRP nanoparticles and assessed by MTT cell viability assay to determine the minimum concentration at which the nanoparticles are cytotoxic (Figure 22).

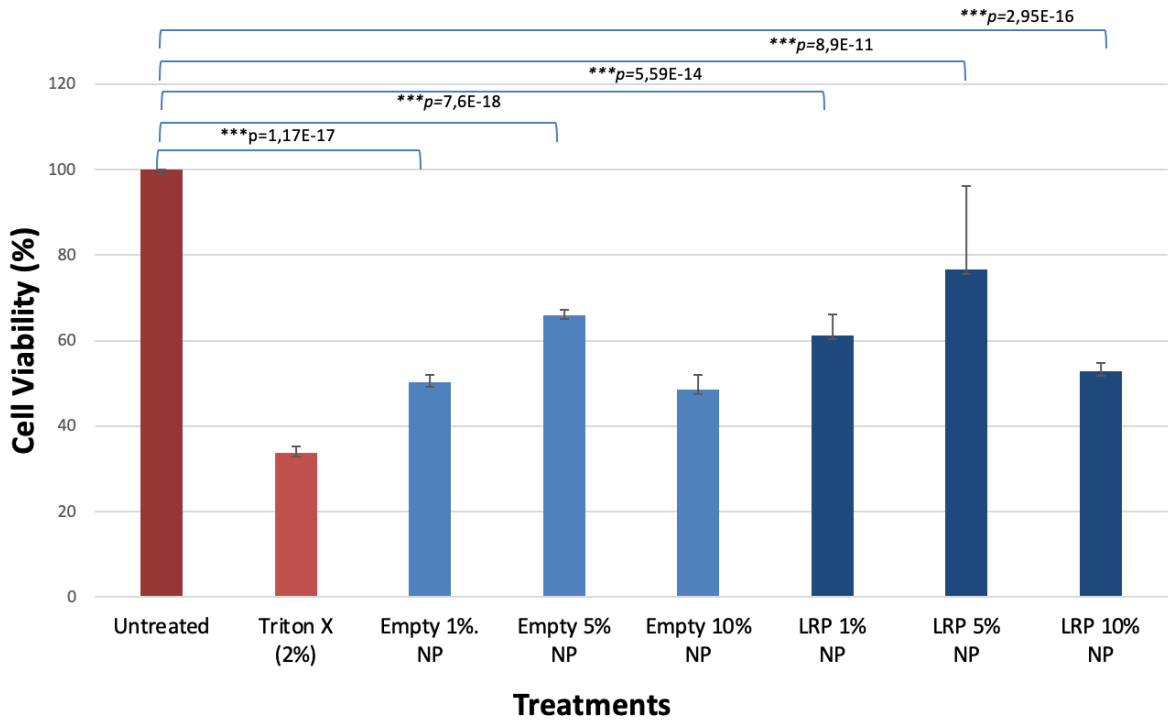

Figure 22. LRP nanoparticle treatments increase SH-SY5Y cell viability as compared to empty nanoparticle treatments. *Initially, all data was normalized and calculated relative to untreated SH-SY5Y sample data. Briefly, quantitative analysis of cell viability indicated that empty nanoparticle treated SH-SY5Y maintains a lower level of cell viability compared to LRP nanoparticle treated SH-SY5Y at increasing concentrations of nanoparticles. Firstly, 1% LRP nanoparticle treatments maintained a 20% higher cell viability compared to 1% empty nanoparticle treatment. Secondly, 5% LRP nanoparticle treatments maintained a 40% higher cell viability compared to 5% empty nanoparticle treatment. Finally, 10% LRP nanoparticle treatments maintained a 9% higher cell viability compared to 10% empty nanoparticle treatment. Standard deviation is shown by the error bars, n = 3 biological repeats. *p<0.05, **p<0.01 and ***p<0.001; Students t-test.*

The neuronal SH-SY5Y cells exhibited a significant increase in cell viability after a 48-hour treatment with the 1%, 5%, and 10% (v/v) LRP PLGA nanoparticles as compared to the cells treated with empty 1%, 5%, and 10% (v/v) empty PLGA nanoparticles. Subsequently, the SH-SY5Y cells treated with 1% (v/v) LRP nanoparticle exhibited a 20% increase in cell viability as compared to the cells treated with 1% (v/v) empty PLGA nanoparticles. Secondly, the 5% (v/v) LRP PLGA nanoparticle treatment maintained a 40% higher cell viability as compared to the 5% (v/v) empty PLGA nanoparticle treated cells. Lastly, when treated with 10% (v/v) LRP PLGA nanoparticles, the SH-SY5Y cells maintained a 9% higher

cell viability compared to the 10% (v/v) empty PLGA nanoparticle treated cells. This therefore indicates that the LRP PLGA nanoparticles have a significant effect on the viability of the neuronal cells as compared to the empty PLGA nanoparticles.

5.3.3. Telomerase activity significantly increases in SH-SY5Y cells after LRP PLGA nanoparticles treatment

As mentioned previously, studies have reported that the increase in expression of TERT is proportional to telomerase activity (Counter *et al.,* 1998). Research has exhibited that LRP::FLAG overexpression enhances expression of hTERT and telomerase activity, and decreases intracellular $A\beta_{42}$ levels and shedding, therefore playing a neuroprotective role by rescuing cells from $A\beta_{42}$ induced cytotoxicity (Otgaar *et al.,* 2017; Bignoux *et al.,* 2019). Thus, telomerase activity was assayed via qPCR in cells treated with 1% and 5% (v/v) empty and LRP encapsulated PLGA nanoparticles. Since there was an effect on cell viability in SH-SY5Y cells, only percentages below 5% (v/v) of nanoparticles will be used for future *in vitro* and *in vivo* treatments. Telomerase activity was represented as ΔCq which is the difference between the Cq value of a gene of interest and the average of the Cq values of the reference genes.

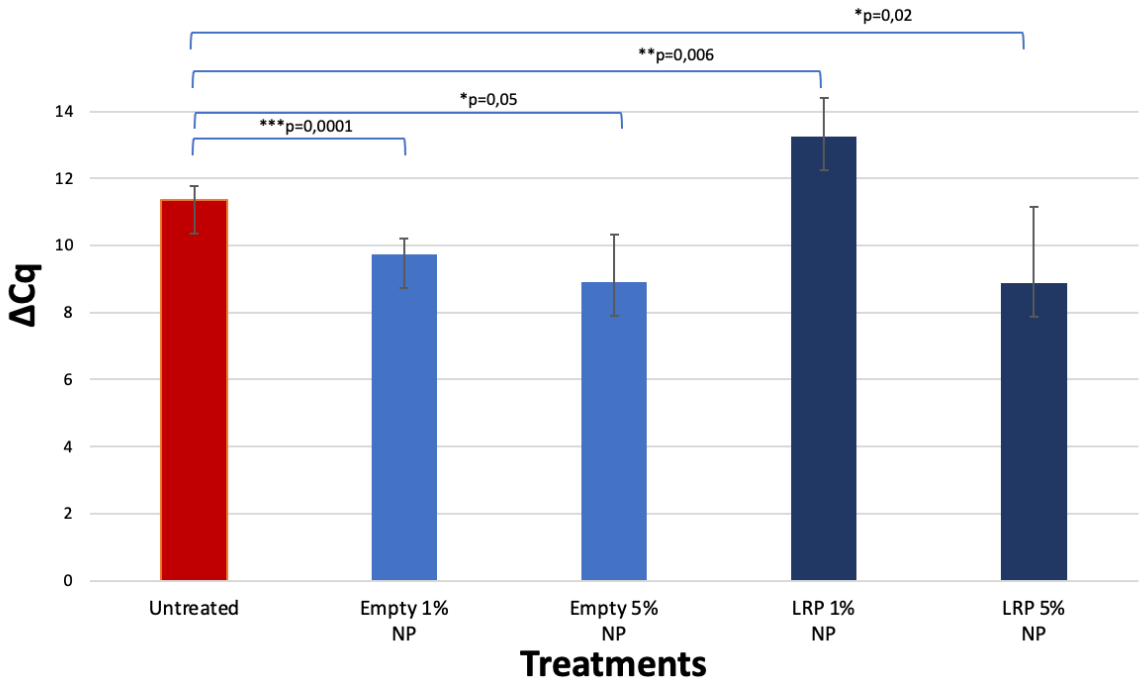

Figure 23. LRP nanoparticle treatments increases telomerase activity in SH-SY5Y cells. ΔCq is significantly increased in the SH-SY5Y cells treated with 1% (v/v) LRP PLGA nanoparticles as compared to the 1% and 5% (v/v) empty PLGA nanoparticles. All values were standardized by subtracting the negative control values from the signal of each sample. The presented data represents the mean value obtained from all biological repeats for each treatment. Standard deviation is shown by the error bars, n = 3 biological repeats. *p<0.05, **p<0.01 and ***p<0.001; Students *t*-test.

Upon quantification of the telomerase activity in the SH-SY5Y (Figure 23), it was revealed that the 1% LRP PLGA nanoparticle treatment exhibited a higher telomerase activity as compared to the untreated cells. Additionally, it was shown that the 1% and 5% (v/v) empty and 5% (v/v) LRP PLGA nanoparticle treated SH-SY5Y cells had a significantly reduced telomerase activity in comparison to the untreated cells.

6. Discussion

6.1. LRP::FLAG *in-vitro* study

LRP/LR is a transmembrane protein that binds to laminin 1, a major component of the extracellular matrix (Mbazima *et al*., 2010). This laminin receptor is involved in a variety of cellular processes including cell migration, adhesion and invasion, as well as signalling pathways which regulate cell proliferation and survival (Chetty *et al.,* 2014). LRP/LR has been implicated in a variety of diseases including cancer, prion disorders, neurodegenerative diseases and ageing (Rao *et al.,* 1989; Zuber *et al*., 2008; Omar *et al.,* 2012; Naidoo *et al.,* 2015; Otgaar *et al.,* 2017). *In-vitro* studies have revealed that the overexpression of LRP::FLAG increases hTERT expression which concurrently decreases telomerase activity while rescuing cells from Aβ-mediated cytotoxicity. Cuttler *et al.* also revealed that LRP::FLAG overexpression decreased phosphorylated tau levels with a concomitant decrease in tauopathy-related proteins. Within PD, *in vitro* studies demonstrated that LRP/LR plays a protective role, through the degradation of α-synuclein and rescuing cells from MPP^+ cytotoxicity. Hence, the role of LRP overexpression in AD and PD was further investigated to elucidate if the overexpression of LRP can provide a novel and potentially effective therapeutic for these diseases. Here, western blotting was performed to assess the effect of LRP::FLAG overexpression on LRP/LR and PINK1 protein levels, as well as the resultant effect on cell viability after treatment with MPP^+, TBHP and $A\beta_{42}$ by MTT analysis.

6.1.1. LRP::FLAG overexpression increases LRP and PINK1 protein levels

The HEK293 cell line was utilized to explore the involvement of LRP/LR in PD and AD. HEK293 cells are often employed in neurological research due to their expression of neuronal markers and their transfectability (Schlachetzki *et al.,* 2013). Briefly, the HEK293 cells were stably transfected using the pCIneo-moLRP-FLAG expression plasmid which increased the total level of LRP within the HEK293 cells (Figure 8). Furthermore, western blot analysis was performed to assess endogenous levels of LRP /LR and PINK1 in the HEK293 control line and the LRP::FLAG transfected HEK293 cells.

After analysis of western blotting it was revealed that LRP::FLAG overexpression significantly elevated LRP/LR and PINK1 protein levels in the HEK293 cells by 11.7% and 8.3%, respectively (Figure 9). The signalling pathway of PINK1/PARKIN is required for the process of mitophagy, which involves the removal dysfunctional mitochondria (Valente *et*

al., 2004; Martin Maestro *et al.,* 2016). The PINK1 protein accumulates in the outer mitochondrial membrane (OMM) in response to a reduced mitochondrial membrane potential (MMP) due to mitochondrial dysfunction/damage (Sugiuria *et al.,* 2014). Subsequently, the accumulation of PINK1 recruits PARKIN from the cytosol to the OMM, where the protein initiates mitophagy via ubiquitination of the mitochondrial protein, resulting in mitochondrial degradation of dysfunctional mitochondria. Many studies indicate that PINK1/PARKIN signalling defects are present in PD and AD (Ye *et al.,* 2015). Therefore, the previously mentioned 8.3% increase in PINK1 protein levels (Figure 9) could have led to increased mitophagy of dysfunctional mitochondria, thereby reducing oxidative stress and cell death (Yang *et al.,* 2006). Thus, LRP/LR could play a neuroprotective role in AD and PD through recruitment of the PINK1/PARKIN signalling pathway. To further investigate the role of LRP/LR in neurodegenerative diseases, cell viability assays were performed on cells treated with MPP^+, TBHP and $A\beta_{42}$ which induce AD and PD like states.

6.1.2. LRP::FLAG overexpression rescues cells from MPP^+ induced cytotoxicity

The neurotoxin, MPP^+ is a harmful substance that blocks complex I in the mitochondrial electron transport chain, this results in a reduction of ATP and eventual death of cells. It is formed as a toxic by-product of MPTP and contributes to PD by destroying dopamine-producing neurons in the substantia nigra (Davis *et al.,* 1979). To investigate how LRP::FLAG overexpression affects cell survival in HEK293 cells exposed to MPP^+, a MTT assay was performed on both treated non-transfected and treated LRP::FLAG transfected cells. The results showed that LRP::FLAG overexpression improved cell viability when compared to MPP^+ treated non-transfected cells. Indeed, compared to the MPP^+ treated non-transfected cells, the LRP::FLAG overexpressing cells treated with 250 µM and 500 µM of MPP^+ exhibited a higher cell viability (Figure 10). According to a study conducted by Gomez-Santos *et al.* in 2002, there was an observed increase in α-synuclein expression in the substantia nigra of rodents with parkinsonism who were treated with MPTP. As noted earlier, the interaction between the CTD and NTD of α-synuclein is crucial in preventing its aggregation. The CTD helps maintain the structure of the full-length α-synuclein, preventing conformational changes that contribute to abnormal aggregation and the development of PD pathology (Hong *et al.,* 2011). The unpublished findings of Burns *et al*. 2021, suggest that overexpressing LRP::FLAG leads to an increase in the α-synuclein CTD. Furthermore, the observed increase in cell viability in MPP+ treated cells that also overexpressed LRP::FLAG

may indicate that the CTD of α-synuclein has a protective effect. These findings suggest that the observed increase in the CTD of α-synuclein following LRP::FLAG transfection may have a rescuing effect on cells exposed to MPP^+, potentially due to the ability of the CTD to prevent aggregation.

Furthermore, a study performed by Verma *et al.* (2020) recently found that a low and chronic dose administration of MPP^+ dysregulates mitophagy and mitochondrial function caused by the depletion of endogenous PINK1 expression. Parkin has also been known to aid in the degradation of α-synuclein and intriguingly, it was shown that parkin levels increase following overexpression of LRP::FLAG (Madhav *et al*, unpublished). The exhibition of the higher cell viability in LRP::FLAG transfected cells, suggests that LRP may rescue cells from the MPP^+ induced cytotoxicity by the neuroprotective signaling between PINK1/PARKIN.

6.1.3. Overexpression of LRP::FLAG rescues HEK293 cells from $A\beta_{42}$ and ROS-induced cytotoxicity

There are key enzymes which form part of the antioxidant system that prevents oxidative stress, and during the progression of AD these enzymes become dysregulated as a result of the accumulation of $A\beta_{42}$ peptides within the mitochondria, contributing to the accumulation of ROS and oxidative stress (Cheignon *et al.*, 2018). It has been established that the accumulation of intracellular $A\beta_{42}$ and NFTs results in cytotoxicity within neuronal cells. (Caetano *et al.,* 2011). Additionally, the $A\beta_{42}$ peptides display the ability to penetrate the mitochondrial membrane and accumulate inside the mitochondria (Hu *et al.,* 2018) which initiates mitochondrial dysfunction and increased production of ROS. Ultimately, this leads to neuronal cell death, intensifying AD progression. Interestingly, studies have shown that TERT gene overexpression can reduce ROS levels through increasing the ratio of reduced to oxidized glutathione (GSH:GSSG) (Indran *et al.,* 2011). In addition to the function TERT plays in ROS regulation, it also has a catalytic subunit of telomerase which is a protein responsible for telomere maintenance and elongation (Kim *et al.,* 1994). Research has shown that AD patients present shorter telomeres lengths (Wang *et al.,* 2015). Recently, it has been demonstrated that enhanced LRP levels results in an increase in telomerase activity and telomere maintenance (Otgaar *et al.,* 2017). Subsequently, this may suggest that LRP::FLAG

overexpression elevates TERT expression levels and telomerase activity while reducing overall ROS levels.

Thus, in order to confirm that the overexpression of LRP::FLAG can maintain viability of cells when exposed to a ROS inducer, an MTT assay was conducted. The results of the experiment showed that cells transfected with LRP::FLAG had a greater viability than non-transfected cells, at all three TBHP concentrations (as shown in Figure 11). These findings indicate that overexpression of LRP::FLAG can prevent the damaging effects of ROS-induced oxidative stress, and thereby improve cellular viability by protecting cells from ROS-induced cytotoxicity. This finding is consistent with previous studies and the hypothesis that increased levels of TERT can protect genomic DNA from damage caused by ROS by promoting the elongation of telomeres and reducing ROS production. Although the exact mechanisms that explain this protective role are not yet fully understood, previous research provides some possible explanations. For instance, it has been observed that when TERT is translocated to the mitochondria, it interacts with mtDNA genes that are responsible for synthesizing subunits 1 and 2 (ND1 and ND2) of the ETC complex I (NADH:ubiquinone oxidoreductase) (Haendeler Judith *et al.,* 2009). Recent research has revealed that ETC complex I is the primary site for ROS production (Galkin and Brandt, 2005). Based on this finding, it is postulated that the interaction between ND1 and ND2 genes with TERT may lead to the formation of a new ETC complex I that functions normally, thereby preventing ROS production and avoiding mitochondrial dysfunction. Essentially, this finding further supports the hypothesis that overexpression of LRP::FLAG and subsequent increase in TERT levels can improve cell viability when exposed to ROS-induced cytotoxicity.

Research has shown that LRP/LR functions as a receptor for $A\beta_{42}$ peptides, according to Da Costa Dias *et al.* 2013 and is involved in the intracellular uptake and build-up of $A\beta_{42}$ (Jovanovic *et al.,* 2014). Furthermore, exposing cells to 500 nM of synthetic $A\beta_{42}$ has been found to mimic the cytotoxicity associated with $A\beta_{42}$ (Da Costa Dias *et al.,* 2014). To investigate whether transfection with LRP::FLAG had an impact on the viability of HEK293 cells exposed to cytotoxic levels of $A\beta_{42}$, an MTT assay was conducted. Interestingly, there was a higher cell viability in the HEK293 transfected cells (Figure 12) as compared to non-transfected cells. Thereby, indicating that LRP::FLAG overexpression rescued the cells from cytotoxicity caused by $A\beta_{42}$. Previous studies have observed the overexpression of

LRP::FLAG resulted in an increase in TERT levels and telomerase activity, with a subsequent reduction in intracellular $A\beta_{42}$ levels and $A\beta_{42}$ shedding (Bignoux *et al.,* 2019). Previous studies, as reported by Da Costa Dias *et al.* (2013) and Otgaar *et al.* (2017), have exhibited co-localization of LRP/LR with hTERT and $A\beta_{42}$ in HEK293 cells. It is suggested that hTERT's ability to interrupt the apoptotic cascade is due to its involvement in adding TTAGGG repeats onto the telomeric ends of chromosomes. This explanation is supported by the fact that telomerase inhibitors can induce apoptosis while telomerase can increase cell viability (Chin *et al.,* 1999). Previous research suggests that TERT can prevent caspase activation before mitochondrial dysfunction occurs and can interact with the tumour suppressor protein p53 through TEP-1 (telomerase-associated protein), both which play a role in the regulation of cell viability (Li *et al.,* 1999).

Furthermore, the 37 kDa LRP has been found to influence cell signalling, through the involvement in the progression of the cell cycle. It has been demonstrated that LRP plays a role in the progression from the Gap phase (G1) to the synthesis phase (S phase) (Scheiman *et al.,* 2010). Additionally, it has been revealed that LRP may be involved in anti-apoptotic signalling, through the suppression of cycle dependent kinase inhibitors such as p21 and surviving (anti-apoptotic protein). Studies have also shown that LRP plays a role in the induction of the mitogen activated protein kinase (MAPK) signalling pathway, which subsequently further regulates cell replication and viability (Givant-Horwittz *et al.,* 2004). Thereby, further indicating that LRP::FLAG overexpression may have assisted in increased in cell survival/viability and proliferation under a cytotoxic environment.

6.2. The structure of 37 kDa LRP protein

As mentioned previously, it is crucial to investigate and understand the structure of the 37 kDa LRP protein on all levels to gain more insight into how the protein is involved in the prevention and impediment of AD and PD. Additionally, the translation of this research to an *in vivo* investigation requires the use of isolated pure 37 kDa LR protein and an effective delivery system. Thus, the second part of this study aimed at overexpressing, purifying, and determining the biophysical characterisations of the protein structure of 37 kDa LRP.

6.2.1. 37 kDa LRP expression and purification

To purify and better understand the structural characterisation of LRP, the full length protein was overexpressed in *E.coli.* A previous study conducted by Jamieson *et al.,* 2008, successfully purified and crystalised the LRP construct containing residues 1-220 (LamR220) (Jamieson *et al.,* 2008). The LamR220 version was used as it could be purified in amounts suitable for crystallization trials, unlike the full length construct of LRP (1-295 residues). Here, this section of the study focused on successfully overexpressing and purifying the 37 kDa (1-295 residue) LRP protein, to produce large amounts of the isolated therapeutic protein for PLGA nanoparticle encapsulation.

Initially, overexpression trials aimed at identifying the optimal conditions for the expression of LRP. It is crucial to optimise these conditions to achieve maximum protein yield without compromising the protein folding, structure, and stability. Two different conditions were trialed using two different concentrations of IPTG. IPTG is a known inducer; it is used to increase galactosidase activity by binding and inhibiting the repressor from the lac operon, thus inducing gene expression (Guzman *et al.,* 1995). Studies revealed that decreasing the concentrations of IPTG can enhance the production of soluble and stable protein (Turner *et al.,* 2005). After induction with 1.0 mM IPTG, incubated at 20°C and at 230 rpm, samples were collected at intervals of 4 hours, 6 hours, 8 hours, and 12 hours. The SDS-PAGE gel (Figure 13 (A)) exhibited higher intensity bands in the pelleted samples which indicated that the protein was highly insoluble, yet at a low concentration. Therefore, a lower concentration of 0.3 mM IPTG was trialed, and a higher concentration of protein was obtained after 8 hours of overexpression, however the protein was still insoluble (Figure 13 (B)). Thus, it was decided that the protein would be overexpressed with a lower concentration of IPTG to produce a higher yield of protein even though it was insoluble.

The solubility of a protein is compromised if the construct includes a transmembrane-spanning region. This is due to the hydrophobic nature and propensity to aggregate and form inclusion bodies (Mohanty and Wiener, 2004). The 37 kDa LRP has a transmembrane region residing in residues 86-105 (Rao *et al.,* 1989), comprising of an α-helical stretch packed against the central structure and a β-strand which forms part of the core β-sheet (DiGiacomo *et al.,* 2016). Thus, due to the challenges associated with the nature of transmembrane

proteins including their insolubility and association with the cell membrane, a detergent solubilisation method was employed to extract soluble protein. This approach involved using detergents to solubilise proteins by disrupting the lipid bilayer and releasing the protein into solution (Lichtenberg *et al*, 2013). Here, the protein was subjected to an extraction protocol where the insoluble 37 kDa LRP was recovered from the cell lysate by low-speed centrifugation (5000 xg) and subsequently, washed with 5% Triton X-100 (w/v). Upon extraction, the resultant SDS-PAGE gel (Figure 14. A and B) indicated that the supernatant collected from wash 1C (W1C) (Figure 14. A) to wash 1E (W1E) (Figure 14. B), contained high yields of soluble 37 kDa LRP. Triton X-100 is a non-ionic detergent which solubilizes protein through the interaction with the hydrophobic regions of the protein (Hare and Holocher, 1994). Triton X-100 is composed of a hydrophobic tail and a hydrophilic head. When added to membrane bound proteins, the detergent molecules interact with the hydrophobic regions of the protein, disrupting the lipid bilayer and releasing it into solution. The detergent molecules then form micelles around the solubilized protein, allowing the hydrophobic regions of the protein to be shielded from water (Schnaitman *et al.,* 1971). As seen in figure 14, a high protein yield was obtained, however, multiple contaminating bands were present, thus, a purification method was employed.

Subsequently, to purify the 37 kDa LRP, the soluble lysate was loaded onto an IMAC column resulting in the flow through of any unbound contaminating proteins. Nickel and cobalt are commonly used metals for purification of histidine-tagged proteins, including transmembrane proteins, through IMAC. Both nickel and cobalt have similar properties and can bind to histidine tags with high affinity (c). However, there are some differences between the metals which may affect their use in purification. Nickel has a higher affinity for histidine tags, as compared to cobalt, thus, it can bind more tightly to the protein, resulting in a higher yield of purified protein (Vançan *et al.,* 2002). Initially, the LRP soluble lysate was loaded onto a nickel IMAC column, and the resultant SDS PAGE gel (Figure 15) revealed that the LRP protein was not completely pure as the eluted fraction contained a few contaminating bands as seen in the elution lane (E3)(Figure 15. A; lane 6). The high levels of non-specifically bound proteins could be accounted for by the low specificity with which histidine-tags bind Ni^{2+}. This is because the nickel-resin has less spatial requirements in its reactive core, thus, binding not only the protein's polyhistadine tag, but also the histidine residues (Bornhorst *et al.,* 2000) Therefore, the soluble lysate was purified using a Co^{2+}-IMAC resin (Figure 16) and although a lower yield of LRP was obtained, less non-specific binding was observed.

Cobalt has a lower affinity for histidine tags than nickel, resulting in a lower protein yield but higher protein purity (Bornhorst *et al.,* 2000) (Figure 16 A: lane 8/9/10).

The samples collected from the Co^{2+}-IMAC were quantitatively and qualitatively assessed using SDS-PAGE (Figure 16. B). The resultant gel showed an anomalous shift in molecular weight, where the molecular weight of LRP was $\approx 47\ kDa$. It has been previously described by Alqahtani *et al.* 2014 that the 37 kDa LRP shows an anomalous electrophoretic mobility at the mass of $\approx 44\ kDa$ (Alqahtani *et al.,* 2014). Studies have shown that membrane proteins have an uncharacteristic migration on SDS-PAGE but has yet to be conclusively explained. It is proposed that the transmembrane sequence of membrane proteins contains helical regions that are embedded within the SDS micelle interior, resulting in a 2-fold greater amount of SDS loading, which has been linked to the abnormally higher molecular weight (Imamura *et al.,* 2002). Thus, using the human anti-LRP/LR IgG-iS18 antibody, a western blot was performed to confirm the presence of the 37 kDa LRP protein and it was observed that the 37 kDa LRP and 67 kDa LRP protein was present in the IMAC eluted fractions (Figure 17). This further confirmed that the 37 kDa LRP protein was purified, despite the higher molecular weight.

Finally, after obtaining the 37 kDa LRP, absorbance spectroscopy was used to determine the protein concentration and to determine if the protein contained nucleic acid contamination. Figure 18 shows an absorbance spectrum that is typical of a protein absorbance spectrum. There is a peak at 280 nm due to the presence of aromatic amino acids (tyrosine, tryptophan and phenylalanine) which absorb at 280 nm. Furthermore, the absorbance at 280 nm was used to calculate the protein concentration of 12.6 µM using the extinction coefficient of 67045 $M^{-1}.cm^{-1}$. There is a shoulder at 295 nm due to the presence of the tryptophan residues which exclusively absorb at 295 nm. The absence of an absorbance at 340 nm indicated that the protein was free from aggregation. Nucleic acids absorb at 260 nm, the A_{280}/A_{260} ratio is 1.54 indicating that the protein is sufficiently free from nucleic acid contamination. (Figure 18). Therefore, the protein overexpression and purification was successful, and it could therefore be used for downstream applications.

6.2.2. 37 kDa LRP structural determination

To incorporate the 37 kDa LRP in nanoparticle production, it was crucial to analyse its properties such as structure and stability. The objective was to verify whether the protein retained its native and active state following the process of overexpression and purification. Initially, the tertiary structure of the 37 kDa LRP was investigated using ITF. In order to verify that the protein had been properly folded, the ITF spectrum was measured both in the presence and absence of a denaturant, 8 M urea, following excitation at 295 and 280 nm. The spectrum of the native protein (in the absence 8 M urea) showed a peak at 345 nm indicating that the tryptophan residues are in the hydrophobic interior of the protein. However, the ITF emission spectrum of the unfolded protein (presence of 8 M urea) showed a single peak at 350 nm. In the presence of urea, the emission maximum is shifted by 5 nm (Figure 19). The crystal structure indicates that the 37 kDa LRP protein contains 10 tryptophan residues which are mainly buried in the hydrophobic core of the protein (Jamieson *et al.,* 2008; Jamieson *et al.,* 2011). This bathochromic shift indicates that the tryptophan residues in the native protein were in a hydrophobic environment and is evidence that the protein was correctly folded during overexpression. If the native protein was unfolded, a bathochromic shift would not occur in the presence of urea.

Furthermore, the secondary structure of the protein was investigated using far-UV CD spectrum (Figure 20). The far UV circular dichroism spectrum was obtained by normalizing the circular dichroism signal (millidegrees) to mean residue ellipticity (MRE), which accounts for protein concentration and the amount of amino acids present. The far-UV CD spectrum of α-helical protein has troughs at 208 nm and 222 nm, and a peak at around 190 nm (Greenfield, 2006). The spectra obtained for the 37 kDa LRP exhibits a trough at 207 nm and a peak at 190 nm, thus, indicating that the protein is predominantly an α-helical protein, as mentioned in previous studies (DiGiacomo *et al.,* 2016). Ould-Abeih *et al.* (2012) demonstrated, by circular dichroism spectrometry, that the NTD, aa 1–209 of LRP is globular, made up of a central β-sheet flanked by α-helices, whereas the CTR, aa 210–295 is intrinsically disordered. The purification and characterisation of the 37 kDa LRP was therefore successful, indicating that the protein was correctly folded and functional and could subsequently be encapsulated in PLGA nanoparticles.

6.3. Assessment of LRP PLGA nanoparticles

Nanotechnologies have become increasingly popular in biomedical applications, specifically for the treatment of neurogenerative disorders, such as AD and PD since these polymers have the ability to cross the BBB due to their adjustable architecture (Leyva-Gomez *et al.,* 2015). Specifically, polymers have demonstrated the ability to improve localised targeted delivery of therapeutics. The encapsulation of drugs in polymers have shown to be more successful than freely delivered drugs as encapsulation allows for a longer half-life (Su and Kang, 2020). In particular, PLGA exhibits ideal physicochemical characteristics of a nanotechnology delivery system, including their biocompatibility, low cytotoxicity, and sustained release of their contents (Leyva-Gomez *et al.,* 2015). Furthermore, it has been shown that small molecules such as nucleic acid and proteins encapsulated in PLGA exhibit enhanced effectiveness in various disease-related applications (Makadia *et al.,* 2011). There has been numerous *in vitro* studies exhibiting the potential use of LRP::FLAG overexpression as a therapeutic for AD and PD, however, the translation of this research *in vivo* requires the employment of an effective delivery system. Hence, this part of the study focused on investigating the effect of empty and LRP encapsulated nanoparticles on cell viability, LRP levels, and telomerase activity in HEK293 and SH-SY5Y cells.

6.3.1. LRP PLGA nanoparticle treated cells exhibit an increase in LRP protein levels in HEK293 cells

Initially, the PLGA nanoparticle production was optimised on empty nanoparticles to ensure that smooth, uniformly sized and spherical nanocapsules within the 200-500 nm size range were obtained. Thereafter, once the LRP protein was purified and isolated, the synthesis of the LRP encapsulated nanoparticles was optimised and compared to empty nanoparticles. Firstly, after encapsulation of LRP in PLGA nanoparticles, the exogenous levels of LRP were investigated, to confirm that the LRP encapsulation was successful. Therefore, western blotting was performed on HEK293 cells which were treated with 1% and 5% (v/v) of empty and LRP encapsulated nanoparticles, and assessed for LRP/LR protein levels. After a 48 hour treatment, the HEK293 cells showed a significant increase in LRP/LR levels by 39% and 17%, respectively, when treated with 1% and 5% (v/v) LRP nanoparticles as compared to the untreated samples (Figure 21. A). Interestingly, the 1% (v/v) LRP nanoparticle treatment exhibited a higher LRP protein level as compared to the 5% (v/v) LRP nanoparticle treatment. There could be several reasons for this, however, one possibility could be that the

physical characteristics such as size and shape of the 5% (v/v) LRP nanoparticles batch may have affected their cellular uptake and drug release. It is possible, that the 1% LRP (v/v) nanoparticles exhibited properties which allowed for more efficient and faster release of the LRP/LR as compared to the 5% (v/v) LRP nanoparticles, however, this would need to be further investigated (Liu *et al.,* 2017). Subsequently, there was a significant increase in LRP/LR protein levels as compared to the empty nanoparticles which reveals that the encapsulated LRP/LR had been released following the 48 hour treatment.

6.3.2. LRP PLGA nanoparticles increases viability of SH-SY5Y cells

After confirming that LRP was successfully encapsulated, the effect of empty and LRP-encapsulated nanoparticles on cell viability was subsequently assessed. The SH-SY5Y cell line is commonly used for neurological studies because they exhibit many of the characteristics of neurons in the brain such as the presence of neurotransmitter receptors and the ability to form synapses (Schlachetzki *et al.,* 2013). Therefore, the cell line was treated with 1%, 5%, and 10% (v/v) of empty and LRP encapsulated nanoparticles and assessed via MTT cell viability assay (Figure 22). After a 48-hour treatment period, there was a significant increase in cell viability in the SH-SY5Y cells treated with varying percentages of LRP-encapsulated nanoparticles compared to those treated with empty PLGA nanoparticles. Specifically, the cells treated with 5% (v/v) LRP PLGA nanoparticle treatment maintained a 40% higher cell viability as compared to the 5% (v/v) empty PLGA nanoparticle treated cells. While the nanoparticles did not affect the viability of SH-SY5Y cells at high concentrations, it was observed that 5% (v/v) was the optimal concentration. Therefore, nanoparticle concentrations of 5% (v/v) (volume nanoparticles/blood volume) and below will be used for *in vivo* treatments. Studies have demonstrated that the surface morphology, particle size range and concentration of nanoparticles are important, as these factors can affect the drug release as well as the foreign body response *in vivo* (Xiong *et al.,* 2013). Cytotoxicity has been found to be correlated with the concentration of nanoparticles that the cells are exposed to. In this study, when the SH-SY5Y cells were exposed to 1%, 5%, and 10% (v/v) of nanoparticles, no toxic effects were observed. Furthermore, a similar pattern was observed in HEK293 cells treated with 1%, 5%, and 10% (v/v) empty and LRP-encapsulated PLGA nanoparticles where a significant increase in cell viability was observed in cells treated with LRP encapsulated nanoparticles as compared to cells treated with the empty PLGA nanoparticles (Bernert *et al.,* 2022, in preparation). This suggests that the morphology, size,

and concentration of the LRP encapsulated nanoparticles are optimal for delivery of the therapeutic.

6.3.3. LRP PLGA nanoparticles significantly increase telomerase activity in SH-SY5Y cells

As noted earlier, Otgaar *et al.* (2017) found that overexpression of LRP::FLAG led to an upregulation of TERT expression, accompanied by an increase in telomerase activity and lengthening of telomeres (Otgaar *et al.,* 2017). There is a suggestion that TERT has a role in decreasing the levels of ROS, apoptosis and mtDNA damage. It has been observed that during AD pathology, TERT is present in the mitochondria of neurons which indicates that TERT may help to lower ROS levels and enhance the functioning of the respiratory chain (Cong and Shay, 2008). Furthermore, numerous studies have found that mitochondrial dysfunction is a pathogenic hallmark that occurs prior to the formation of amyloid plaques. While the mechanisms are not fully understood, studies have shown that mitochondrial dysfunction increases ROS production, thereby increasing $A\beta_{42}$ accumulation (Lee *et al.,* 2017). Previous research by Wang *et al.* (2015) has demonstrated an antagonistic relationship between $A\beta_{42}$ and telomerase activity. Furthermore, it has been shown that overexpression of LRP::FLAG can decrease $A\beta_{42}$ levels (Bignoux *et al*., 2019), the telomerase activity of the empty and LRP-encapsulated PLGA nanoparticles were assessed. The telomerase activity was assayed via qPCR in the SH-SY5Y cells that were treated with 1% and 5% (v/v) empty and LRP-encapsulated PLGA nanoparticles. Here, it was established that the 1% (v/v) LRP PLGA nanoparticle treatment exhibited a higher telomerase activity as compared to the untreated cells. This correlates with previous studies that have shown that LRP::FLAG overexpression increased hTERT levels and telomerase activity (Otgaar *et al.,* 2017). LRP has been shown to play a role in TERT translational processing by interacting with the ribosomal complex. Furthermore, elevated TERT levels are caused by LRP interaction with the nuclear envelope, which allows chromatin remodelling, exposing the TERT gene and leading to increased transcription (Sato *et al.,* 1996). Overall, the results indicated that the LRP-encapsulated nanoparticles increased telomerase activity and viability and could thus be a possible therapeutic for conditions related to cellular degeneration and decreased telomerase activity such as ageing and age-related diseases including AD and PD.

7. Conclusion

Conclusively, the first part of the study confirms that the overexpression of LRP::FLAG in HEK293 cells provides a potentially effective treatment for AD and PD. It was shown that the overexpression of LRP::FLAG increased LRP/LR and PINK1 protein levels. Furthermore, the overexpression of LRP::FLAG rescued cells from MPP^+, $A\beta_{42}$, and ROS-induced TBHP cytotoxicity. Thus, confirming the potential role in which LRP/LR may play in neuroprotection and as a therapeutic for neurodegenerative diseases.

The *in vitro* overexpression of LRP::FLAG in previous studies (Bignoux *et al.,* 2019; Cuttler *et al.,* 2019) and the current study presented an opportunity to test the LRP protein *in vivo*. However, prior to testing *in vivo*, the protein had to be isolated and encapsulated. Therefore, the second part of this study aimed to overexpress, purify, and characterize the 37 kDa LRP. Initially, optimal conditions for overexpression were determined using two different concentrations of IPTG (1.0 mM and 0.3 mM). Although a higher concentration of protein was obtained with 0.3 mM of IPTG after 8 hours of overexpression, the protein remained insoluble. Therefore, to extract the soluble protein, a detergent extraction method was employed using 0.5% Triton X-100 due to the challenges associated with transmembrane proteins, including their insolubility and association with the cell membrane. A high yield of the LRP was obtained, but multiple contaminating bands were present, necessitating a purification method. Thus, the soluble lysate was loaded onto an IMAC column, resulting in the flow-through of any unbound contaminating proteins. Initially, a nickel-IMAC column was used, which resulted in a high yield of low purity LRP. Therefore, a cobalt-IMAC column was used, which resulted in a lower yield of LRP but with less non-specific binding. A western blot was performed using the human anti-LRP/LR IgG-iS18 antibody to confirm the presence of the LRP protein, and it was observed that the 37 kDa LRP protein were present in the IMAC eluted fractions, further confirming the purification of the LRP protein despite the higher molecular weight. Finally, absorbance spectroscopy indicated a protein concentration of 12.6 µM and an A_{280}/A_{260} ratio of 1.54.

Moreover, in order to assess whether the 37 kDa LRP retained its native and active state subsequent to the process of overexpression and purification, various characterisation techniques were employed. To examine the tertiary structure of the LRP, ITF was used, while far UV-CD was utilised to investigate the secondary structure. The results revealed that the

protein was properly folded and functionally active, with a secondary structure consisting of α-helices, consistent with existing literature. Therefore, indicating that the LRP protein could be encapsulated in PLGA nanoparticles. PLGA is well-established for the delivery of pharmaceutical agents, such as proteins. PLGA nanoparticles offer several advantages, including controlled release and protection of the protein within their polymeric matrix, which makes them a useful option for drug delivery (Feczkó *et al.,* 2011). Thus, the third part of the study investigated the effect of empty and LRP-encapsulated PLGA nanoparticles on cell viability, LRP levels, and telomerase activity in HEK293 and SH-SY5Y cells. The results showed that LRP-encapsulated nanoparticles had a significant increase in LRP/LR protein levels in HEK293 cells and higher cell viability than empty PLGA nanoparticles in treated SH-SY5Y cells. Additionally, LRP-encapsulated nanoparticles significantly increased telomerase activity in SH-SY5Y cells. These findings suggest that LRP-encapsulated nanoparticles are an effective delivery system for LRP, which has the potential therapeutic for conditions related to cellular degeneration and decreased telomerase activity such as ageing and age-related diseases including AD and PD. Although similar results were obtained in the LRP::FLAG and LRP-encapsulated nanoparticle treatments, future studies would hold interest in assessing the effect of the empty and LRP-encapsulated nanoparticles on cells treated with MPP^+, TBHP, and $A\beta_{42}$.

8. References

Abhilash, M., 2010. Potential applications of Nanoparticles. *International Journal of Pharma and Bio Sciences*, *1*(1), pp.1-12.

Ahmed, S., Passos, J.F., Birket, M.J., Beckmann, T., Brings, S., Peters, H., Birch-Machin, M.A., von Zglinicki, T. and Saretzki, G., 2008. Telomerase does not counteract telomere shortening but protects mitochondrial function under oxidative stress. *Journal of cell science*, *121*(7), pp.1046-1053.

Alqahtani, F., Mahdavi, J., Wheldon, L.M., Vassey, M., Pirinccioglu, N., Royer, P.J., Qarani, S.M., Morroll, S., Stoof, J., Holliday, N.D. and Teo, S.Y., 2014. Deciphering the complex three-way interaction between the non-integrin laminin receptor, galectin-3 and Neisseria meningitidis. *Open biology*, *4*(10), p.140053.

Avila, J., 2006. Tau phosphorylation and aggregation in Alzheimer's disease pathology. *FEBS letters*, *580*(12), pp.2922-2927.

Barratt, G.M., 2000. Therapeutic applications of colloidal drug carriers. *Pharmaceutical Science & Technology Today*, *3*(5), pp.163-171.

Basarkar, A. and Singh, J., 2007. Nanoparticulate systems for polynucleotide delivery. *International journal of nanomedicine*, *2*(3), pp.353.

Beeler, J.A., Frank, M.J., McDaid, J., Alexander, E., Turkson, S., Bernandez, M.S., McGehee, D.S. and Zhuang, X., 2012. A role for dopamine-mediated learning in the pathophysiology and treatment of Parkinson's disease. *Cell reports*, *2*(6), pp.1747-1761.

Bekris, L.M., Yu, C.E., Bird, T.D. and Tsuang, D., 2011. The Genetics of Alzheimer's Disease and Parkinson's Disease. *Neurochemical Mechanisms in Disease*, pp.695-755.

Bignoux, M.J., Cuttler, K., Otgaar, T.C., Ferreira, E., Letsolo, B.T. and Weiss, S.F., 2019. LRP:: FLAG rescues cells from amyloid-β-mediated cytotoxicity through increased TERT levels and telomerase activity. *Journal of Alzheimer's Disease*, *69*(3), pp.729-741.

Bornhorst, J.A. and Falke, J.J., 2000. Purification of proteins using polyhistidine affinity tags. *Academic Press*, *326,* pp.245-254

Braungart, E., Gerlach, M., Riederer, P., Baumeister, R. and Hoener, M. C., 2004. Caenorhabditis elegans MPP+ model of Parkinson's disease for high-throughput drug screenings. *Neuro-degenerative diseases*, *1*(4-5), pp.175–183.

Briand, L., Marcion, G., Kriznik, A., Heydel, J. M., Artur, Y., Garrido, C., Seigneuric, R. and Neiers, F., 2016. A self-inducible heterologous protein expression system in Escherichia coli. *Scientific reports*, *6*, pp.33037.

Butò, S., Tagliabue, E., Ardini, E., Magnifico, A., Ghirelli, C., Van Den Brûle, F., Castronovo, V., Colnaghi, M.I., Sobel, M.E. and Ménard, S., 1998. Formation of the 67-kDa laminin receptor by acylation of the precursor. *Journal of cellular biochemistry*, *69*(3), pp.244-251.

Caetano, F.A., Beraldo, F.H., Hajj, G.N., Guimaraes, A.L., Jürgensen, S., Wasilewska-Sampaio, A.P., Hirata, P.H., Souza, I., Machado, C.F., Wong, D.Y.L. and De Felice, F.G., 2011. Amyloid-beta oligomers increase the localization of prion protein at the cell surface. *Journal of neurochemistry*, *117*(3), pp.538-553.

Castronovo, V., Taraboletti, G. and Sobel, M.E., 1991. Functional domains of the 67-kDa laminin receptor precursor. *Journal of Biological Chemistry*, *266*(30), pp.20440-20446.

Cente, M., Filipcik, P., Pevalova, M., Novak, M., 2006. Expression of a truncated tau protein induces oxidative stress in a rodent model of tauopathy. *European Journal of Neuroscien*ce, *24*, pp.1085–1090.

Cheignon, C., Tomas, M., Bonnefont-Rousselot, D., Faller, P., Hureau, C. and Collin, F., 2018. Oxidative stress and the amyloid beta peptide in Alzheimer's disease. *Redox biology*, *14*, pp.450-464.

Choi, S.H., Kim, Y.H., Hebisch, M., Sliwinski, C., Lee, S., D'Avanzo, C., Chen, H., Hooli, B., Asselin, C., Muffat, J. and Klee, J.B., 2014. A three-dimensional human neural cell culture model of Alzheimer's disease. *Nature*, *515*(7526), pp.274-278.

Cong, Y.S., Wright, W.E. and Shay, J.W., 2002. Human telomerase and its regulation. *Microbiology and molecular biology reviews*, *66*(3), pp.407-425.

Cong, Y. and Shay, J.W., 2008. Actions of human telomerase beyond telomeres. *Cell research*, *18*(7), pp.725-732.

Couvreur, P., Dubernet, C. and Puisieux, F., 1995. Controlled drug delivery with nanoparticles: current possibilities and future trends. *European journal of pharmaceutics and biopharmaceutics*, *41*(1), pp.2-13.

Cummings, J.L. and Cole, G., 2002. Alzheimer disease. *Jama*, *287*(18), pp.2335-2338.

Danhier, F., Ansorena, E., Silva, J. M., Coco, R., Le Breton, A. and Préat, V., 2012. PLGA-based nanoparticles: An overview of biomedical applications. *Journal of Controlled Release*, *161*(2), pp.505–522.

Dauer, W. and Przedborski, S., 2003. Parkinson's disease: mechanisms and models. *Neuron*, *39*(6), pp.889-909.

Dias, B.D.C., Jovanovic, K., Gonsalves, D., Moodley, K., Reusch, U., Knackmuss, S., Penny, C., Weinberg, M.S., Little, M. and Weiss, S.F., 2013. Anti-LRP/LR specific antibody IgG1-iS18 and knock-down of LRP/LR by shRNAs rescue cells from Aβ 42 induced cytotoxicity. *Scientific reports*, *3*(1), pp.1-8.

DiGiacomo, V. and Meruelo, D., 2015. Looking into laminin receptor: critical discussion regarding the non-integrin 37/67-kDa laminin receptor/RPSA protein. *Biological Reviews, 91(2)*, pp.288-310.

Emamzadeh, F.N., 2016. Alpha-synuclein structure, functions, and interactions. *Journal of research in medical sciences: the official journal of Isfahan University of Medical Sciences, 21*, pp.29.

Falke, J. J., and Corbin, J. A., 2013. Affinity Tags for Protein Purification. *Encyclopedia of Biological Chemistry (2)*(2), pp.61–63.

Fatehullah, A., Doherty, C., Pivato, G., Allen, G., Devine, L., Nelson, J. and Timson, D.J., 2010. Interactions of the 67 kDa laminin receptor and its precursor with laminin. *Bioscience reports*, *30*(2), pp.73-79.

Feczkó, T., Tóth, J., Dósa, G. and Gyenis, J., 2011. Optimization of protein encapsulation in PLGA nanoparticles. *Chemical Engineering and Processing: Process Intensification*, *50*(8), pp.757–765.

Friedlich, A.L. and Beal, M.F., 2000. Prospects for redox-based therapy in neurodegenerative diseases. *Neurotoxicity research*, *2*(2), pp.229-237.

Galkin, A and Brandt, U. (2005). Superoxide radical formation by pure complex I (NADH:ubiquinone oxidoreductase) from Yarrowia lipolytica. *The Journal of biological chemistry*, *280*(34), pp.30129–30135.

Garrido, C., Galluzzi, L., Brunet, M., Puig, P.E., Didelot, C. and Kroemer, G., 2006. Mechanisms of cytochrome c release from mitochondria. *Cell Death & Differentiation*, *13*(9), pp.1423-1433.

Garti, N. and Bisperink, C., 1998. Double emulsions: progress and applications. *Current opinion in colloid & interface science*, *3*(6), pp.657-667.

Gauczynski, S., Peyrin, J. M., Ha.k, S., Leucht, C., Hundt, C., Rieger, R., Krasemann, S., Deslys, J. P., Dormont, D., Lasm.zas, C. I. and Weiss, S., 2001. The 37-kDa/67-kDa laminin receptor acts as the cell-surface receptor for the cellular prion protein. *The EMBO journal, 20*(21), pp.5863–5875.

Ghisaidoobe, Amar B T, and Sang J Chung. Intrinsic tryptophan fluorescence in the detection and analysis of proteins: a focus on Förster resonance energy transfer techniques. *International journal of molecular sciences, 5*(12), pp. 22518-38.

Gilder, A. S and Gómez, S. M. (2013). Protein detection and quantitation technologies for gel-based proteome analysis. I*nternational journal of proteomics, 13*, pp.709176.

Givant-Horwitz, V., Davidson, B. and Reich, R. (2004). Laminin-induced signaling in tumor cells: the role of the M(r) 67,000 laminin receptor. *Cancer research*, *64*(10), pp.3572–3579.

Greenfield N. J. (2006). Using circular dichroism spectra to estimate protein secondary structure. *Nature protocols*, *1*(6), pp.2876–2890.

Goedert, M. and Spillantini, M.G., 2006. A century of Alzheimer's disease. *Science*, *314*(5800), pp.777-781.

Hernandez-Zimbron, L.F., Luna-Muñoz, J., Mena, R., Vazquez-Ramirez, R., Kubli-Garfias, C., Cribbs, D.H., Manoutcharian, K. and Gevorkian, G., 2012. Amyloid-β peptide binds to cytochrome C oxidase subunit 1. *PloS one*, *7*(8), pp.42344.

Hu, W., Wang, Z. and Zheng, H., 2018. Mitochondrial accumulation of amyloid β (Aβ) peptides requires TOMM22 as a main Aβ receptor in yeast. *The Journal of biological chemistry*, *293*(33), pp.12681–12689.

Jamieson, K.V., Wu, J., Hubbard, S.R. and Meruelo, D., 2008. Crystal structure of the human laminin receptor precursor. *Journal of Biological Chemistry*, *283*(6), pp.3002-3005.

Jamieson, K. V., Hubbard, S. R. and Meruelo, D., 2011. Structure-guided identification of a laminin binding site on the laminin receptor precursor. *Journal of molecular biology*, *405*(1), pp.24–32.

Jarrett, J.T., Berger, E.P. and Lansbury Jr, P.T., 1993. The C-Terminus of the β Protein is Critical in Amyloidogenesis a. *Annals of the New York Academy of Sciences*, *695*(1), pp.144-148.

Jovanovic, K., Chetty, C.J., Khumalo, T., Da Costa Dias, B., Ferreira, E., Malindisa, S.T., Caveney, R., Letsolo, B.T. and Weiss, S.F., 2015. Novel patented therapeutic approaches targeting the 37/67 kDa laminin receptor for treatment of cancer and Alzheimer's disease. Expert opinion on therapeutic patents, 25(5), pp.567-582.

Jovanovic, K., Gonsalves, D., Da Costa Dias, B., Moodley, K., Reusch, U., Knackmuss, S., Penny, C., Weinberg, M., Little, M. and Weiss, S., 2013. Anti-LRP/LR specific antibodies and shRNAs impede amyloid beta shedding in Alzheimer's disease. *Scientific Reports, 3(1).*

Jovanovic, K., Loos, B., Da Costa Dias, B., Penny, C. and Weiss, S., 2014. High Resolution Imaging Study of Interactions between the 37 kDa/67 kDa Laminin Receptor and APP, Beta-Secretase and Gamma-Secretase in Alzheimer's Disease. *PLoS ONE, 9(6*), pp.100373.

Haendeler, J., Dröse, S., Büchner, N., Jakob, S., Altschmied, J., Goy, C., Spyridopoulos, I., Zeiher, A. M., Brandt, U. and Dimmeler, S., 2009. Mitochondrial telomerase reverse transcriptase binds to and protects mitochondrial DNA and function from damage. *Arteriosclerosis, thrombosis, and vascular biology*, *29*(6), pp.929–935.

Hu, Q. and Wang, G., 2016. Mitochondrial dysfunction in Parkinson's disease. *Translational neurodegeneration*, *5*(1), pp.1-8.

Irving, B., 2007. Nanoparticle drug delivery systems. *Inno Pharm Biotechnol*, *24*, pp.58-62.

Kaur, D., Yantiri, F., Rajagopalan, S., Kumar, J., Mo, J.Q., Boonplueang, R., Viswanath, V., Jacobs, R., Yang, L., Beal, M.F. and DiMonte, D., 2003. Genetic or pharmacological iron chelation prevents MPTP-induced neurotoxicity in vivo: a novel therapy for Parkinson's disease. *Neuron*, *37*(6), pp.899-909.

Landowski, T.H., Uthayakumar, S. and Starkey, J.R., 1995. Control pathways of the 67 kDa laminin binding protein: surface expression and activity of a new ligand binding domain. *Clinical & experimental metastasis*, *13*(5), pp.357-372.

Leucht, C., Simoneau, S., Rey, C., Vana, K., Rieger, R., Lasm.zas, C. and Weiss, S., 2003. The 37 kDa/67 kDa laminin receptor is required for PrP Sc propagation in scrapie-infected neuronal cells. EMBO reports, 4(3), pp.290-295.

Li, C.H., Nguyen, X., Narhi, L., Chemmalil, L., Towers, E., Muzammil, S., Gabrielson, J. and Jiang, Y., 2011. Applications of circular dichroism (CD) for structural analysis of proteins: qualification of near-and far-UV CD for protein higher order structural analysis. *Journal of pharmaceutical sciences*, *100*(11), pp.4642-4654.

Li, J. and Sabliov, C., 2013. PLA/PLGA nanoparticles for delivery of drugs across the blood-brain barrier. *Nanotechnology Reviews, 2*(3), pp. 241-257.

Lichtenberg, D., Ahyayauch, H., Alonso, A. and Goñi, F.M., 2013. Detergent solubilization of lipid bilayers: a balance of driving forces. *Trends in biochemical sciences*, *38*(2), pp.85-93.

Linnane, A., Ozawa, T., Marzuki, S. and Tanaka, M., 1989. Mitochondrial DNA mutations as an important contributor to ageing and degenerative diseases. *The Lancet*, *333*(8639), pp.642-645.

Lin, X., Parisiadou, L., Sgobio, C., Liu, G., Yu, J., Sun, L., Shim, H., Gu, X.L., Luo, J., Long, C.X. and Ding, J., 2012. Conditional expression of Parkinson's disease-related mutant α-synuclein in the midbrain dopaminergic neurons causes progressive neurodegeneration and degradation of transcription factor nuclear receptor related 1. *Journal of Neuroscience*, *32*(27), pp.9248-9264

Liu, J., Huang, Y. and Kumar, A., 2017. Understanding the factors affecting the cellular uptake of nanoparticles: A review of recent advances and challenges. Archives of pharmacal research, 40(3), 264-278.

Lotharius, J. and Brundin, P., 2002. Pathogenesis of Parkinson's disease: dopamine, vesicles and α-synuclein. *Nature reviews neuroscience*, *3*(12), pp.932-942.

Mandel, S., Grünblatt, E., Riederer, P., Gerlach, M., Levites, Y. and Youdim, M.B., 2003. Neuroprotective strategies in Parkinson’s disease: an update on progress. *CNS drugs*, *17*, pp.729-762.

Martín-Maestro, P., Gargini, R., Perry, G., Avila, J. and García-Escudero, V., 2016. PARK2 enhancement is able to compensate mitophagy alterations found in sporadic Alzheimer's disease. *Human molecular genetics*, *25*(4), pp.792-806.

Makadia, H.K. and Siegel, S.J., 2011. Poly lactic-co-glycolic acid (PLGA) as biodegradable controlled drug delivery carrier. *Polymers*, *3*(3), pp.1377-1397.

Matsuda, S., Kitagishi, Y. and Kobayashi, M., 2013. Function and characteristics of PINK1 in mitochondria. *Oxidative medicine and cellular longevity*, *2013*, pp.601587.

Mayeux, R. and Stern, Y., 2012. Epidemiology of Alzheimer disease. *Cold Spring Harbor perspectives in medicine*, *2*(8), pp.006239.

Meade, R.M., Fairlie, D.P. and Mason, J.M., 2019. Alpha-synuclein structure and Parkinson's disease–lessons and emerging principles. *Molecular neurodegeneration*, *14*(1), pp.1-14.

Miklya, I., Göltl, P., Hafenscher, F. and Pencz, N., 2014. The role of parkin in Parkinson's disease. *Neuropsychopharmacologia Hung*,*16*(2), pp.67-76.

Mizuno, Y., Hattori, N., Mori, H., Suzuki, T. and Tanaka, K., 2001. Parkin and Parkinson's disease. *Current opinion in neurology*, *14*(4), pp.477-482

Moon, H.E. and Paek, S.H., 2015. Mitochondrial dysfunction in Parkinson's disease. *Experimental neurobiology*, *24*(2), pp.103.

Moraitou, M., Hadjigeorgiou, G., Monopolis, I., Dardiotis, E., Bozi, M., Vassilatis, D., Vilageliu, L., Grinberg, D., Xiromerisiou, G., Stefanis, L. and Michelakakis, H., 2011. β-Glucocerebrosidase gene mutations in two cohorts of Greek patients with sporadic Parkinson's disease. *Molecular genetics and metabolism*, *104*(1-2), pp.149-152.

Muangpaisan, W., Mathews, A., Hori, H. and Seidel, D., 2011. A systematic review of the worldwide prevalence and incidence of Parkinson's disease. *Journal of the Medical Association of Thailand*, *94*(6), pp.749–755.

Mudshinge, S. R., Deore, A. B., Patil, S. and Bhalgat, C. M., 2011. Nanoparticles: Emerging carriers for drug delivery. *Saudi Pharmaceutical Journal*, *19*(3), pp.129–141.

Murphy, K.E., Gysbers, A.M., Abbott, S.K., Tayebi, N., Kim, W.S., Sidransky, E., Cooper, A., Garner, B. and Halliday, G.M., 2014. Reduced glucocerebrosidase is associated with increased α-synuclein in sporadic Parkinson's disease. *Brain*, *137*(3), pp.834-848.

Nakamura, T.M. and Cech, T.R., 1998. Reversing time: origin of telomerase. *Cell*, *92*(5), pp.587-590.

Naidoo, K., Malindisa, S., Otgaar, T., Bernert, M., Da Costa Dias, B., Ferreira, E., Reusch, U., Knackmuss, S., Little, M., Weiss, S. and Letsolo, B., 2015. Knock-Down of the 37kDa/67kDa Laminin Receptor LRP/LR Impedes Telomerase Activity. *PLOS ONE, 10*(11), pp.0141618.

Nelson, J., McFerran, N. V., Pivato, G., Chambers, E., Doherty, C., Steele, D. and Timson, D. J., 2008. The 67 kDa laminin receptor: structure, function and role in disease. *Bioscience reports*, *28*(1), pp.33–48.

Neugroschl, J. and Wang, S., 2011. Alzheimer's Disease: Diagnosis and Treatment Across the Spectrum of Disease Severity. *Mount Sinai Journal of Medicine: A Journal of Translational and Personalized Medicine*, *78*(4), pp.596–612.

Nussbaum, R.L. and Ellis, C.E., 2003. Alzheimer's disease and Parkinson's disease. *New england journal of medicine*, *348*(14), pp.1356-1364.

Oertel, W. and Schulz, J.B., 2016. Current and experimental treatments of Parkinson disease: a guide for neuroscientists. *Journal of neurochemistry*, *139*, pp.325-337.

Omar, A., Reusch, U., Knackmuss, S., Little, M. and Weiss, S.F., 2012. Anti-LRP/LRspecific antibody IgG1-iS18 significantly reduces adhesion and invasion of metastatic lung, cervix, colon and prostate cancer cells. Journal of molecular biology, 419(1-2), pp.102-109.

Otgaar, T. C., Ferreira, E., Malindisa, S., Bernert, M., Letsolo, B. T. and Weiss, S., 2017. 37 kDa LRP::FLAG enhances telomerase activity and reduces senescent markers in vitro. *Oncotarget, 8*(49), pp.86646–86656.

Paillard, T., Rolland, Y. and de Souto Barreto, P., 2015. Protective effects of physical exercise in Alzheimer's disease and Parkinson's disease: a narrative review. *Journal of clinical neurology (Seoul, Korea)*, *11*(3), pp.212.

Pardridge W. M., 2012. Drug transport across the blood-brain barrier. *Journal of cerebral blood flow and metabolism : official journal of the International Society of Cerebral Blood Flow and Metabolism*, *32*(11), pp.1959–1972.

Perez-Ortiz, J.M. and Swerdlow, R.H., 2019. Mitochondrial dysfunction in Alzheimer's disease: Role in pathogenesis and novel therapeutic opportunities. *British journal of pharmacology*, *176*(18), pp.3489-3507.

Pinnock, E.C., Jovanovic, K., Pinto, M.G., Ferreira, E., Dias, B.D.C., Penny, C., Knackmuss, S., Reusch, U., Little, M., Schatzl, H.M. and Weiss, S.F., 2016. LRP/LR Antibody Mediated Rescuing of Amyloid-β-Induced Cytotoxicity is Dependent on PrP c in Alzheimer's Disease. *Journal of Alzheimer's Disease*, *49*(3), pp.645-657.

Poulopoulos, M., Levy, O.A. and Alcalay, R.N., 2012. The neuropathology of genetic Parkinson's disease. *Movement Disorders*, *27*(7), pp.831-842.

Reeve, A., Simcox, E. and Turnbull, D., 2014. Ageing and Parkinson's disease: why is advancing age the biggest risk factor?. *Ageing research reviews*, *14*, pp.19-30.

Reitz, C., Brayne, C. and Mayeux, R., 2011. Epidemiology of Alzheimer disease. *Nature Reviews Neurology*, *7*(3), pp.137-152.

Rodriguez, M., Rodriguez-Sabate, C., Morales, I., Sanchez, A. and Sabate, M., 2015. Parkinson's disease as a result of aging. *Aging cell*, *14*(3), pp.293-308.

Royer, C.A., 1995. Fluorescence spectroscopy. *Protein stability and folding: Theory and practice*, pp.65-89.

Scheiman, J., Tseng, J. C., Zheng, Y. and Meruelo, D. (2010). Multiple functions of the 37/67-kd laminin receptor make it a suitable target for novel cancer gene therapy. *Molecular therapy : the journal of the American Society of Gene Therapy*, *18*(1), pp.63–74.

Schlachetzki, J., Saliba, S.W. and Oliveira, A.C.P.D., 2013. Studying neurodegenerative diseases in culture models. *Brazilian Journal of Psychiatry*, *35*, pp.92-100.

Santos, J.H., Meyer, J.N. and Van Houten, B., 2006. Mitochondrial localization of telomerase as a determinant for hydrogen peroxide-induced mitochondrial DNA damage and apoptosis. *Human molecular genetics*, *15*(11), pp.1757-1768.

Seirafi, M., Kozlov, G. and Gehring, K., 2015. Parkin structure and function. *The FEBS journal*, *282*(11), pp.2076-2088.

Selkoe, D.J., 1996. Amyloid β-protein and the genetics of Alzheimer's disease. *Journal of Biological Chemistry*, *271*(31), pp.18295-18298.

Semete, B., Booysen, L., Lemmer, Y., Kalombo, L., Katata, L., Verschoor, J. and Swai, H. S., 2010. In vivo evaluation of the biodistribution and safety of PLGA nanoparticles as drug delivery systems. *Nanomedicine : nanotechnology, biology, and medicine*, *6*(5), pp.662–671.

Serrano-Pozo, A., Frosch, M.P., Masliah, E. and Hyman, B.T., 2011. Neuropathological alterations in Alzheimer disease. *Cold Spring Harbor perspectives in medicine*, *1*(1), pp.006189.

Sharma, N.K., Reyes, A., Green, P., Caron, M.J., Bonini, M.G., Gordon, D.M., Holt, I.J. and Santos, J.H., 2012. Human telomerase acts as a hTR-independent reverse transcriptase in mitochondria. *Nucleic acids research*, *40*(2), pp.712-725.

Shay, J.W. and Wright, W.E., 2004. Telomeres are double-strand DNA breaks hidden from DNA damage responses. *Molecular cell*, *14*(4), pp.420-421.

Singh, N., Pillay, V. and Choonara, Y.E., 2007. Advances in the treatment of Parkinson's disease. *Progress in neurobiology*, *81*(1), pp.29-44.

Stebbins, G.T. and Murphy, C.M., 2009. Diffusion tensor imaging in Alzheimer's disease and mild cognitive impairment. *Behavioural neurology*, *21*(1, 2), pp.39-49.

Song, D.D., Shults, C.W., Sisk, A., Rockenstein, E. and Masliah, E., 2004. Enhanced substantia nigra mitochondrial pathology in human α-synuclein transgenic mice after treatment with MPTP. *Experimental neurology*, *186*(2), pp.158-172.

Song, P., Li, S., Wu, H., Gao, R., Rao, G., Wang, D., Chen, Z., Ma, B., Wang, H., Sui, N. and Deng, H., 2016. Parkin promotes proteasomal degradation of p62: implication of selective vulnerability of neuronal cells in the pathogenesis of Parkinson's disease. *Protein & cell*, *7*(2), pp.114-129

Sugiura, A., McLelland, G.L., Fon, E.A. and McBride, H.M., 2014. A new pathway for mitochondrial quality control: mitochondrial-derived vesicles. *The EMBO journal*, *33*(19), pp.2142-2156.

Sveinbjornsdottir, S., 2016. The clinical symptoms of Parkinson's disease. *Journal of neurochemistry*, *139*, pp.318-324.

Tarakad, A. and Jankovic, J., 2017, April. Diagnosis and management of Parkinson's disease. In *Seminars in neurology*, *37*(02) , pp.118-126.

Thomas, P., O'Callaghan, N.J. and Fenech, M., 2008. Telomere length in white blood cells, buccal cells and brain tissue and its variation with ageing and Alzheimer's disease. *Mechanisms of ageing and development*, *129*(4), pp.183-190.

Yang, Y., Gehrke, S., Imai, Y., Huang, Z., Ouyang, Y., Wang, J.W., Yang, L., Beal, M.F., Vogel, H. and Lu, B., 2006. Mitochondrial pathology and muscle and dopaminergic neuron degeneration caused by inactivation of Drosophila Pink1 is rescued by Parkin. *Proceedings of the National Academy of Sciences*, *103*(28), pp.10793-10798.

Yasuda, T. and Mochizuki, H., 2010. The regulatory role of α-synuclein and parkin in neuronal cell apoptosis; possible implications for the pathogenesis of Parkinson's disease. *Apoptosis*, *15*(11), pp.1312-1321.

Ye, X., Sun, X., Starovoytov, V. and Cai, Q., 2015. Parkin-mediated mitophagy in mutant hAPP neurons and Alzheimer's disease patient brains. *Human molecular genetics*, *24*(10), pp.2938-2951.

Valente, E.M., Abou-Sleiman, P.M., Caputo, V., Muqit, M.M., Harvey, K., Gispert, S., Ali, Z., Del Turco, D., Bentivoglio, A.R., Healy, D.G. and Albanese, A., 2004. Hereditary early-onset Parkinson's disease caused by mutations in PINK1. *Science*, *304*(5674), pp.1158-1160.

Veeriah, S., Taylor, B.S., Meng, S., Fang, F., Yilmaz, E., Vivanco, I., Janakiraman, M., Schultz, N., Hanrahan, A.J., Pao, W. and Ladanyi, M., 2010. Somatic mutations of the Parkinson's disease–associated gene PARK2 in glioblastoma and other human malignancies. *Nature genetics*, *42*(1), pp.77.

Von Coelln, R., Dawson, V.L. and Dawson, T.M., 2004. Parkin-associated Parkinson's disease. *Cell and tissue research*, *318*(1), pp.175-184.

Xiong, S., George, S., Yu, H., Damoiseaux, R., France, B., Ng, K. W. and Loo, J. S. (2013). Size influences the cytotoxicity of poly (lactic-co-glycolic acid) (PLGA) and titanium dioxide (TiO(2)) nanoparticles. *Archives of toxicology*, *87*(6), pp.1075–1086.

Zecca, L., Casella, L., Albertini, A., Bellei, C., Zucca, F.A., Engelen, M., Zadlo, A., Szewczyk, G., Zareba, M. and Sarna, T., 2008. Neuromelanin can protect against iron-mediated oxidative damage in system modeling iron overload of brain aging and Parkinson's disease. *Journal of neurochemistry*, *106*(4), pp.1866-1875.

Zidane, N., Ould-Abeih, M., Petit-Topin, I. and Bedouelle, H., 2012. The folded and disordered domains of human ribosomal protein SA have both idiosyncratic and shared functions as membrane receptors. *Bioscience Reports, 33*(1).